Cy 113

~~SECRET~~

DTL020,329

Operation

SUN BEAM

SHOT SMALL BOY

DNA1.950515.002

POR-2249
(WT-2249)

This document consists of 107 pages

No. 113 of 205 copies, Series A

L-146/79

PROJECT OFFICERS REPORT—PROJECT 7.13

F-100F/GAM-83B SIMULATION ~~(U)~~

TECHNICAL LIBRARY
of 1953 /63
of the
13 NOV 1963
DEFENSE ATOMIC
SUPPORT AGENCY

~~PLEASE RETURN TO
RAMAS MIDYKE
BURLINGTON, MASS.~~

Bernard C. Lorenz, Capt, USAF
Project Officer

Aeronautical Systems Division
Air Force Systems Command
Wright-Patterson AFB, Ohio

and

Paul W. Lappin, Major, USAF

6570th Aerospace Medical
Research Laboratories
Wright-Patterson AFB, Ohio

~~GROUP-1
Excluded from automatic
downgrading and declassification.~~

~~FORMERLY RESTRICTED DATA~~

~~Handle as Restricted Data in foreign dissemination. Section 144b, Atomic Energy Act of 1954.~~

~~This material contains information affecting the national defense of the United States within the meaning of the espionage laws, Title 18, U.S.C., Secs. 793 and 794, the transmission or revelation of which in any manner to an unauthorized person is prohibited by law.~~

Issuance Date: October 24, 1968

PORTIONS OF DOCUMENT(S) RELEASED UNDE
FREEDOM OF INFORMATION ACT
DNA CASE NO. 90-073
DATE

~~SECRET~~

68-008, 904

HRE-1182

SECRET

POR-2249
(WT-2249)

OPERATION SUN BEAM

SHOT SMALL BOY

PROJECT OFFICERS REPORT—PROJECT 7.13

F-100F/GAM-83B SIMULATION (U)

Bernard C. Lorenz, Capt, USAF
Project Officer

Aeronautical Systems Division
Air Force Systems Command
Wright-Patterson AFB, Ohio

and

Paul W. Lappin, Major, USAF

6570th Aerospace Medical
Research Laboratories
Wright-Patterson AFB, Ohio

Qualified requesters may obtain copies of this report from DDC

GROUP-1
Excluded from automatic downgrading and declassification

FORMERLY RESTRICTED DATA
Handle as Restricted Data in foreign dissemination. Section 144b, Atomic Energy Act of 1954.

This material contains information affecting the national defense of the United States within the meaning of the espionage laws, Title 18, U.S.C., Secs. 793 and 794, the transmission or revelation of which in any manner to an unauthorized person is prohibited by law.

This document is the author(s) report to the Chief, Defense Atomic Support Agency, of the results of experimentation sponsored by that agency during nuclear weapons effects testing. The results and findings in this report are those of the author(s) and not necessarily those of the DOD. Accordingly, reference to this material must credit the author(s). This report is the property of the Department of Defense and as such, may be reclassified or withdrawn from circulation as appropriate by the Defense Atomic Support Agency.
DEPARTMENT OF DEFENSE
WASHINGTON 25, D.C.

SECRET

ABSTRACT

The objectives of this experiment were to determine F-100F response to measured loads imposed from weapons in the GAM-83B yield range, verify existing structural analysis of an F-100F exposed to these loads, and evaluate the effectiveness of devices designed to protect eyes from flash blindness and retinal burns.

The F-100F was programmed to fly a normal GAM-83B level, offset-delivery flight path and was controlled by MSQ-1A ground positioning radar so as to arrive over a predetermined point at time of detonation. This desired location was where the F-100F might have been had the aircraft actually delivered the weapon. The aircraft was instrumented to measure loads imposed, and to measure rigid body response and dynamic response to these loads. The rear seat observer was outfitted with a special visor, developed by the Aeromedical Laboratory, to protect his eyes from flash blindness and retinal burns. The observer had one eye protected with a patch and viewed the detonation with the unpatched eye through the protective visor.

The aircraft was positioned within the stringent requirements necessary to obtain meaningful data. Postshot examination of the aircraft showed no signs of damage. No retinal burns were found on the observer and he stated that he did not experience any flash blindness or after image.

SECRET

PREFACE

Due to the two completely separate problems involved in safely performing the GAM-83B Mission, this report is written in two distinctly separated parts. Part I, written by the Project Officer Capt. Bernard C. Lorenz, is concerned only with the aircraft response to the weapon effects. Part II, written by Major Paul W. Lappin, 6570th Aerospace Medical Research Laboratories is concerned only with the effects of the detonation on the eyes, the protection afforded by the experimental eye visor and the ability of the pilot to perform the mission.

This mission was successfully accomplished because the aircraft was precisely positioned at time of detonation. Due to the uncanny positioning skills required, and the danger inherent in the mission, it seems fitting to pay particular tribute to the MSQ Operator, Capt. Russell X. Greenfield, the rear seat observer, Capt. Lucien D. Wise, and the pilot, Capt. Larry D. McClain.

SECRET

CONTENTS

ABSTRACT ---------- 5

PREFACE ---------- 6

PART 1 NUCLEAR WEAPON EFFECTS ON F-100F SIMULATING DELIVERY OF GAM-83B ---------- 11

CHAPTER 1 INTRODUCTION ---------- 11

1.1 Objectives ---------- 11
1.2 Background ---------- 11
1.3 Theory ---------- 12

CHAPTER 2 PROCEDURE ---------- 14

2.1 Operations ---------- 14
2.1.1 Ground Radar ---------- 14
2.1.2 Site Office ---------- 15
2.1.3 Flight Path ---------- 15
2.1.4 Rehearsals ---------- 16
2.2 Positioning ---------- 16
2.2.1 Limiting Effects ---------- 16
2.2.2 Positioning for Limiting Effects ---------- 17
2.2.3 Flight Pattern Control ---------- 19
2.3 Instrumentation ---------- 21

CHAPTER 3 RESULTS ---------- 28

3.1 Aircraft Position ---------- 28
3.2 Aircraft Damage ---------- 29
3.3 Data Presentation ---------- 29

CHAPTER 4 DISCUSSION ---------- 64

4.1 Flight Path Control Concept ---------- 64
4.2 Nuclear Radiation ---------- 64
4.3 Thermal Radiation ---------- 64
4.4 Rigid-Body Data ---------- 66
4.5 Overpressure Data ---------- 67
4.6 Lateral Accelerations ---------- 68
4.7 Normal Accelerations ---------- 68

SECRET

4.8 Shear Stress in Fuselage Side Panels ---------- 71

CHAPTER 5 CONCLUSIONS ---------- 74

5.1 Flight Pattern Concept ---------- 74
5.2 Position Analysis ---------- 74
5.3 Rigid-Body Response ---------- 74
5.4 Dynamic Response ---------- 74

PART 2 EYE PROTECTION IN F-100F/GAM-83B SIMULATION --- 75

CHAPTER 6 INTRODUCTION ---------- 75

6.1 Objectives ---------- 75
6.2 Background ---------- 75
6.3 Theory ---------- 76

CHAPTER 7 PROCEDURE ---------- 78

7.1 Experimental Design ---------- 78
7.2 Instrumentation ---------- 79

CHAPTER 8 RESULTS ---------- 80

8.1 Visual ---------- 80
8.2 Calculated ---------- 80

CHAPTER 9 DISCUSSION ---------- 81

CHAPTER 10 THEORETICAL ANALYSIS ---------- 84

10.1 Discussion ---------- 84
10.2 Calculation of Irradiance on the Retina ---------- 84
10.2.1 Energy from the Second Pulse ---------- 84
10.2.2 Energy from the First Pulse ---------- 89

CHAPTER 11 CONCLUSIONS AND RECOMMENDATIONS -------- 92

APPENDIX INSTRUMENTATION LOCATIONS AND CONFIGURATIONS ---------- 93

REFERENCES ---------- 105

TABLES

2.1 Aircraft Position ---------- 19
3.1 Aircraft Position at Detonation ---------- 28
3.2 Aircraft Position at Time of Shock Arrival ---------- 29
3.3 Nuclear Radiation ---------- 32

SECRET

FIGURES

2.1 Flight path geometry ---------- 24
2.2 Limit aircraft positions ---------- 25
2.3 Flight pattern ---------- 26
2.4 Strain gage calibration ---------- 27
3.1 Aircraft flight path ---------- 33
3.2 Thermal radiation ---------- 34
3.3 Overpressure and rigid-body time histories ---------- 35
3.4 Rigid-body time histories, elapsed time 6.1 to 6.9 seconds --- 36
3.5 Rigid-body time histories, elapsed time −1 to 9 seconds ----- 37
3.6 Lateral acceleration time histories, fuselage nose (FS 28) and center of gravity (FS 271) ---------- 38
3.7 Lateral acceleration time histories, vertical stabilizer tip (front spar) and fuselage tail (FS 464) ---------- 39
3.8 Normal acceleration time histories, fuselage tail (FS 440) and fuselage nose (FS 16) ---------- 40
3.9 Normal acceleration time histories, right wingtip (front spar) and center of gravity (FS 269) ---------- 41
3.10 Normal acceleration time histories, left wingtip (front spar) and right wingtip (rear spar) ---------- 42
3.11 Strain gage locations ---------- 43
3.12 Zero stress determination, strain gage Channel 4 -------- 44
3.13 Zero stress determination, strain gage Channel 5 -------- 45
3.14 Zero stress determination, strain gage Channel 6 -------- 46
3.15 Zero stress determination, strain gage Channel 7 -------- 47
3.16 Zero stress determination, strain gage Channel 8 -------- 48
3.17 Zero stress determination, strain gage Channel 9 -------- 49
3.18 Zero stress determination, strain gage Channel 10 -------- 50
3.19 Zero stress determination, strain gage Channel 11 -------- 51
3.20 Zero stress determination, strain gage Channel 12 -------- 52
3.21 Zero stress determination, strain gage Channel 13 -------- 53
3.22 Zero stress determination, strain gage Channel 14 -------- 54
3.23 Zero stress determination, strain gage Channel 15 -------- 55
3.24 Positive shear sign convention ---------- 56
3.25 Side panel stress at shock arrival, strain gage Channels 9 and 11 ---------- 57
3.26 Side panel stress at shock arrival, strain gage Channels 15 and 10 ---------- 58
3.27 Side panel stress at shock arrival, strain gage Channels 13 and 14 ---------- 59
3.28 Side panel stress at shock arrival, strain gage Channels 12 and 7 ---------- 60
3.29 Side panel stress at shock arrival, strain gage Channels 5 and 8 ---------- 61

SECRET

3.30 Side panel stress at shock arrival, strain gage Channels 4 and 6 ---------- 62
3.31 Peak stresses inside panels ---------- 63
9.1 Retinal irradiance ---------- 83
A.1 General aircraft instrumentation ---------- 94
A.2 Legend ---------- 95
A.3 Attitude gyro installation, FS 189.898 ---------- 96
A.4 Rate gyro installation, FS 189.898 ---------- 97
A.5 Lateral and vertical accelerometer installation, FS 275.50 ---------- 98
A.6 Accelerometer installation, FS 15.75 ---------- 99
A.7 Vertical stabilizer accelerometer installation ---------- 100
A.8 Accelerometer installation, FS 464.16 ---------- 101
A.9 Accelerometer installation, FS 28.50 ---------- 102
A.10 Wingtip accelerometer installation, right wing ---------- 103
A.11 Wingtip accelerometer installation, left wing ---------- 104

SECRET

CHAPTER 1

INTRODUCTION

1.1 OBJECTIVES

The primary objectives of this experiment were to obtain data on: (1) gust and diffraction loadings imposed on an aircraft using offset-delivery techniques to deliver a GAM-83B, and (2) F-100F response to loadings imposed by [redacted] detonation.

The secondary objective was to verify an existing analysis of F-100D/F aircraft having vertical gusts imposed from delivery of a GAM-83B (Reference 2).

1.2 BACKGROUND

The GAM-83B was developed after the nuclear weapon testing moratorium and is soon scheduled to be operational.

Lack of specific proven data has seriously limited the confidence in USAF ability to determine safe separation distances between delivery aircraft and GAM-83B missiles. Very conservative assumptions are necessitated to insure safe separation.

The data from this experiment will measurably increase the knowledge available and permit less conservative assumptions and a greater degree of accuracy in predicting safe separation distances.

1.3 THEORY

A structural analysis of the F-100D/F has been conducted by North American Aviation (Reference 1). The analysis defines specific aircraft limitations to various effects of nuclear detonations in the yield range of the GAM-83B warhead. Two conditions at time of shock arrival were investigated, one in which the shock strikes the aircraft on the bottom at varying angles, and the other in which the shock strikes the aircraft on the side. This experiment is only concerned with the former case, as is the remainder of this discussion.

The analysis shows that the aircraft has a limit of 3 psi in overpressure. Limiting gust velocity is shown to be dependent upon the gust impingement angle, aircraft velocity and steady-state G load at time of shock arrival.

All GAM-83B delivery escape maneuvers specify a 4g breakaway turn to be maintained through shock arrival, therefore, during this experiment, the F-100F was programmed to be in a steady 4g turn at time of shock impingement. The aircraft velocity was set at [redacted] and positioned so that the impingement angle would be 90 degrees. Under these conditions the limiting gust velocity is [redacted] for the F-100F (extrapolated value based on F-100D gust limits) and [redacted] for the F-100D. The critical point on the aircraft to gust loading is the fuselage side panel, Fuselage Stations 334 to 389. This panel would fail in shear.

SECRET

Safe-escape studies indicate that the delivery aircraft would encounter 3-psi overpressure as a limiting criteria only when delivering the GAM-83B with very small offset distances (Reference 2).

Gust becomes limiting on the aircraft with greater offset distances, requiring a maximum separation distance at time of burst when the burst takes place at an angle somewhat less than 45 degrees off the nose of the aircraft. The escape maneuver of the aircraft would then carry it to a point where the gusts would be imposed.

No test data is available to verify these studies for the F-100D or F.

SECRET

CHAPTER 2

PROCEDURE

The experiment took place in conjunction with Shot Small Boy which had a yield [redacted] d a height of burst of 10 feet above ground. This particular shot was desirable [redacted] and is always a ground burst.

2.1 OPERATIONS

2.1.1 Ground Radar. One MSQ-1A (ground-installed positioning radar) was used to accurately control the F-100F so the aircraft would arrive at a predetermined point at time of detonation. The aircraft was equipped with an APW 11A radar beacon to facilitate radar pickup.

The MSQ-1A ground positioning radar included a plotting board and an automatic pen follower which followed the actual position of the aircraft. Ground zero and the desired flight path up to 15 seconds prior to time of detonation were located on the board.

Voice communication between MSQ and the aircraft was maintained by ultra high frequency radio, 340.0 Mc. The MSQ equipment was placed in a position which enabled it to have an uninterrupted view of the aircraft throughout its flight path and was turned off at 15 seconds prior to time of detonation.

SECRET

2.1.2 Site Office. A project office was set up at the test site. Communications between the project office and the MSQ site were maintained by DOD radio. Voice countdown was also received on this radio at the MSQ site.

2.1.3 Flight Path. The F-100F departed Nellis Air Force Base, Las Vegas, Nevada with drop tanks installed, on the date of the test. With drop tanks, there was enough fuel for approximately 50 minutes at the test site. The tanks were dropped in a clear area approximately 25 minutes prior to detonation. The aircraft assumed a holding pattern to the southwest of ground zero under control of MSQ. The aircraft departed the holding pattern so as to arrive at a point [redacted] from ground zero at time of detonation. The detonation took place approximately 35 degrees to the right of the flight path. The aircraft maintained a ground speed of [redacted] and an altitude of 1,500 feet above burst throughout its flight path.

The pilot was instructed to execute a normal escape maneuver at zero time or at arrival at a point [redacted] from ground zero (GZ), whichever occurred first. A ground-located visual marker identified the [redacted] point. The escape maneuver consisted of a 4g, coordinated turn to the left, continuing until after time of shock arrival.

After the experiment, the aircraft landed at Indian Springs Air Force Base, Indian Springs, Nevada for decontamination.

SECRET

2.1.4 Rehearsals. All equipment was in place and ready for operation by 1 June 1962. Rehearsals took place frequently after this date until the date of the test.

2.2 POSITIONING

The aircraft was positioned to receive the effects from a weapon having a maximum predicted yield o[redacted] detonated at 3000 feet mean sea level. The aircraft was to have a velocity of [redacted] flying 1,500 feet above burst, approaching ground zero, offset to the left in straight and level flight. After detonation the aircraft was to initiate a 4g level breakaway turn to the left and be fully established in this turn 3 seconds after detonation. The aircraft was to remain in this turn until after shock arrival. (See Figure 2.1 for flight-path geometry).

2.2.1 Limiting Effects. For the F-100F aircraft, flying at [redacted], 4500 feet altitude (mean sea levels) and in a 4g load factor turn, the limit normal gust velocity is

$$Wp \text{ Sin } \theta = [redacted]$$

Where:

Wp = gust velocity, ft/sec

θ = impingement angle, degrees

The impingement angle is the angle between the fuselage reference line and the direction of the gust velocity. The value of [redacted] was obtained by utilizing extrapolated F-100D dynamic data (Reference 1). Eighty percent of limit normal gust velocity was used.

SECRET

Therefore the limit normal gust velocity for this experiment was [redacted]

The overpressure limit for the F-100D aircraft is 3 psi (Reference 3). There is no apparent reason for suspecting that the limit overpressure on the F-100F is significantly different than that of the F-100D, therefore a limit overpressure of 3 psi was used for this experiment.

A total nuclear radiation limit of 5 rem was set for each individual participating in the Small Boy experiment.

For the purposes of this experiment a thermal radiation limit on the unprotected crew was set at 2 cal/cm^2 since this is the approximate pain threshold for humans.

2.2.2 Positioning for Limiting Effects. Since the aircraft response to gust effects was the desired data, the ideal position for the aircraft was along a flight path such that the normal component of the gust imposed on the aircraft was maximum [redacted] and the other effects were not critical.

For a given total-gust velocity, it is evident that the component of gust velocity normal to the aircraft is greatest when the impingement angle is 90 degrees. Thus, for any desired normalgust velocity component, the aircraft would be at maximum distance from the detonation at time of shock arrival, if the impingement angle of the gust was 90 degrees. This arrangement would cause the aircraft to be at the greatest possible distance

SECRET

from ground zero at time of detonation and thus diminish the effects of thermal and nuclear radiation. A further advantage of this positioning approach is that any deviation from desired longitudinal position along the flight path at T_o would cause a decrease in impingement angle and a corresponding decrease in the normal gust-velocity component. This afforded a built-in factor of safety as a protection against positioning errors during the test, since the desired normal gust component was the maximum value attainable.

Having a known desired gust velocity, a known yield and height of burst and a known altitude of the receiver aircraft, the required slant-range envelope and time of shock arrival to that curve was computed (Reference 4).

After determining the locus of points defining the [redacted] gust, the exact point where the flight path of the aircraft would be tangent to this curve was determined, and then the aircraft was backed up along its flight path to the point it would be at time of burst.

Table 2.1 shows the planned aircraft location in relation to ground zero at time of detonation and time of shock arrival.

Figure 2.2 shows the planned aircraft trajectory through the final phase of the flight path, and limiting positions at detonation and shock arrival times for a limit normal gust velocity of

[redacted]

SECRET

TABLE 2.1 AIRCRAFT POSITION

	Time of Detonation	Time of Shock Arrival
Horizontal Range	[redacted]	[redacted]
Offset Distance	[redacted]	[redacted]
Ground Range	[redacted]	[redacted]
Slant Range	[redacted]	[redacted]
Impingement Angle		θ = 90 degrees

2.2.3 Flight Pattern Control. The positioning pattern was drawn on the plotting board of the MSQ-1A. The pattern terminated at the point for which the aircraft was programmed at time of detonation (see Figure 2.3).

The pattern consisted of two parallel lines lying on a 058-degree-true heading separated by a distance equal to the diameter of a 2-minute turn of an F-100 traveling a[redacted] true.

One track terminated at the desired location for the aircraft at time of detonation (T_o). This was the inbound track for the final run of the aircraft. This track was marked in 5-second increments [redacted] outbound from the T_o point. The time marks represented desired aircraft position on the inbound leg in relation to time to go.

The displaced track (displaced to the northwest) was the outbound leg. This track was also marked in 5-second increments

SECRET

outbound from the T_o point, except that starting at a point opposite the T_o location the initial time mark was 2 minutes to go.

The aircraft was turned onto the outbound track at approximately 8 minutes to go and flown outbound until the time to go on the voice count equalled the time-to-go hash mark that the aircraft was passing on the outbound leg. At this time the aircraft was put into a 2-minute turn to the inbound leg.

Upon rollout on the inbound leg, the aircraft was very nearly merged with time-to-go countdown and time marks, and slight corrections were made with speed change to account for these errors.

At T minus 15 seconds, the aircraft was [redacted] behind the pre-programed position and [redacted] to the left of the desired flight path. At this time, the MSQ-1A was turned off, and no further control was accomplished. This was due to the limitations placed on radar transmissions by other participating projects.

From the T-minus-15-seconds point, the aircraft was kept on the last assigned heading and airspeed until time of detonation or arrival at the visual marker, whichever occurred first. At this time the pilot initiated the programmed escape maneuver. See Figure 2.3 for diagram of flight pattern.

This flight pattern is a departure from past patterns used for positioning for nuclear testing. It was developed because of two primary reasons: (1) Terrain features severely limited the maneuvering space available, (2) Possibility of shot delay and resumption of countdown late in the time sequencing required a position pattern which would provide accurate positioning with a minimum of available time.

SECRET

2.3 INSTRUMENTATION

The instrumentation on the F-100F was established to measure and record rigid body and dynamic response to gust, overpressure, thermal radiation and nuclear radiation. The system consisted of accelerometers, strain gages, gyros, potentiometers, a radiometer, a calorimeter, pressure transducers, and dosimeters. Calibration of these devices was performed in the laboratory, with the exception of the strain gages.

Because of the short lead time and aircraft structure involved, it was not practical to remove the side panels from the aircraft in order to calibrate the strain gages. In-flight calibration was accomplished by plotting stress versus velocity for zero g maneuvers and extrapolating back to zero velocity using the 1g plot as a guide. Using this approach it is possible to obtain stress values the same as if the panel were unloaded. These values would have an accuracy of ± 10 percent (see Figure 2.4).

Most of the instrumentation used on the F-100F was externally mounted. Time available for instrumentation precluded removing skin panels to allow for internal mounting. Lead wires to the instruments were also externally affixed to the aircraft with an epoxy base binding agent. The instrumentation arrangement necessitated limiting the aircraft to a 15,000-foot maximum altitude because of temperature limitations of the binder.

A standard oscillograph recording system was used to record the outputs of the various transducers.

SECRET

The following parameters were recorded:

a. Airspeed

b. Altitude

c. Angle of Attach

d. Angle of Yaw

e. Pitch Rate

f. Yaw Rate

g. Roll Rate

h. Roll Angle

i. C. G. Vertical g

j. Tail Vertical g

k. Nose Vertical g

l. Strain Gage (Upper) 334 Left

m. Strain Gage (Lower) 334 Left

n. Strain Gage (Upper) 334 Right

o. Strain Gage (Lower) 334 Right

p. Strain Gage (Upper) 362 Left

q. Strain Gage (Lower) 362 Left

r. Strain Gage (Upper) 362 Right

s. Strain Gage (Lower) 362 Right

t. Strain Gage (Upper) 390 Left

u. Strain Gage (Lower) 390 Left

v. Strain Gage (Upper) 390 Right

w. Strain Gage (Lower) 390 Right

SECRET

x. Vertical Accel Right Wing Tip, Front Spar

x. Vertical Accel Left Wing Tip, Front Spar

aa. Vertical Accel Fuselage C. G.

bb. Vertical Accel Near Nose

cc. Vertical Accel Near Aft End

dd. Lateral Accel Fuselage C. G.

ee. Lateral Accel Fuselage Nose

ff. Lateral Accel Fuselage Aft

gg. Lateral Accel Vertical Stabilizer, Front Spar, Tip

hh. Longitudinal Accel Fuselage C. G.

ii. Pressure Transducer (Overpressure) Left Side Fuselage Forward

jj. Pressure Transducer (Overpressure) Left Side Fuselage Mid

kk. Pressure Transducer (Overpressure) Left Side Fuselage Vertical Fin

ll. Calorimeter

mm. Radiometer

SECRET

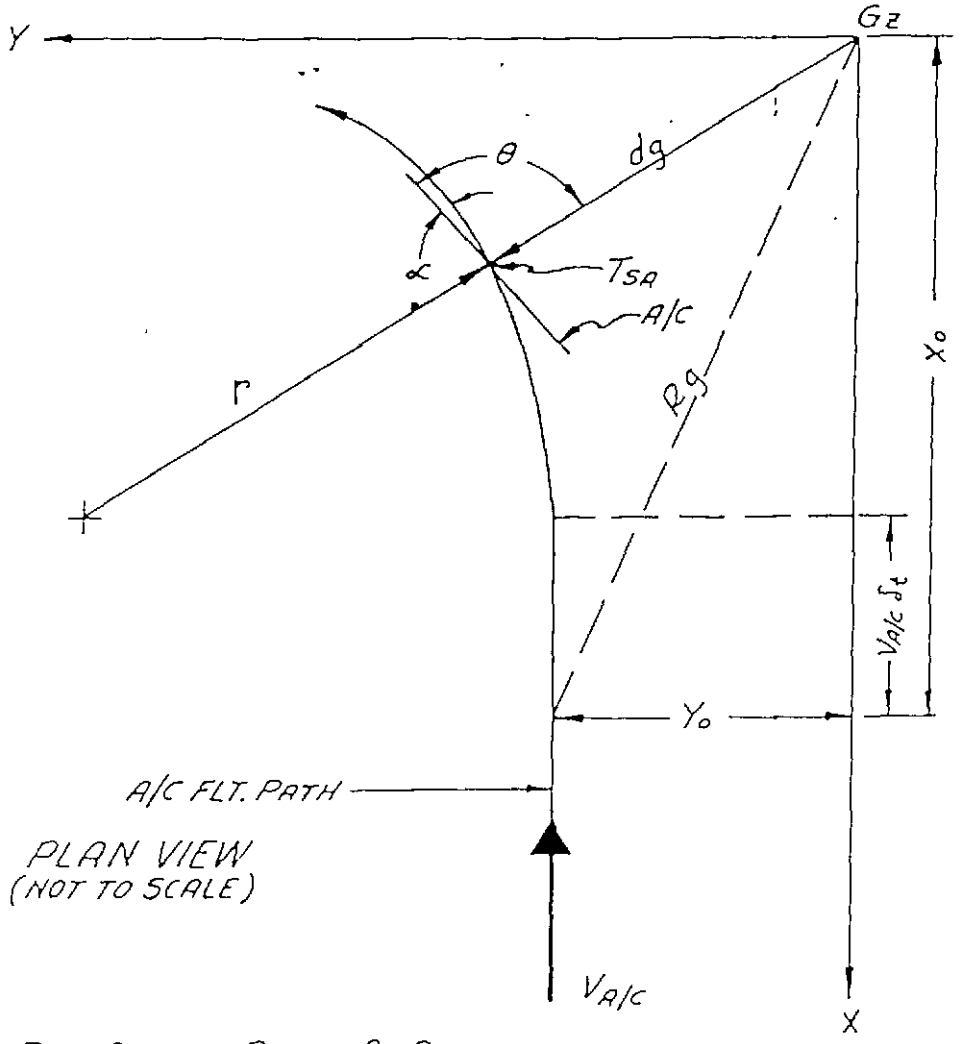

WHERE: R_g = GROUND RANGE AT DETONATION
$V_{A/C}$ = AIRCRAFT VELOCITY
δt = REACTION TIME, 3 SECONDS
θ = SHOCK IMPINGEMENT
r = TURN RADIUS
α = ANGLE OF ATTACK
Gz = GROUND ZERO
T_{SA} = TIME OF SHOCK ARRIVAL [redacted]
X_o = HORIZONTAL RANGE AT T_o
Y_o = OFFSET DISTANCE AT T_o
d_g = GROUND RANGE AT T_{SA}

Figure 2.1 Flight path geometry.

SECRET

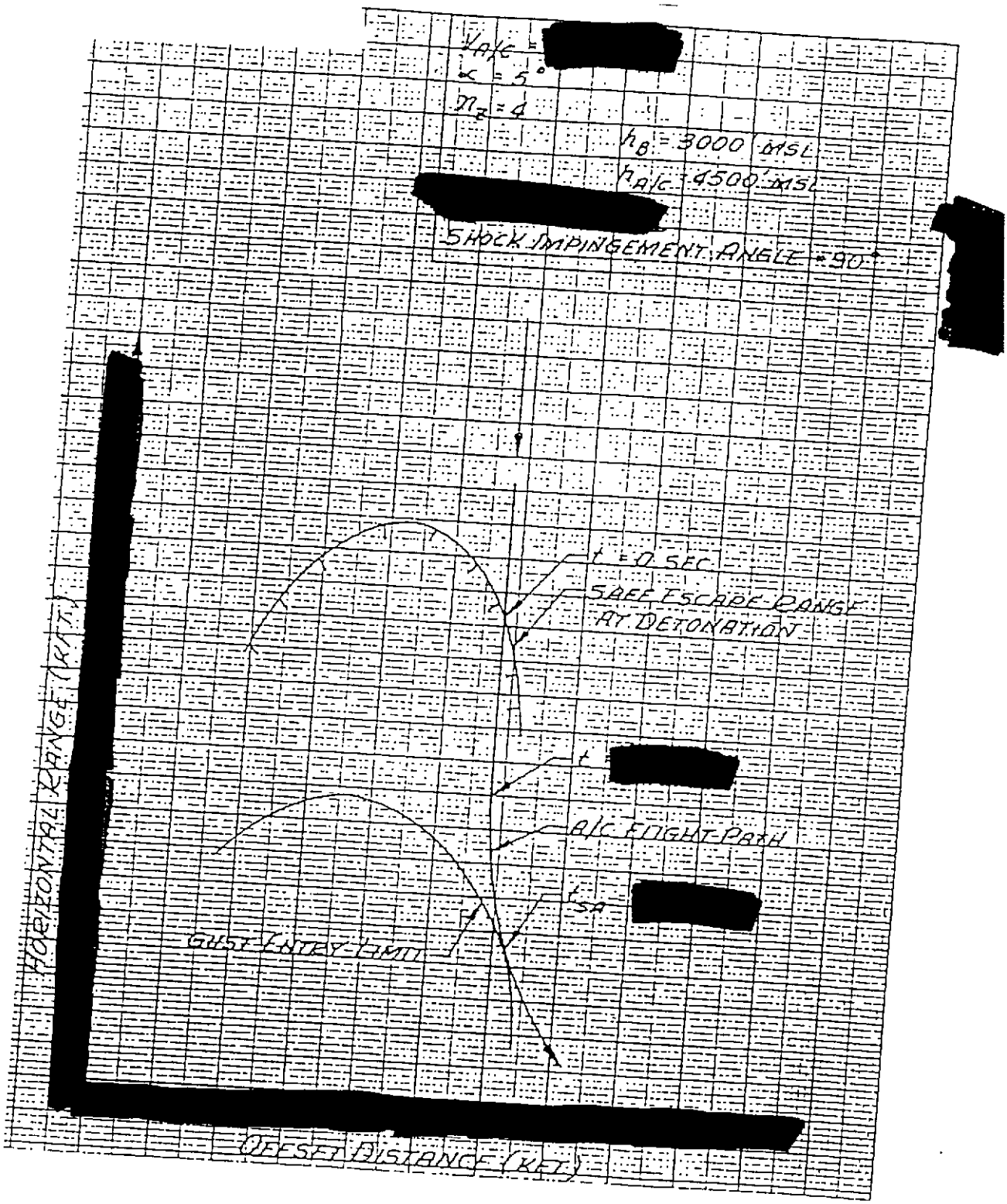

Figure 2.2 Limit aircraft positions.

SECRET

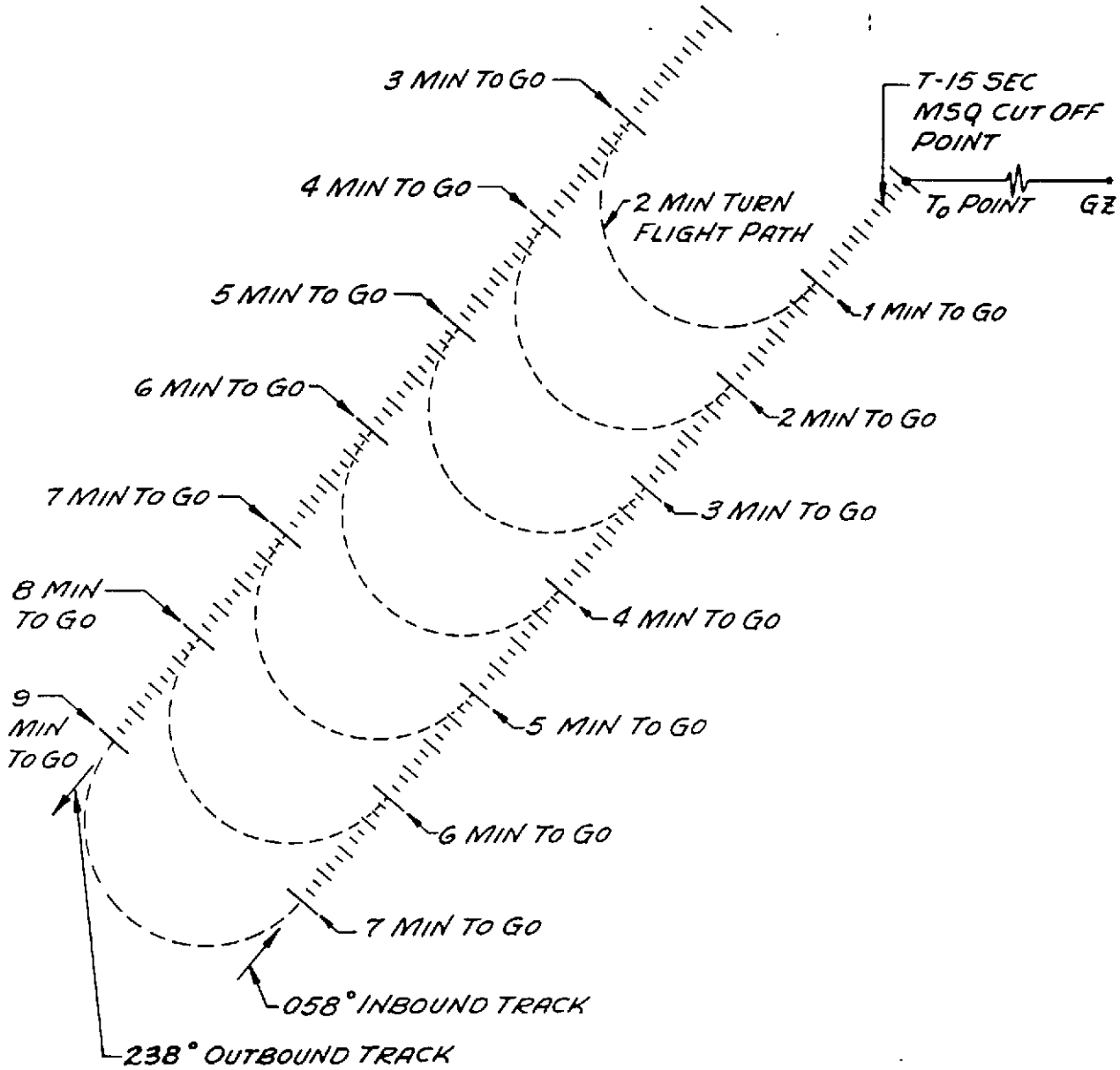

Figure 2.3 Flight pattern.

SECRET

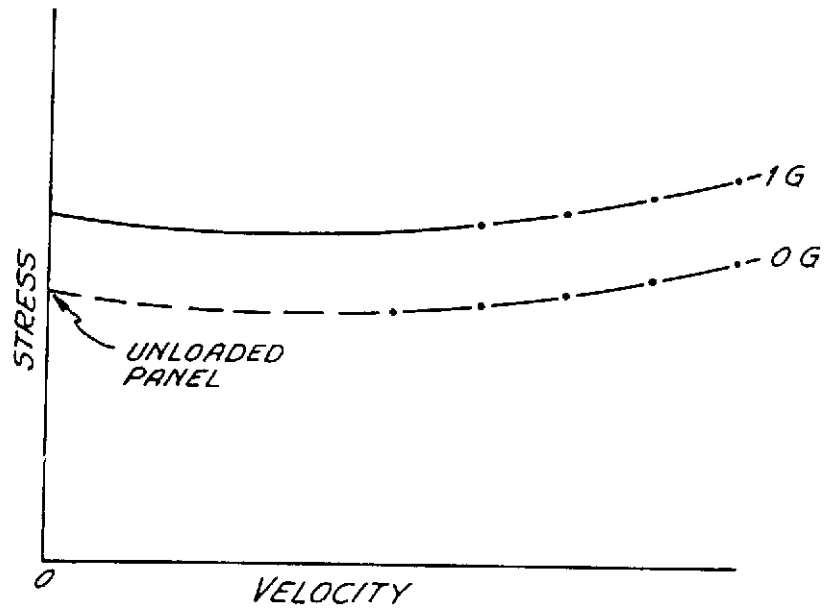

Figure 2.4 Strain gage calibration.

~~SECRET~~

CHAPTER 3

RESULTS

3.1 AIRCRAFT POSITION

As a result of accurate ground radar equipment and continuous practice, the radar controller was able to position the aircraft within the stringent requirements necessary to obtain meaningful data. At T minus 15 seconds the aircraft was [redacted] behind the pre-programmed position and [redacted] to the left of the desired flight path. (Ground radar was shut off 15 seconds prior to detonation so as not to interfere with other projects near ground zero). The aircraft position at time of detonation was determined by using flight parameter readouts from instruments installed in the aircraft.

TABLE 3.1 AIRCRAFT POSITION AT DETONATION

	Pre-Programmed Position	Test Day Position
Offset Distance	[redacted]	[redacted]
Horizontal Range	[redacted]	[redacted]
Ground Range	[redacted]	[redacted]
Slant Range	[redacted]	[redacted]

The aircraft position at time of shock arrival was also determined by use of instrument readouts, and verified by the time elapsed until shock arrival.

SECRET

TABLE 3.2 AIRCRAFT POSITION AT TIME OF SHOCK ARRIVAL

	Pre-Programmed Position	Test Day Position
Offset Distance	[redacted]	[redacted]
Horizontal Range	[redacted]	[redacted]
Ground Range	[redacted]	[redacted]
Slant Range	[redacted]	[redacted]
Impingement angle	[redacted]	[redacted]
Time of Shock Arrival	[redacted]	[redacted]

The increasing error between actual and desired position was due to: (1) initial aircraft velocity error, (2) being established in the 4-g turn too early, (3) initial positioning errors, and (4) decreasing airspeed in the breakaway turn.

A plan view of the desired and actual final phase of the flight path is shown in Figure 3.1.

3.2 AIRCRAFT DAMAGE

A thorough check of the aircraft was accomplished at Indian Springs AFB after the test. No aircraft damage was discovered. A second check was made at Majors Field, Texas during the reconfiguration phase and this too showed no damage.

3.3 DATA PRESENTATION

Reduced data obtained during the test are presented in Table 3.3 and Figures 3.2 through 3.31. The data is discussed in Chapter 4. In presenting the data, time zero (T−0) is chosen

SECRET

as the time at weapon detonation. Thus, for example, an elapsed time of 3 seconds means 3 seconds after weapon detonation. For the most part, the data are presented in two types of time histories: (1) A time history covering the period from just previous to shock-wave impingement to approximately 1 second after shock-wave impingement; and (2) A time history covering the period from 1 second previous to weapon detonation to 3 seconds after shock-wave impingement, excluding the time period covered in (1).

In evaluating the accelerometer data, cognizance of a significant fact is important. Previous to the actual test, instrumentation checkout flights had revealed the presence of a considerable amount of high-frequency noise in the accelerometer traces, particularly under high g maneuvers. Apparently a wingtip buffet condition was the primary cause. It was felt that in order to obtain meaningful accelerometer data in the actual test, installation of filters in the accelerometer circuits was mandatory. Accordingly, this was done, with the result that the high-frequency components in the accelerometer traces are sharply attenuated. The filters cause negligible attenuation in the low-frequency range, however. Consequently, when evaluating the accelerometer data it must be realized that the values shown are not strictly valid in regions where high-frequency components predominate. As will be seen however, the high-frequency components contribute very little to the stress levels experienced by aircraft primary structure. It is at the low frequencies associated with the fundamental modes that maximum stresses occur.

SECRET

In reducing the accelerometer data subsequent to shock-wave impingement the time increment used for plotting purposes was usually 0.005 seconds. Thus, the reduced data differs from the oscillograph traces in some areas, in that some of the very high frequency components have been manually filtered out. This is considered unimportant however, for the same reason as given above.

SECRET

TABLE 3.3 NUCLEAR RADIATION

Badge No.	Location	Facing	Reading (Rem)
1	Pilot Top Dash Center	Upward	.100
2	Pilot Right Side Below Console	Left Side	.085
3	Pilot Top Left Seat	Upward	.100
4	Pilot Top Right Seat	Upward	.140
5	Center Rail Front Left Side	Forward	.073
6	Center Rail Front Right Side	Forward	.120
7	Observer Left Console	Upward	.073
8	Observer Right Console	Upward	.098
9	Observer Top Left Side	Upward	.110
10	Observer Top Right Side	Upward	.140

SECRET

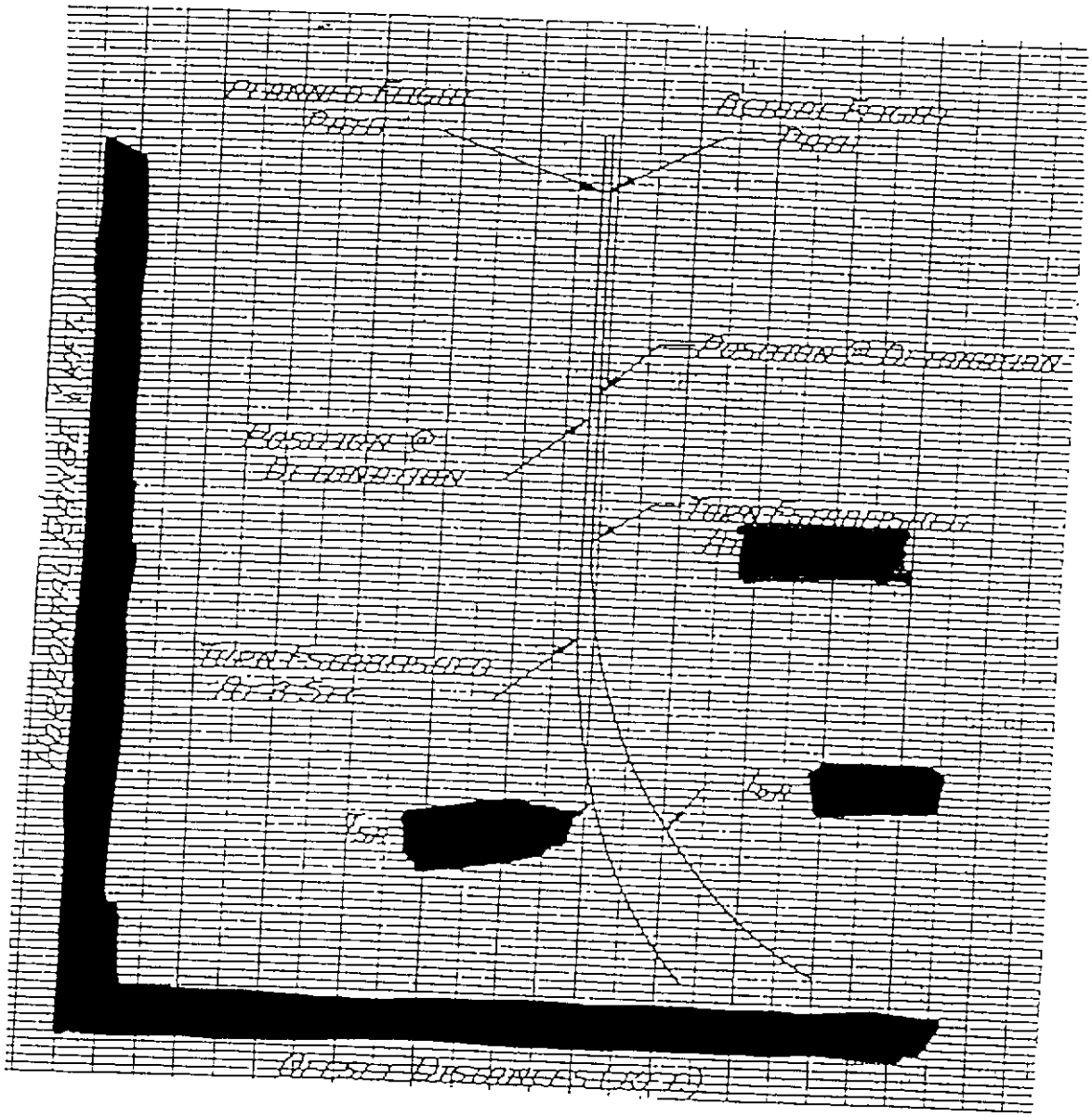

Figure 3.1 Aircraft flight path.

SECRET

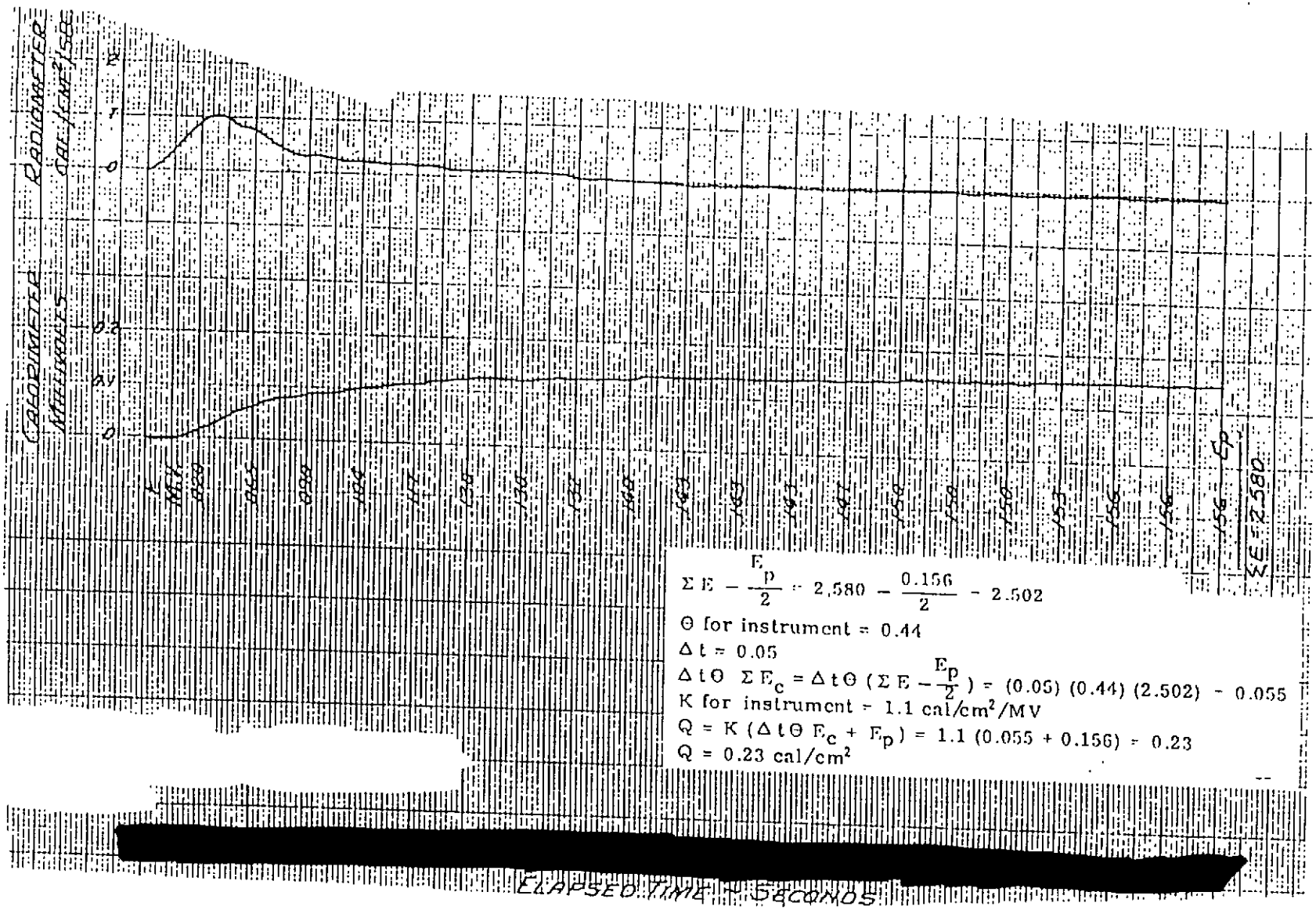

$$\Sigma E - \frac{E_p}{2} = 2.580 - \frac{0.156}{2} = 2.502$$

Θ for instrument = 0.44

$\Delta t = 0.05$

$$\Delta t \Theta \ \Sigma E_c = \Delta t \Theta \left(\Sigma E - \frac{E_p}{2}\right) = (0.05)(0.44)(2.502) = 0.055$$

K for instrument = 1.1 cal/cm²/MV

$$Q = K(\Delta t \Theta E_c + E_p) = 1.1\,(0.055 + 0.156) = 0.23$$

$Q = 0.23$ cal/cm²

Figure 3.2 Thermal radiation.

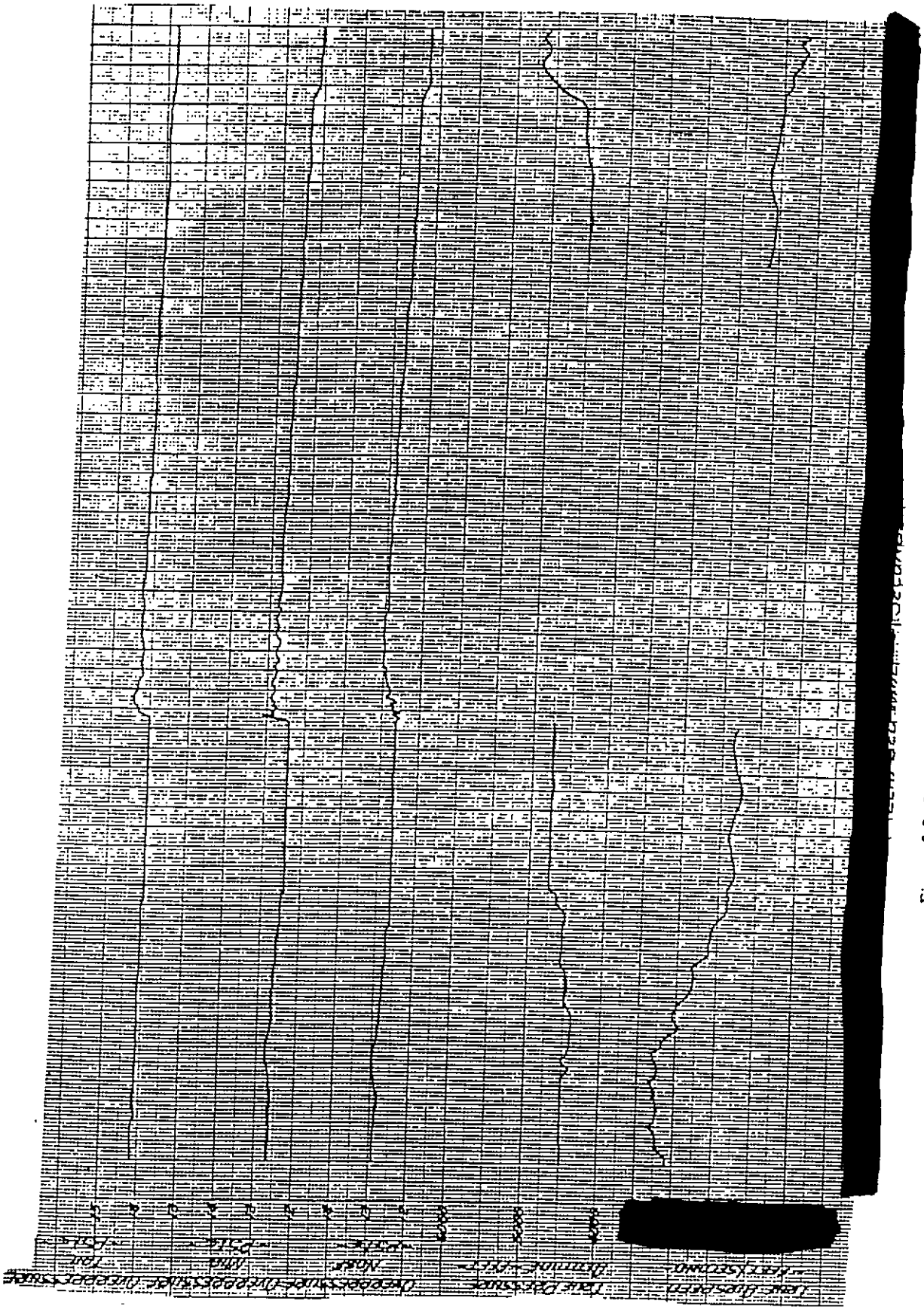

Figure 3.3 Overpressure and rigid-body time histories.

SECRET

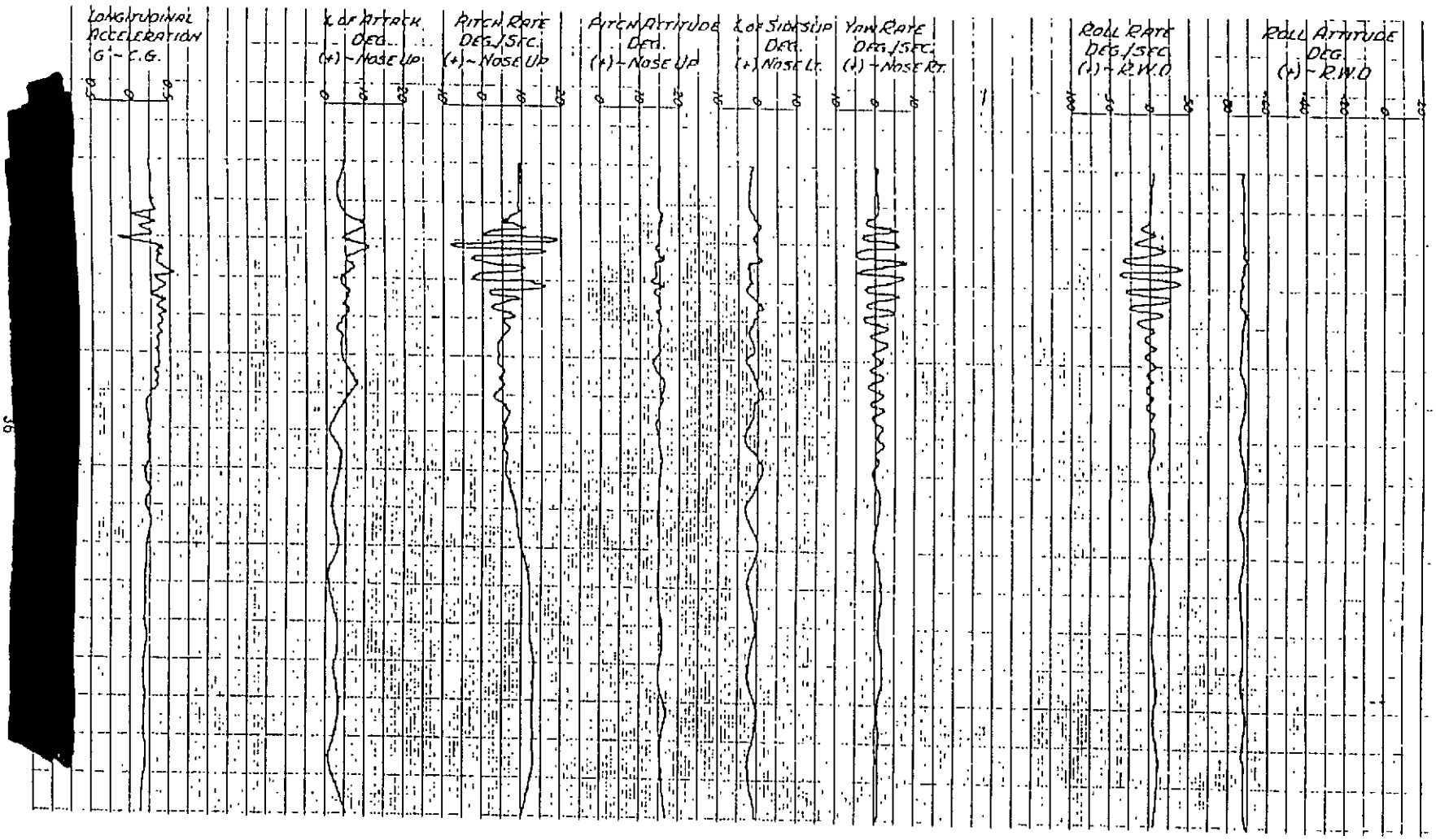

Figure 3.4 Rigid-body time histories, elapsed t[redacted]

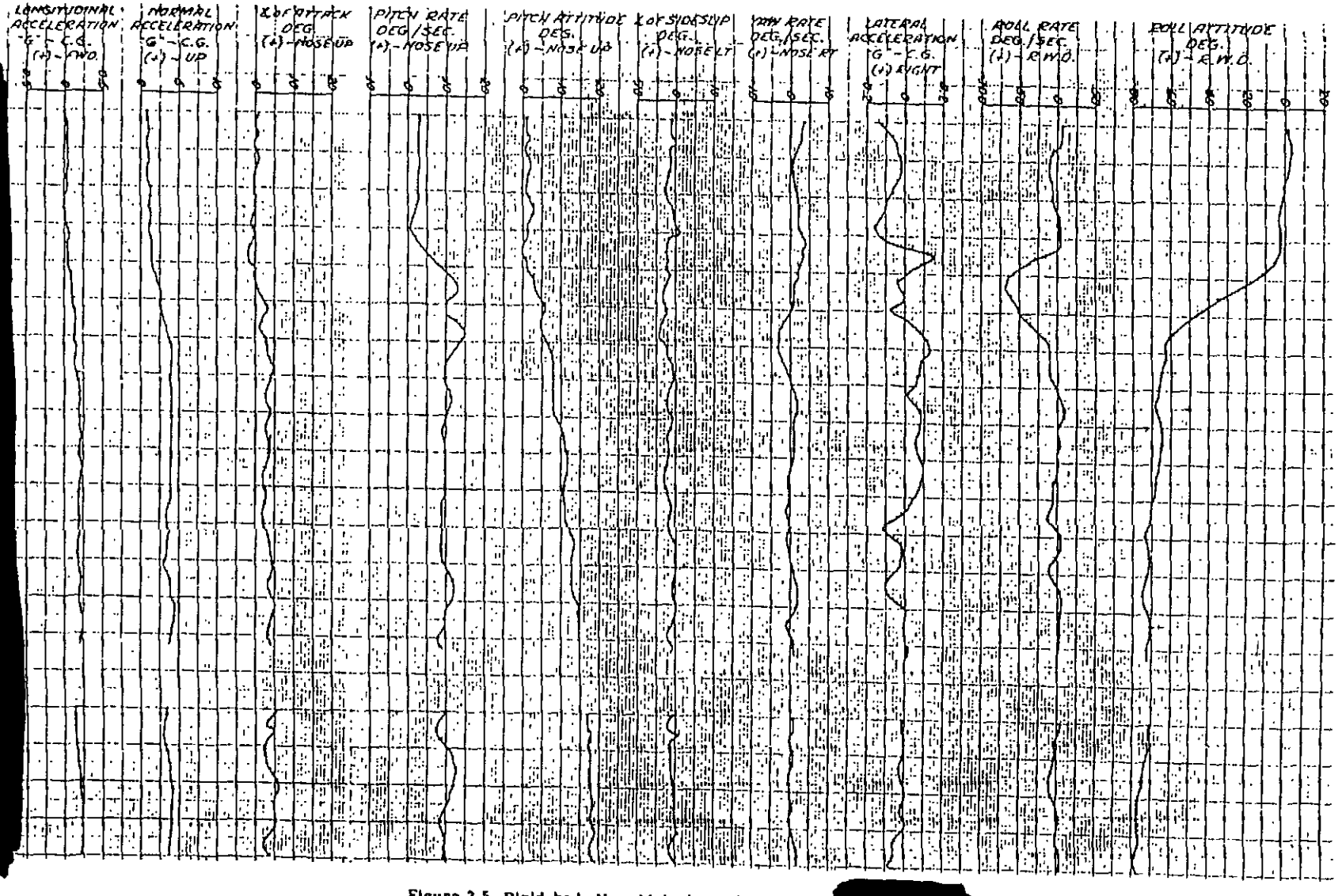

Figure 3.5 Rigid-body time histories, elapsed time [redacted]

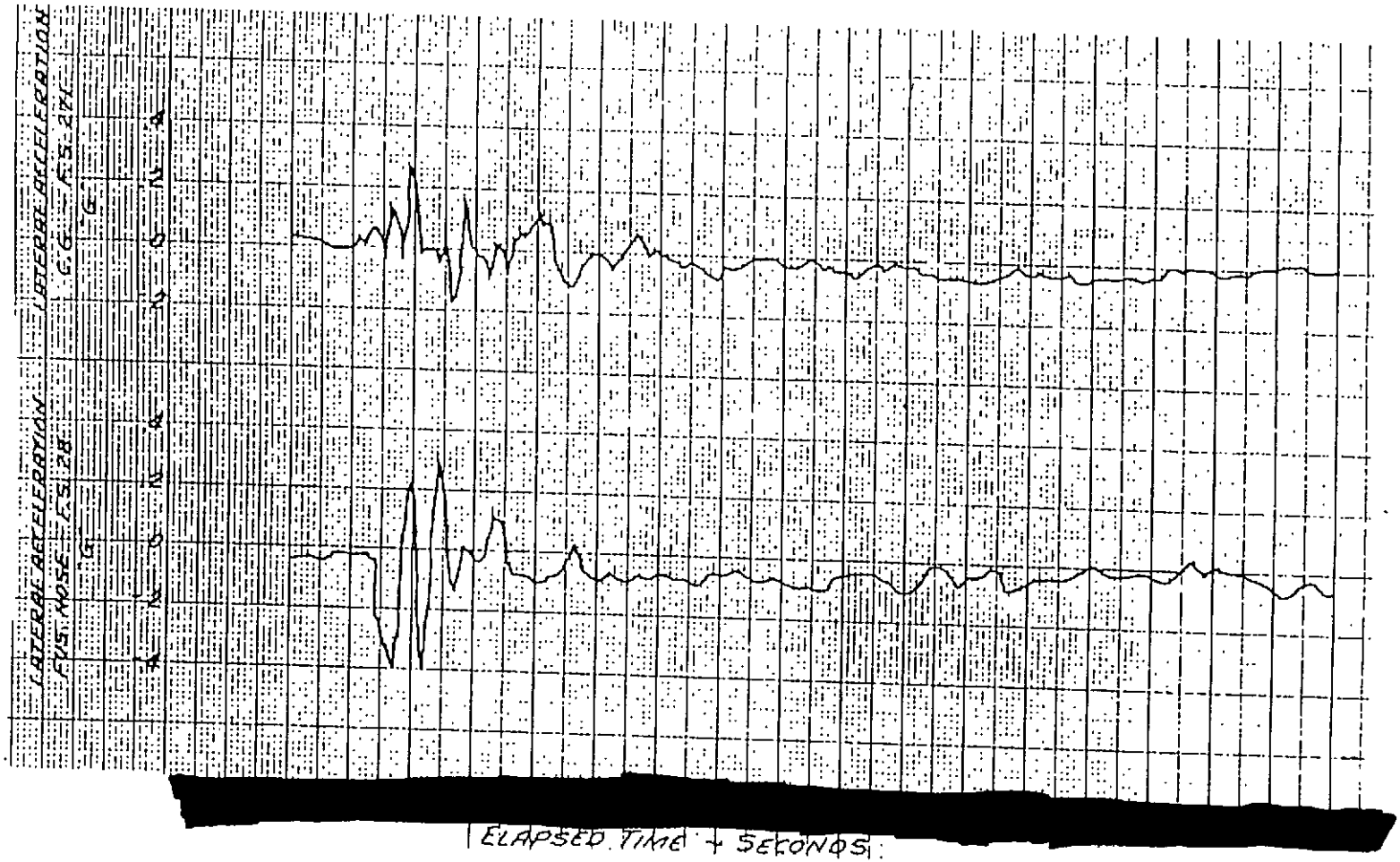

Figure 3.6 Lateral acceleration time histories, fuselage nose (FS 28) and center of gravity (FS 271).

SECRET

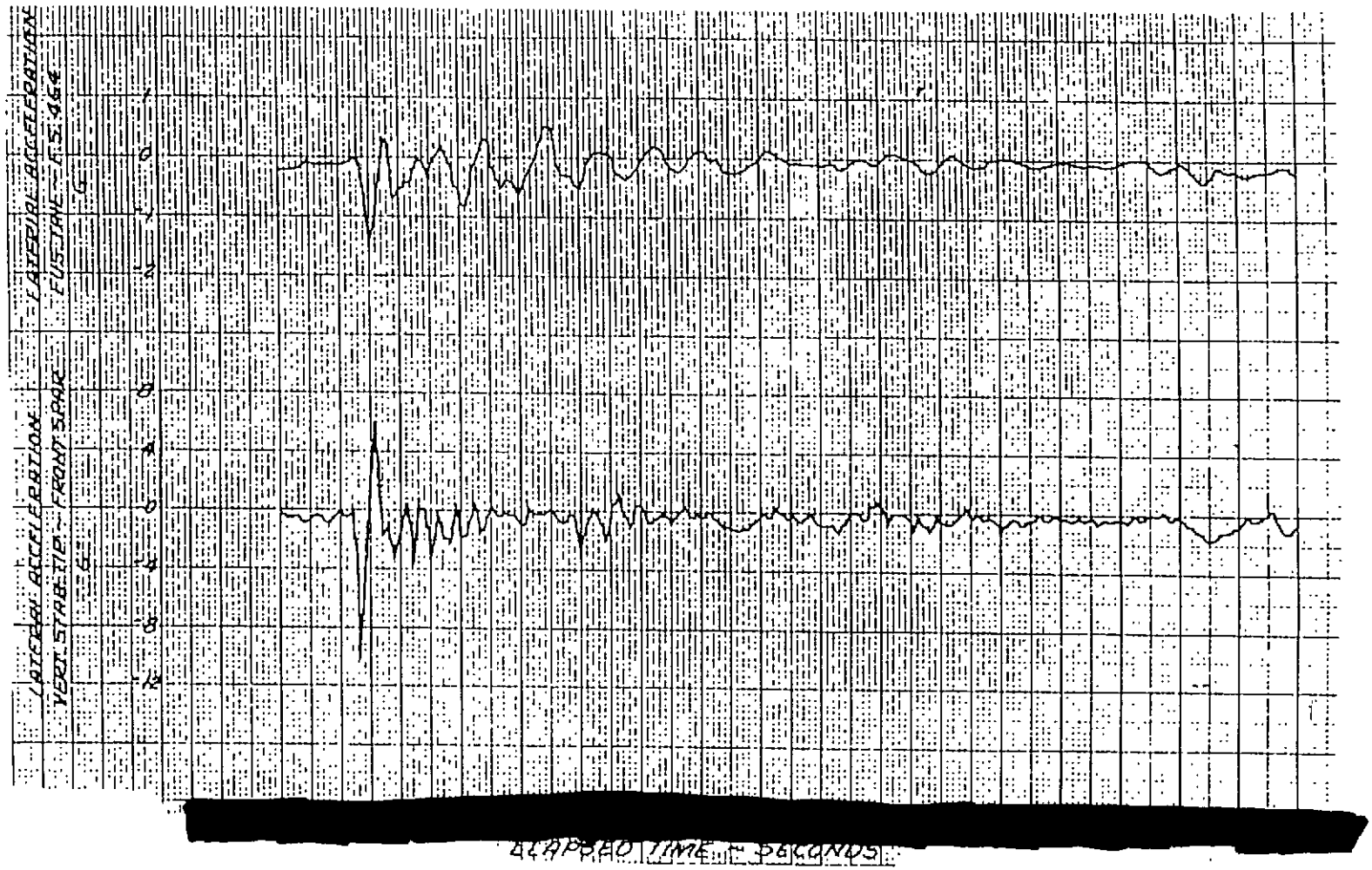

Figure 3.7 Lateral acceleration time histories, vertical stabilizer tip (front spar) and fuselage tail (FS 464).

SECRET

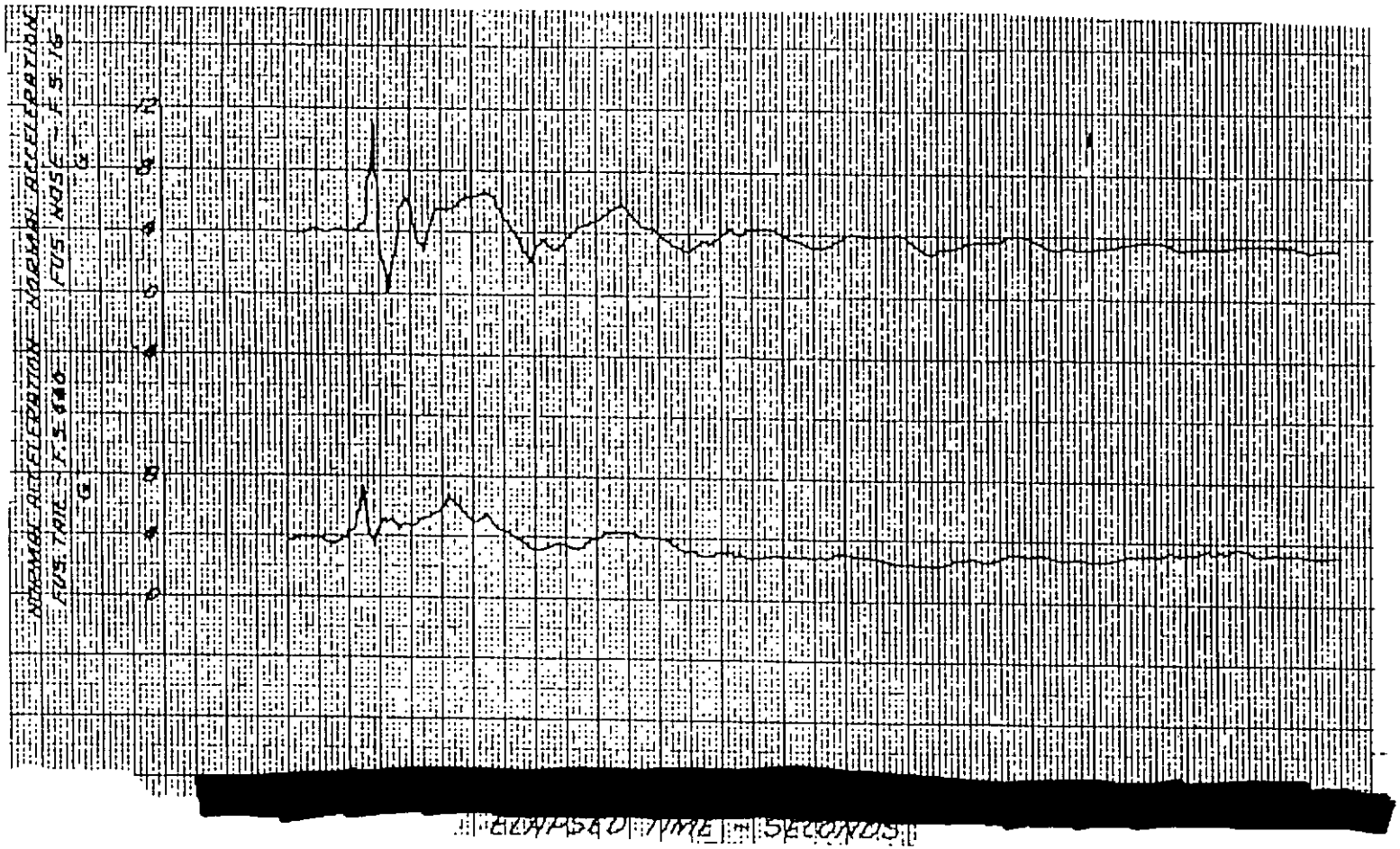

Figure 3.8 Normal acceleration time histories, fuselage tail (FS 440) and fuselage nose (FS 16).

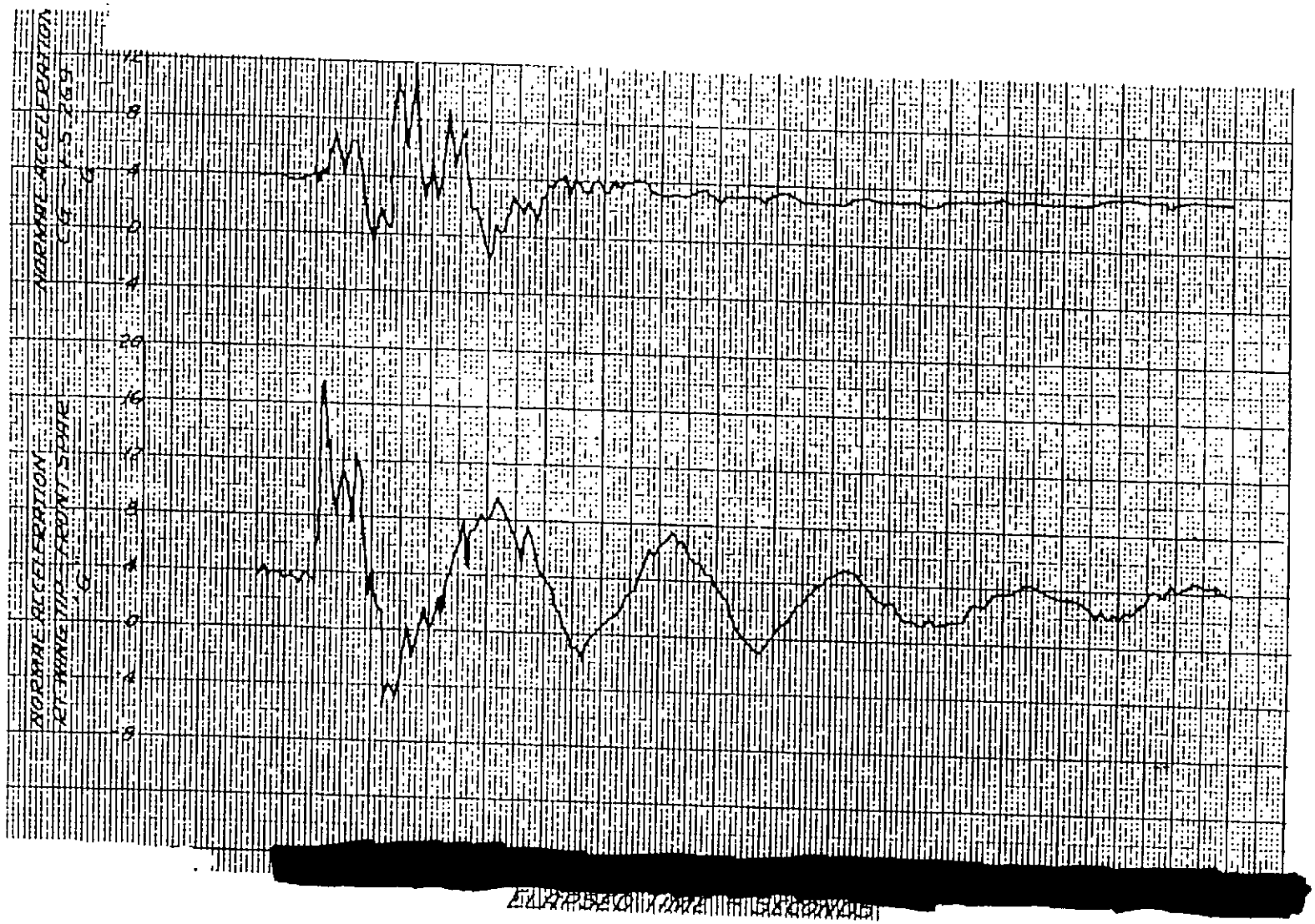

Figure 3.9 Normal acceleration time histories, right wingtip (front spar) and center of gravity (FS 269).

SECRET

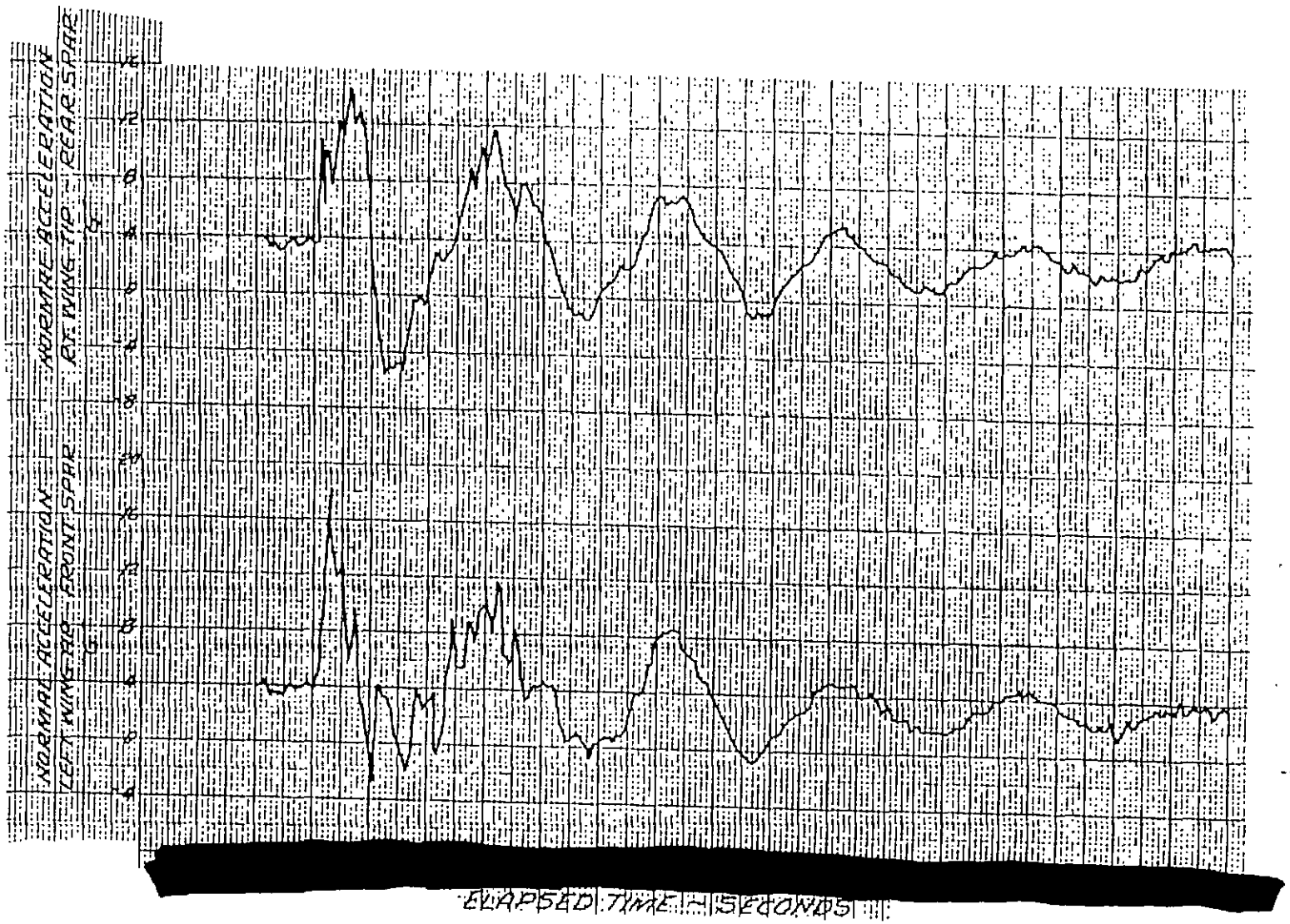

Figure 3.10 Normal acceleration time histories, left wingtip (front spar) and right wingtip (rear spar).

STRAIN GAGE CHANNEL Nº (OSCILLOGRAPH)	STRAIN GAGE LOCATION		STRAIN GAGE Nº
	POSITION	FUS. STA.	
4	UP. LEFT	337	1
5	LOW. LEFT	385	6
6	UP. RIGHT	337	7
7	UP. RIGHT	385	11
8	LOW. RIGHT	360	12
9	LOW. LEFT	360	4
10	UP. RIGHT	360	9
11	LOW. RIGHT	360	10
12 (NO DATA)	UP. LEFT	385	5
13	LOW. LEFT	337	2
14 (NO DATA)	LOW. RIGHT	337	8
15	UP. LEFT	360	3

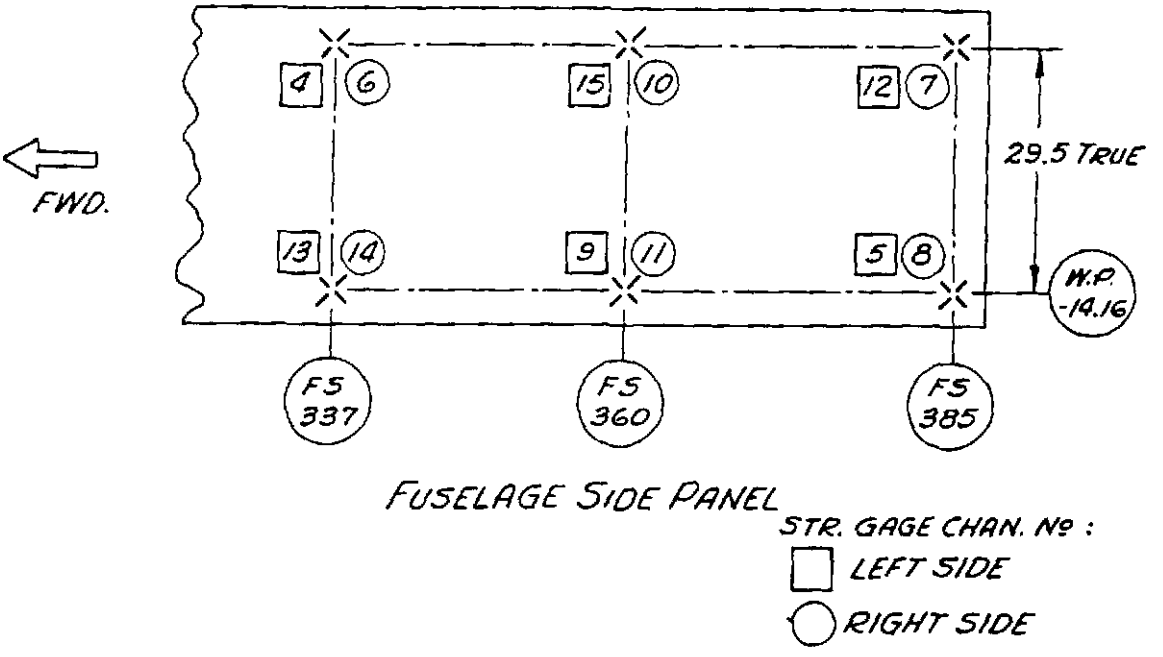

Figure 3.11 Strain gage locations.

SECRET

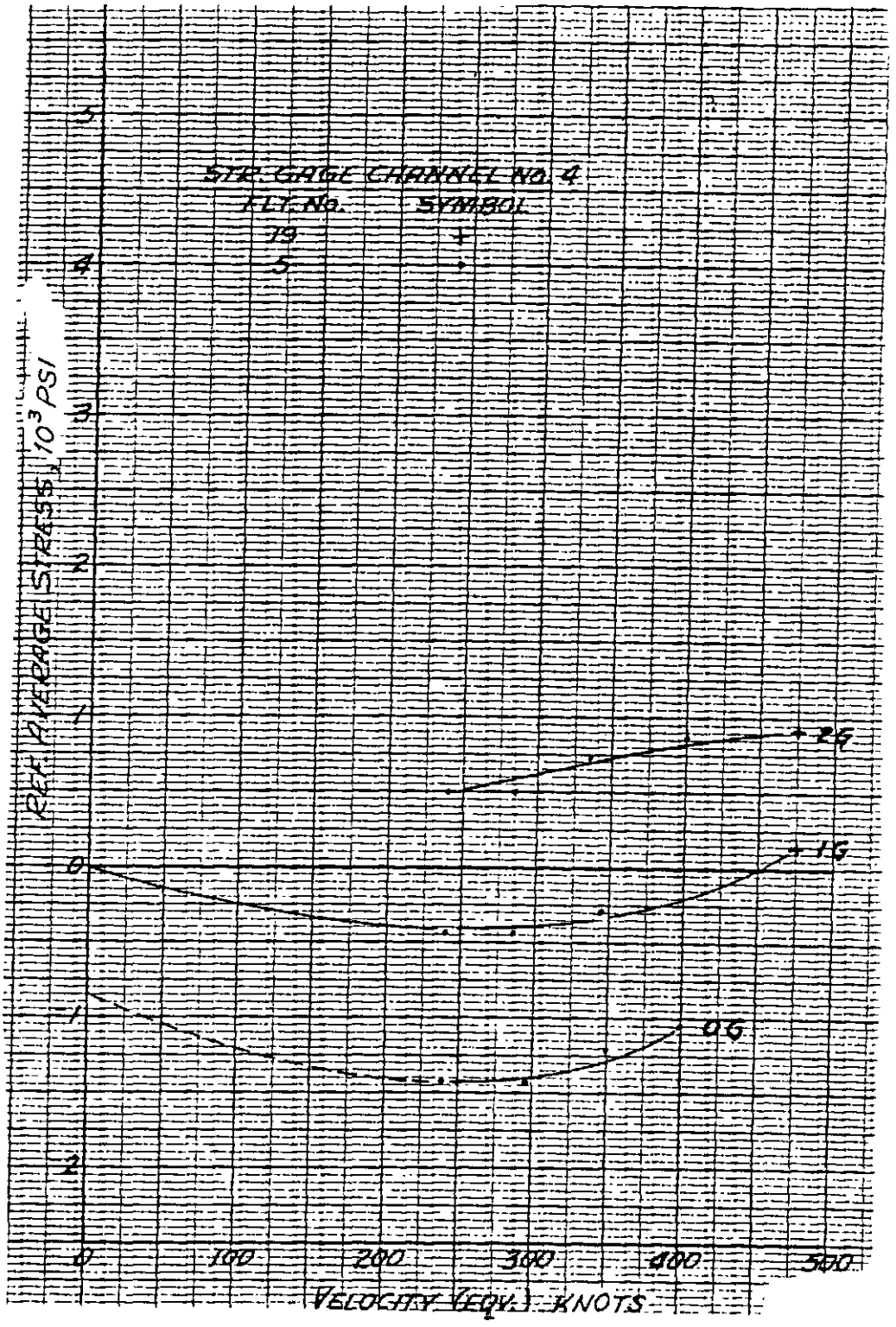

Figure 3.12 Zero stress determination, strain gage Channel 4.

SECRET

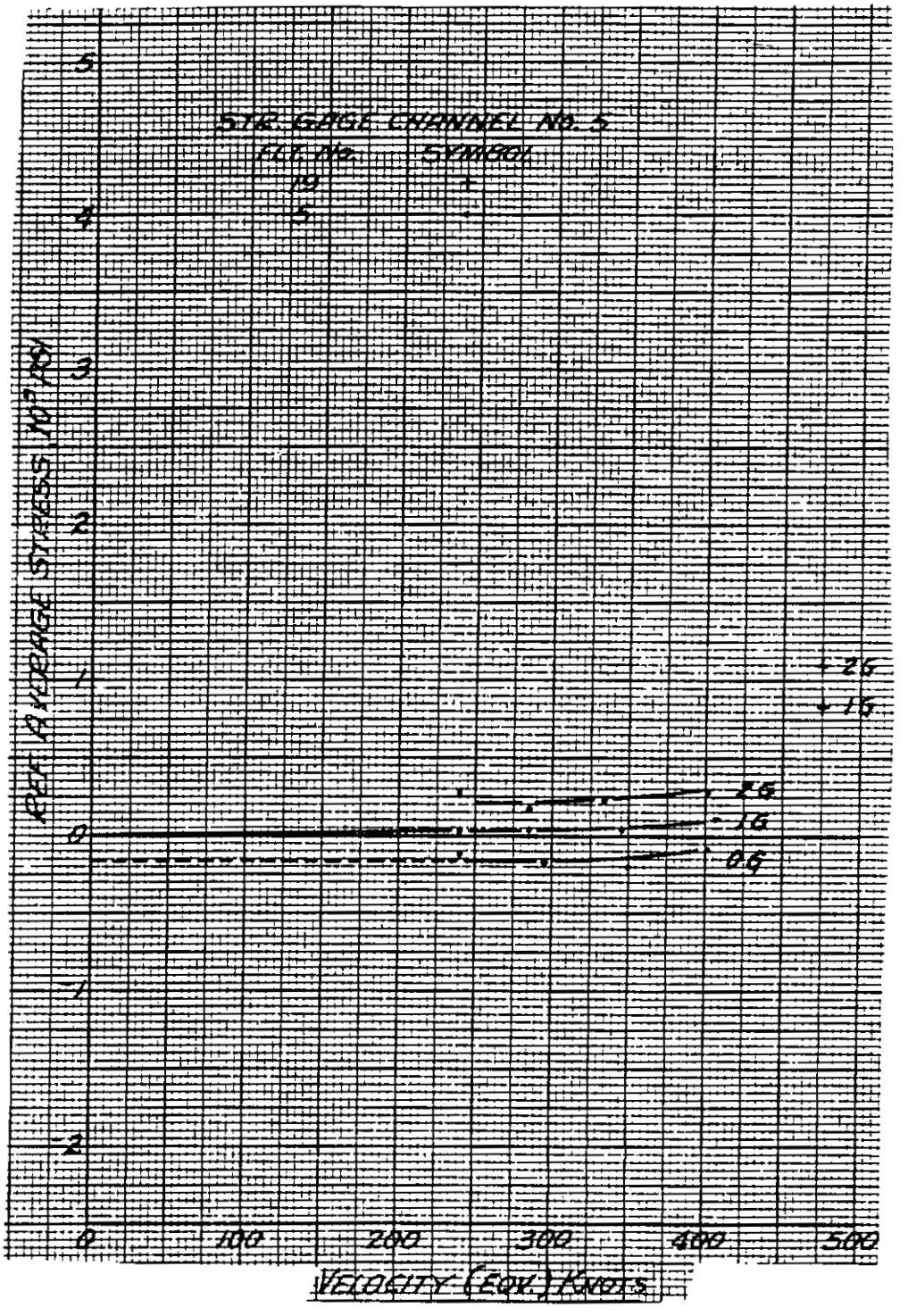

Figure 3.13 Zero stress determination, strain gage Channel 5.

SECRET

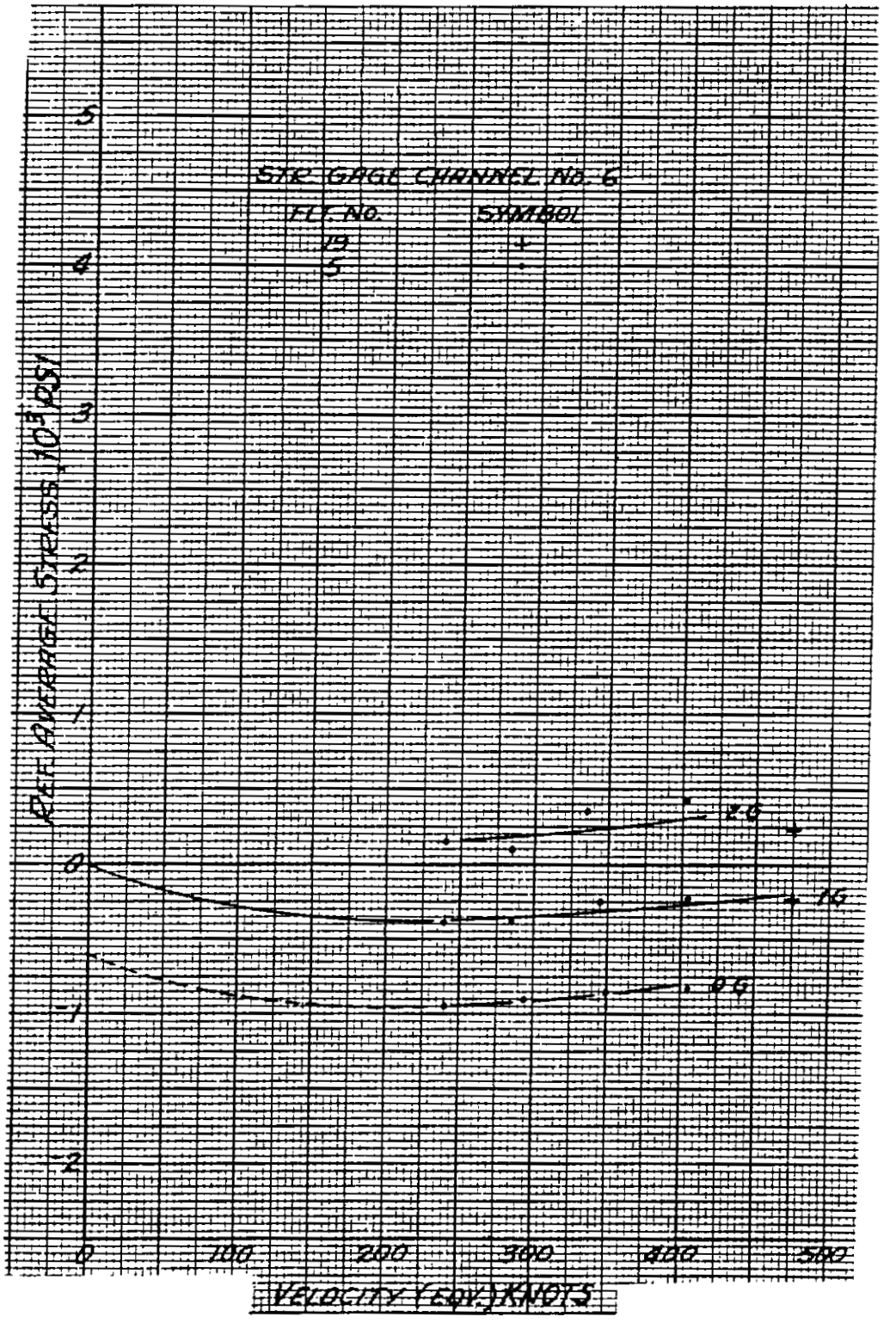

Figure 3.14 Zero stress determination, strain gage Channel 6.

SECRET

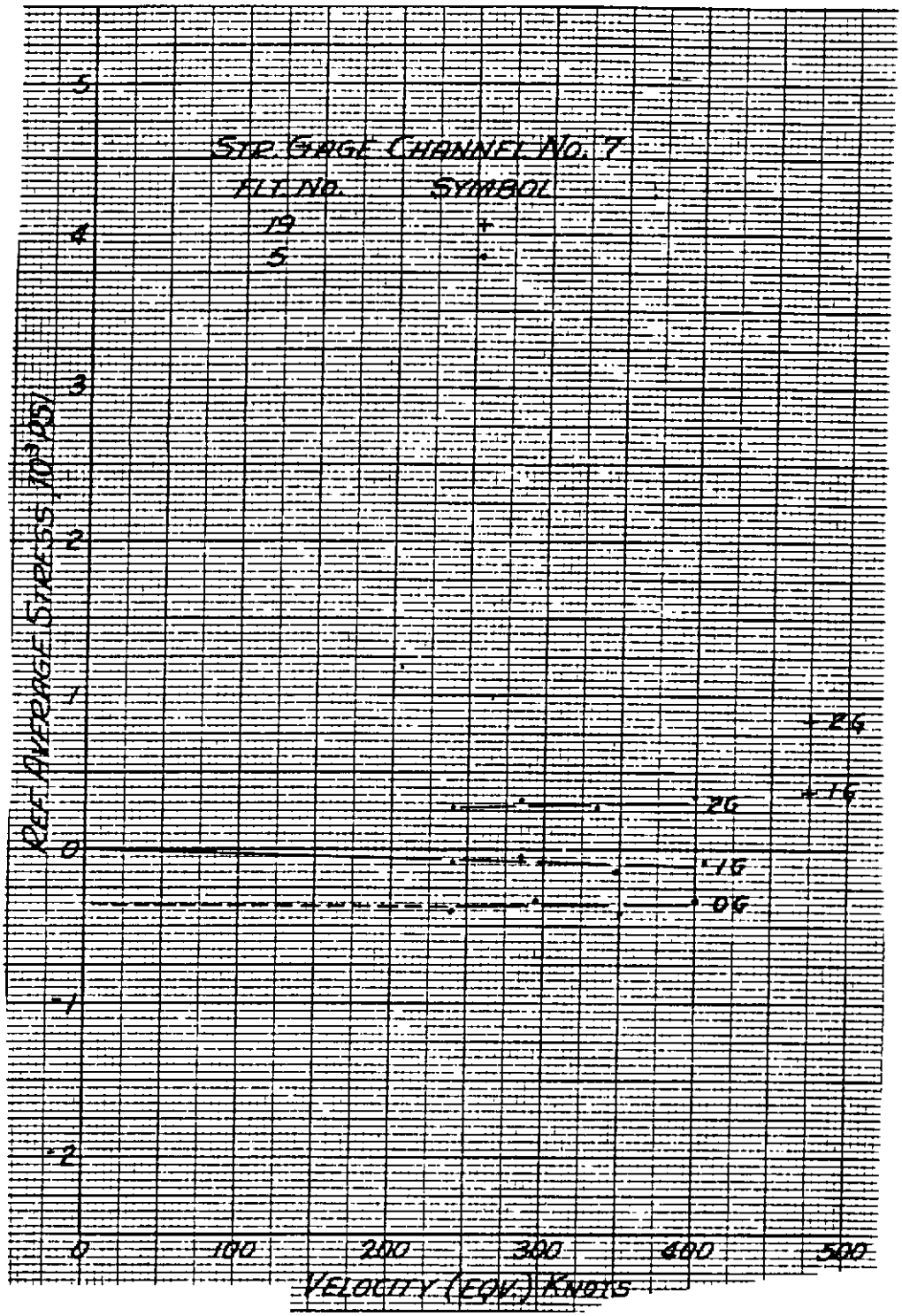

Figure 3.15 Zero stress determination, strain gage Channel 7.

SECRET

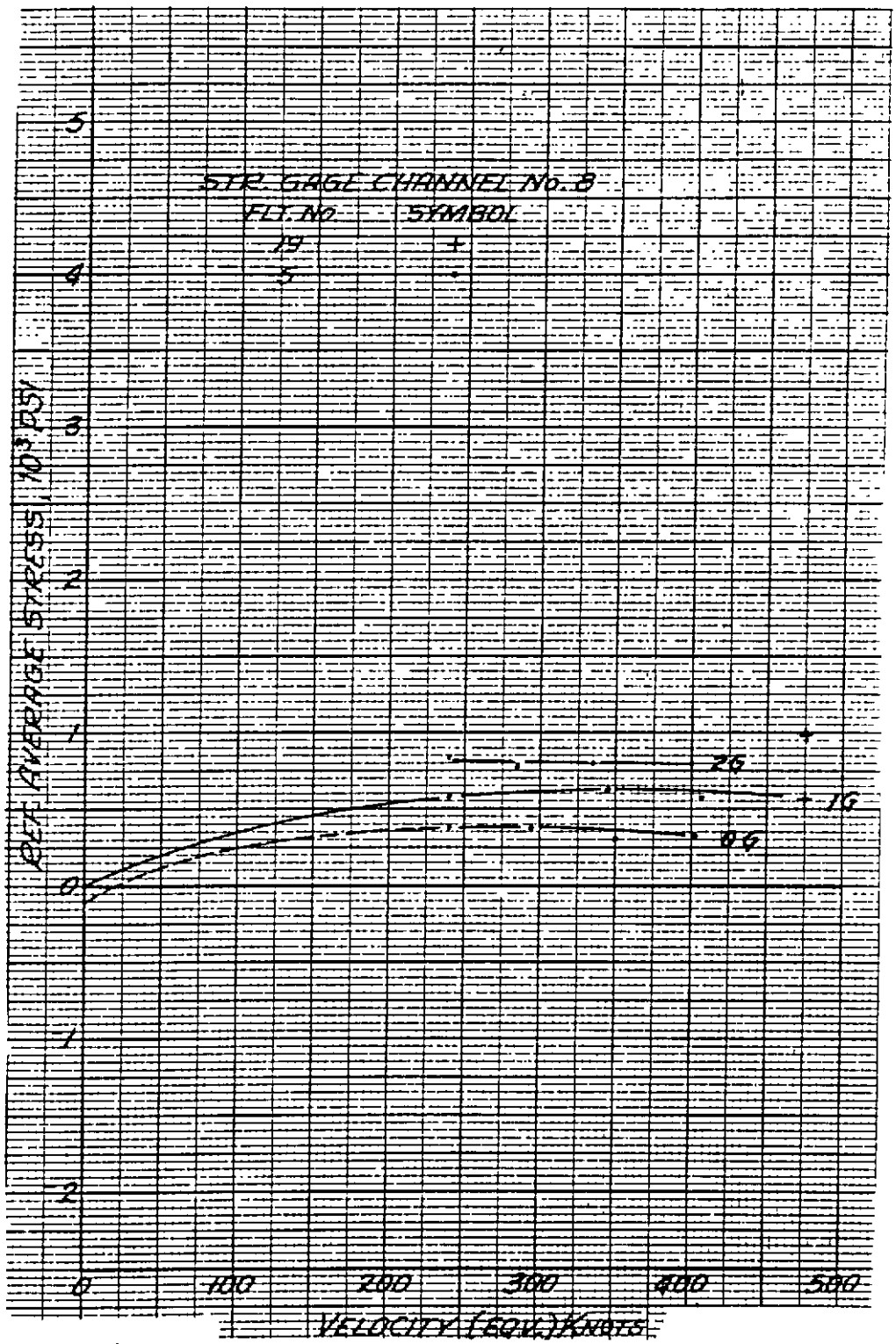

Figure 3.16 Zero stress determination, strain gage Channel 8.

SECRET

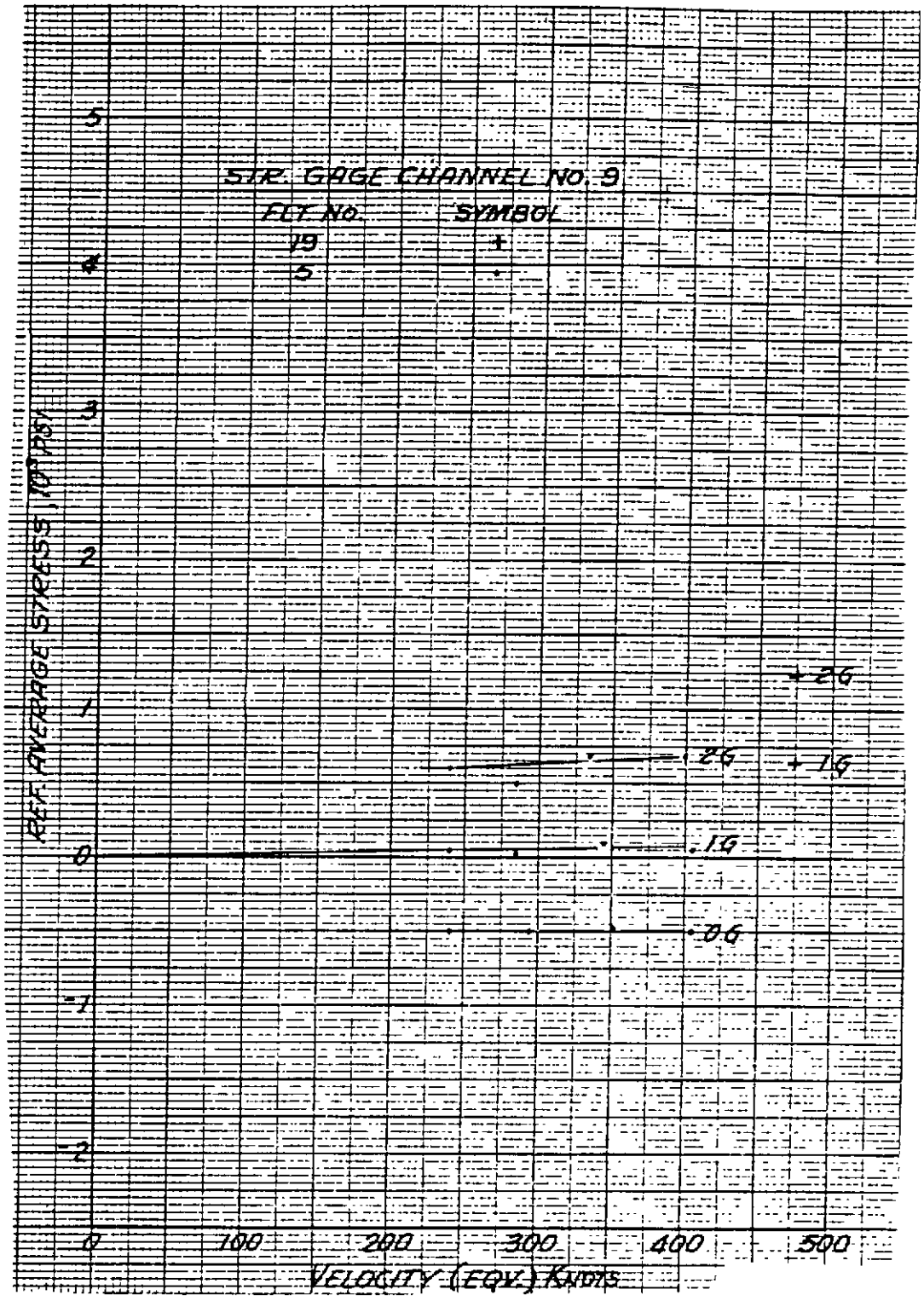

Figure 3.17 Zero stress determination, strain gage Channel 9.

SECRET

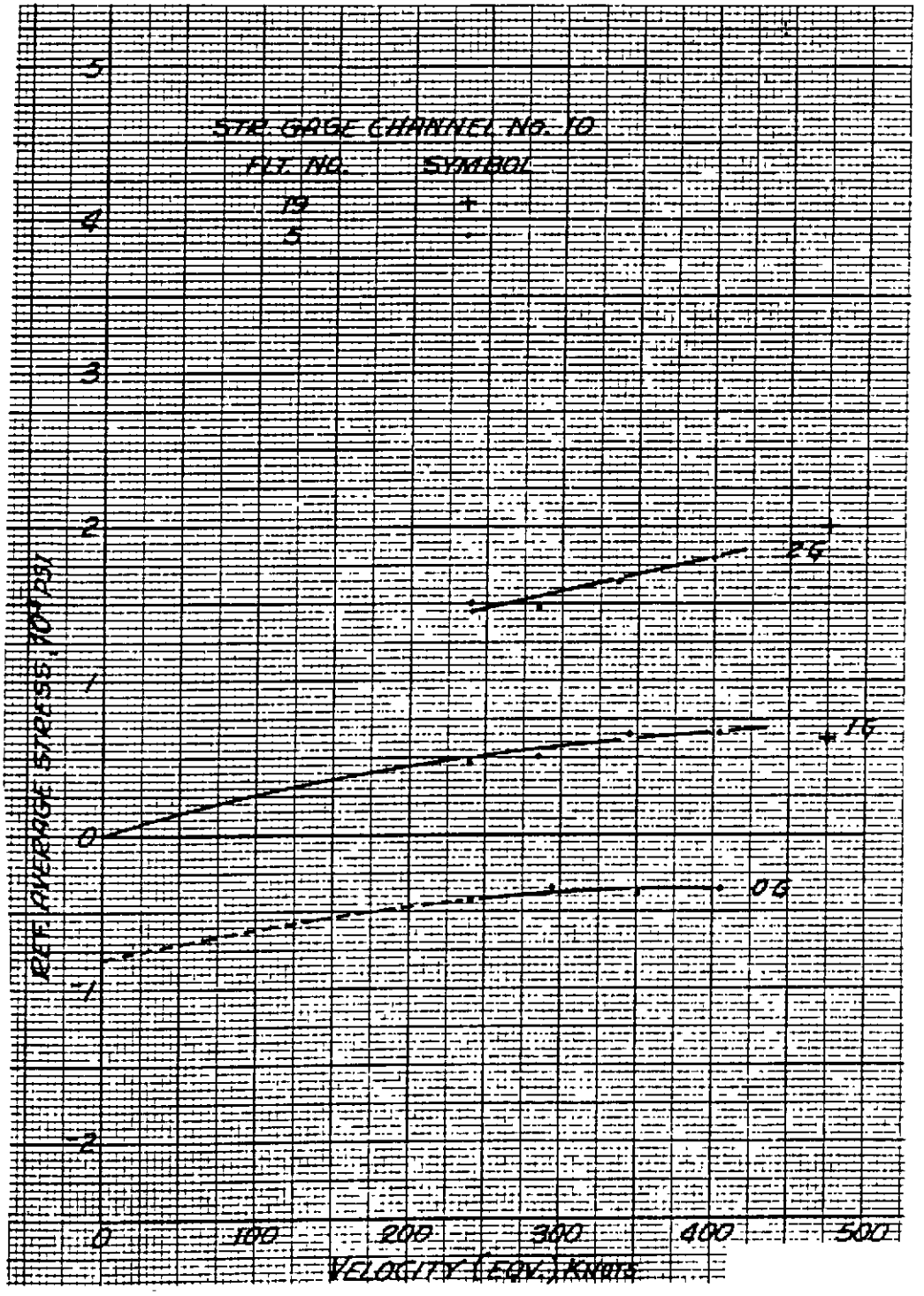

Figure 3.18 Zero stress determination, strain gage Channel 10.

SECRET

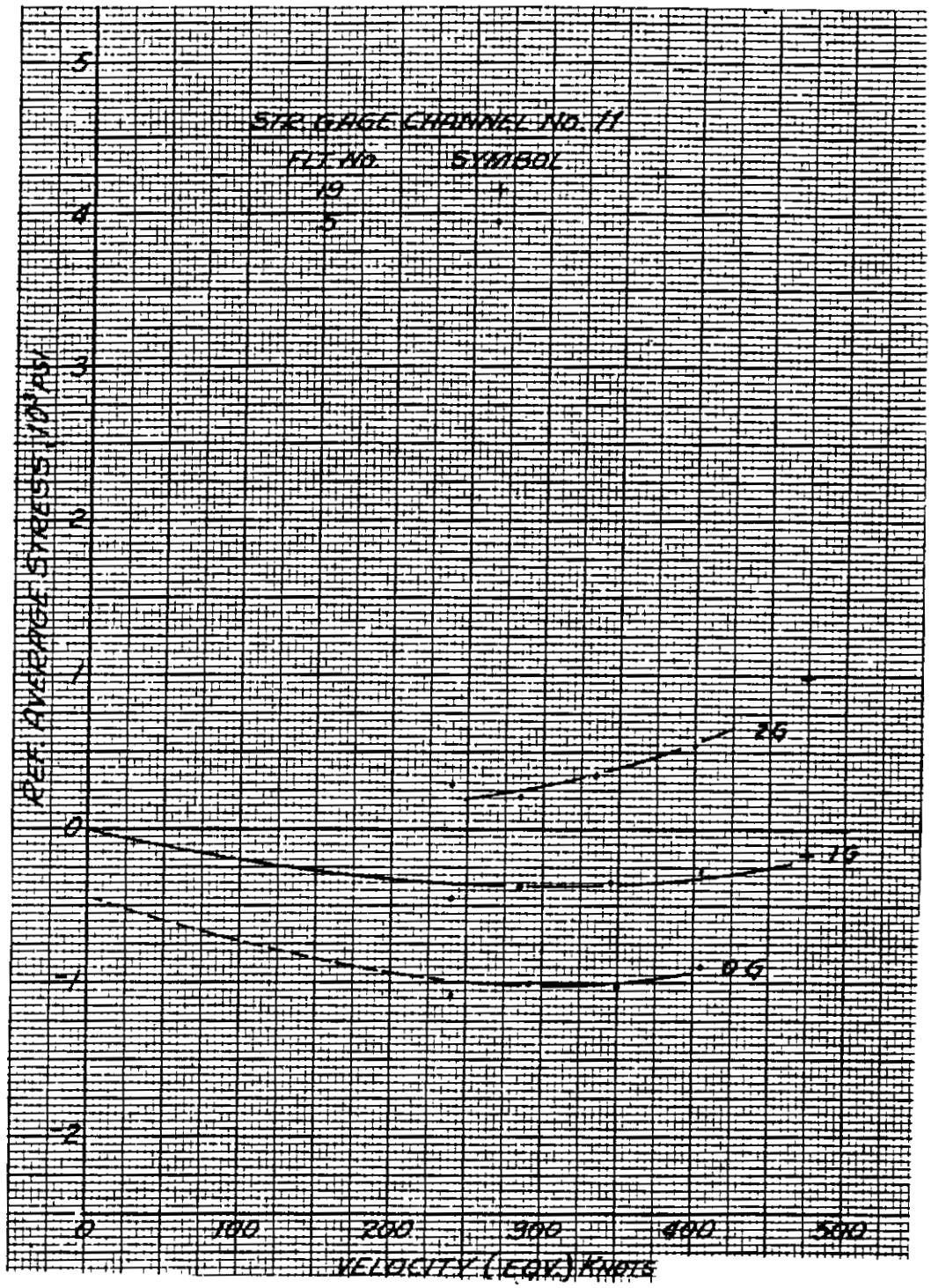

Figure 3.19 Zero stress determination, strain gage Channel 11.

SECRET

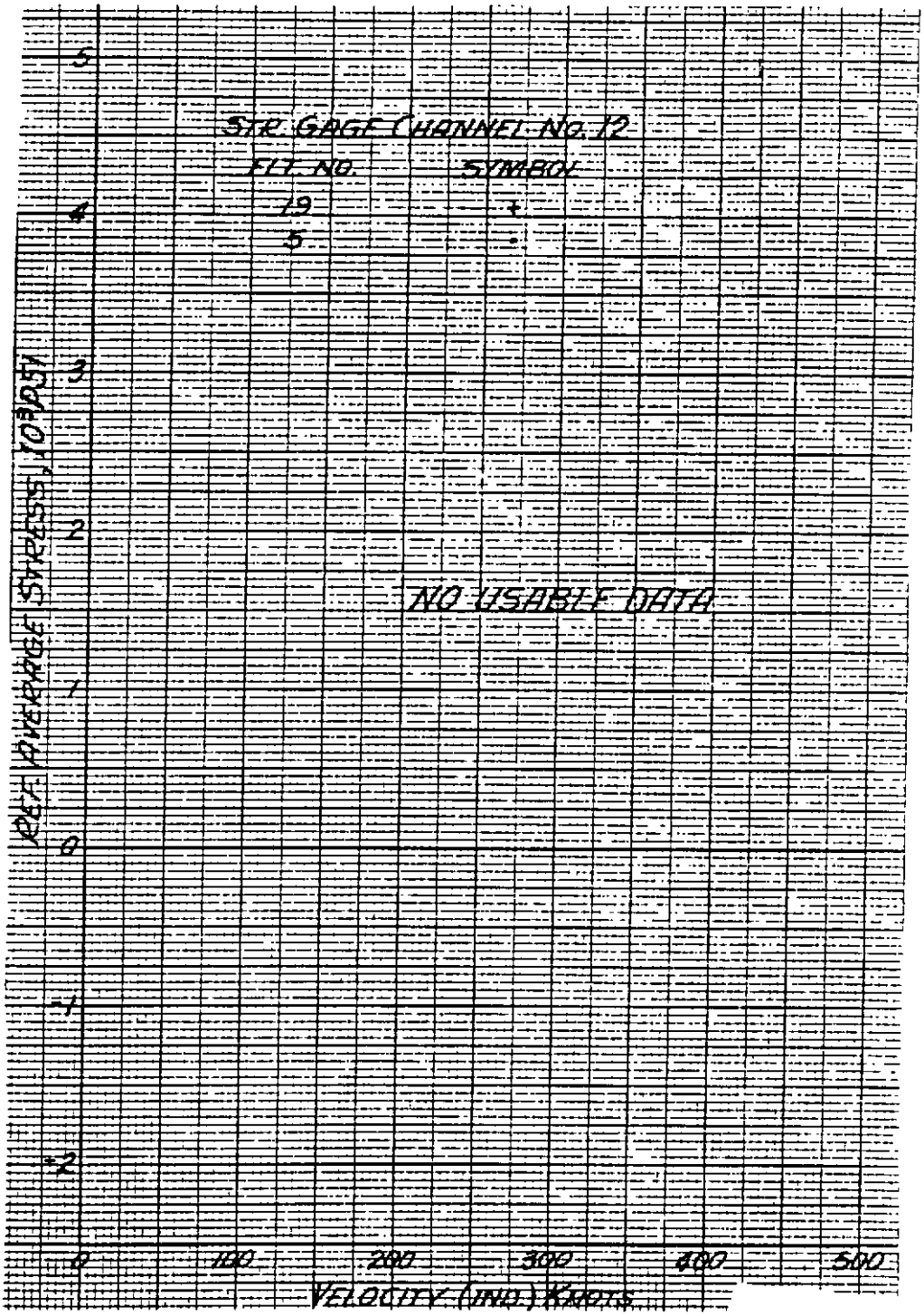

Figure 3.20 Zero stress determination, strain gage Channel 12.

SECRET

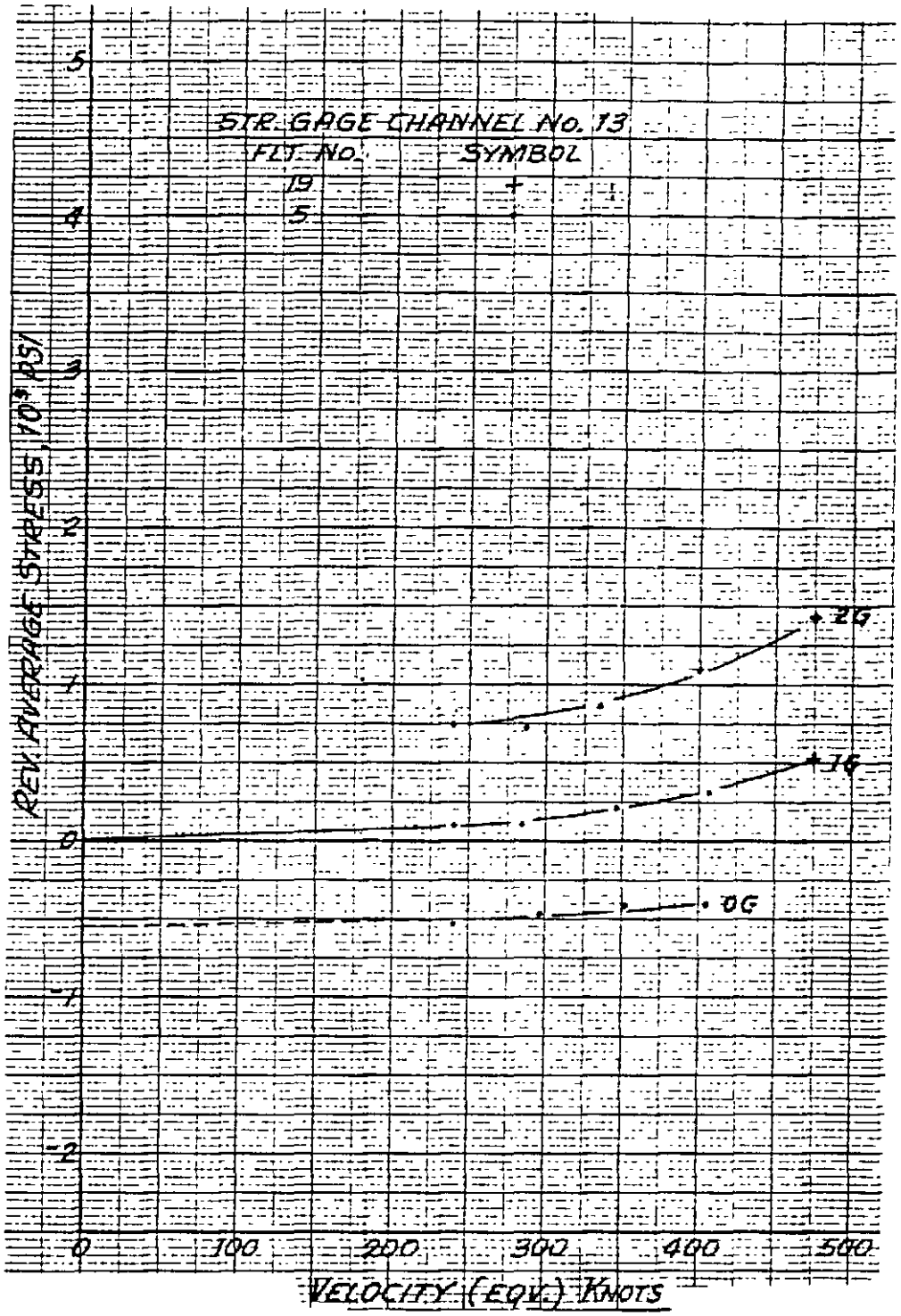

Figure 3.21 Zero stress determination, strain gage Channel 13.

SECRET

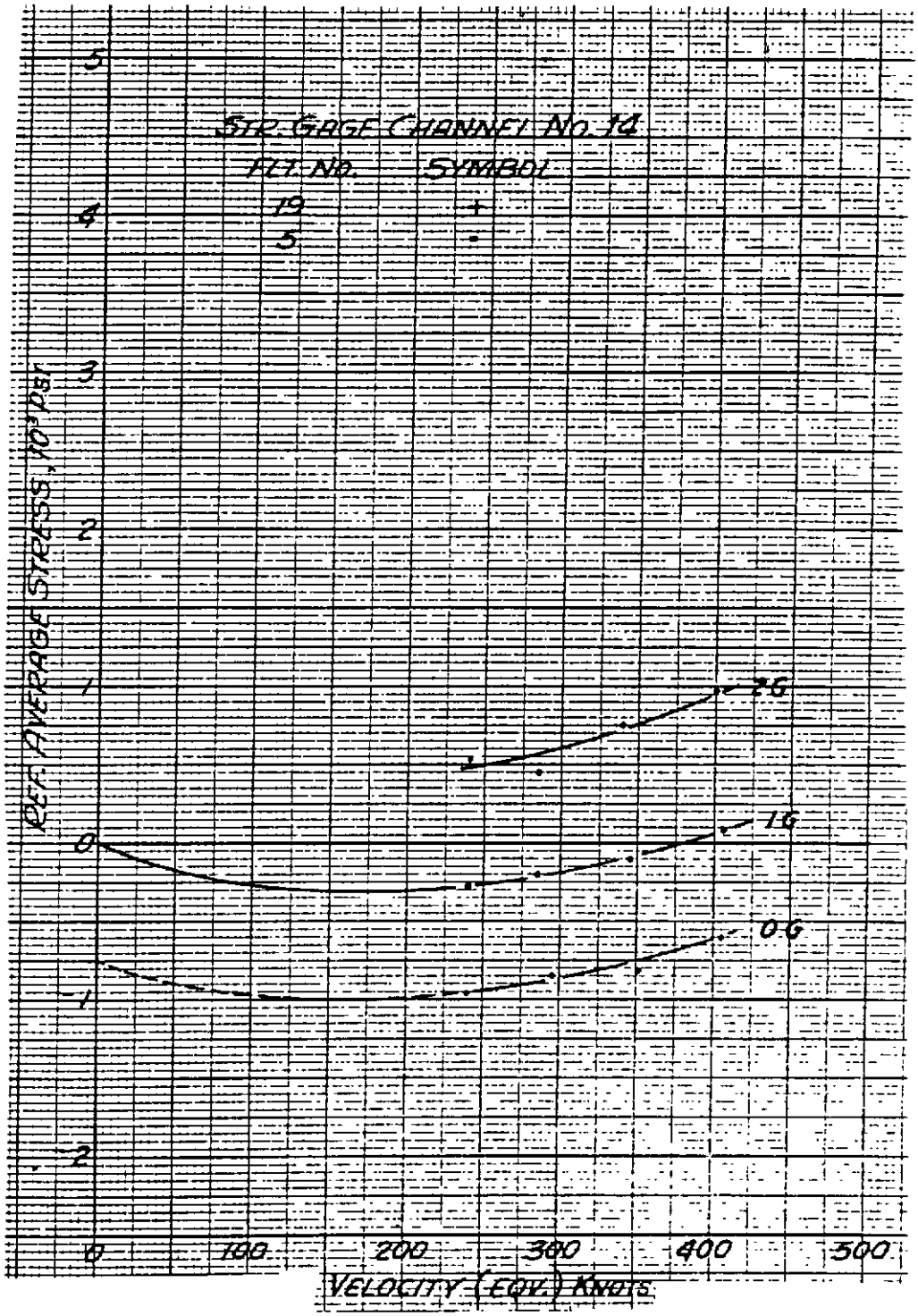

Figure 3.22 Zero stress determination, strain gage Channel 14.

SECRET

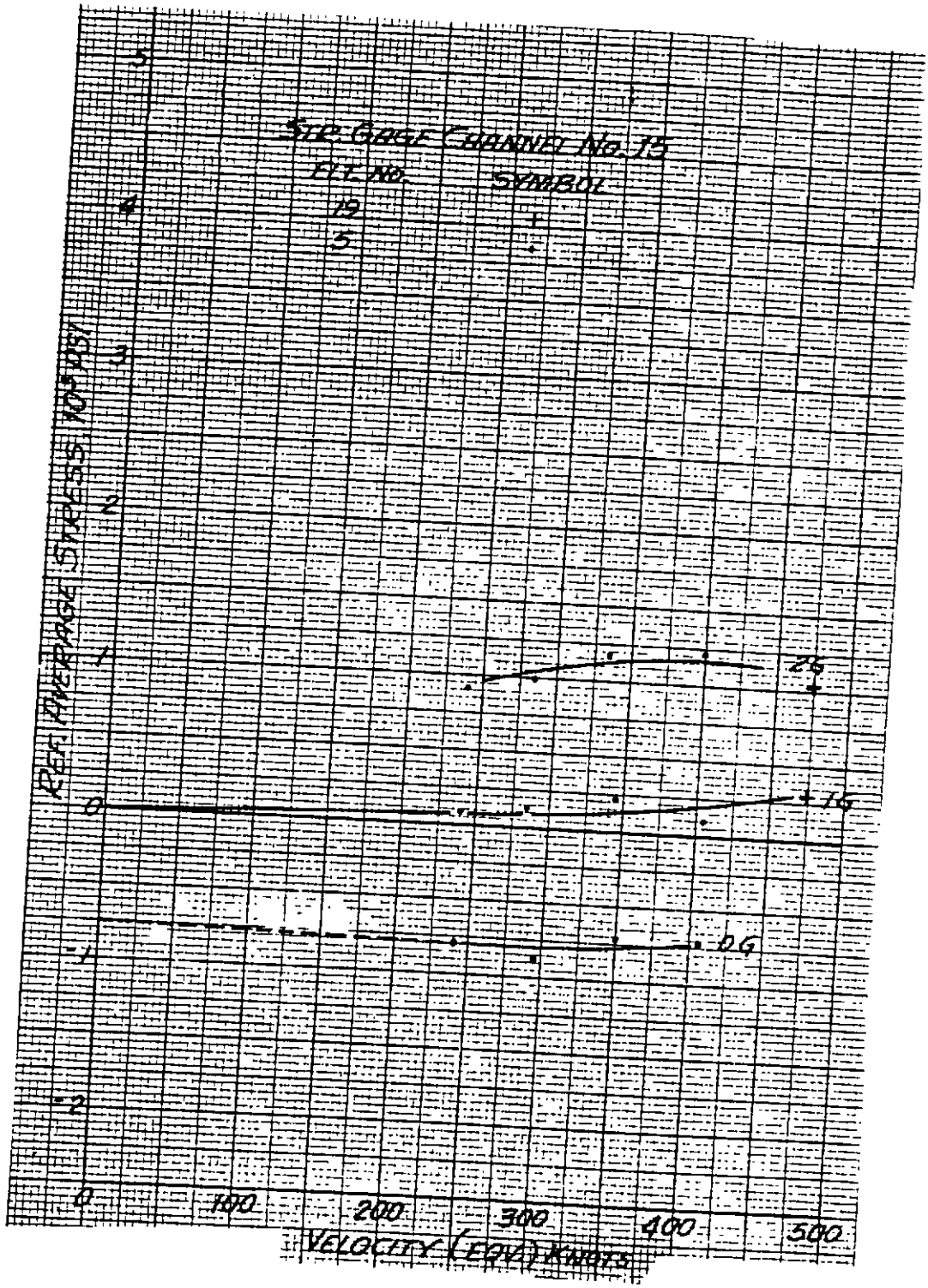

Figure 3.23 Zero stress determination, strain gage Channel 15.

SECRET

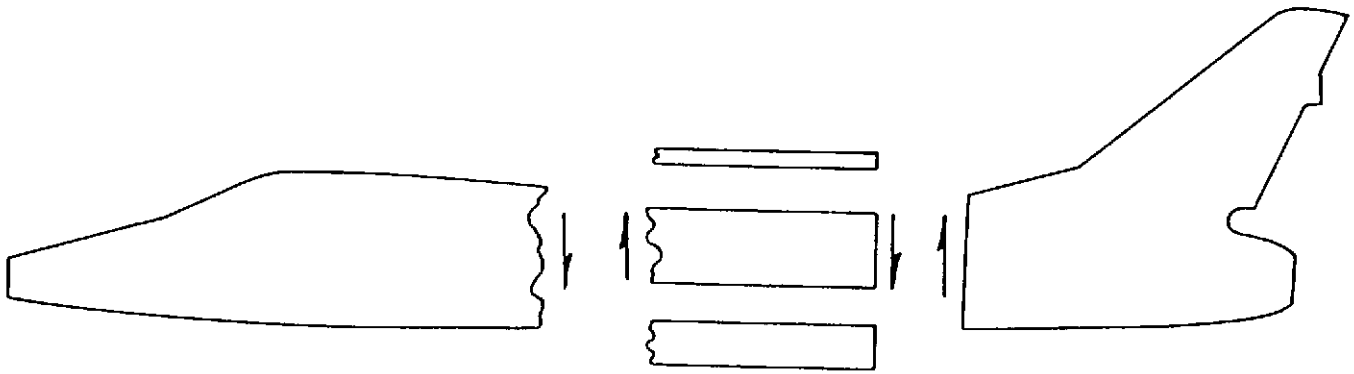

Figure 3.24 Positive shear sign convention.

SECRET

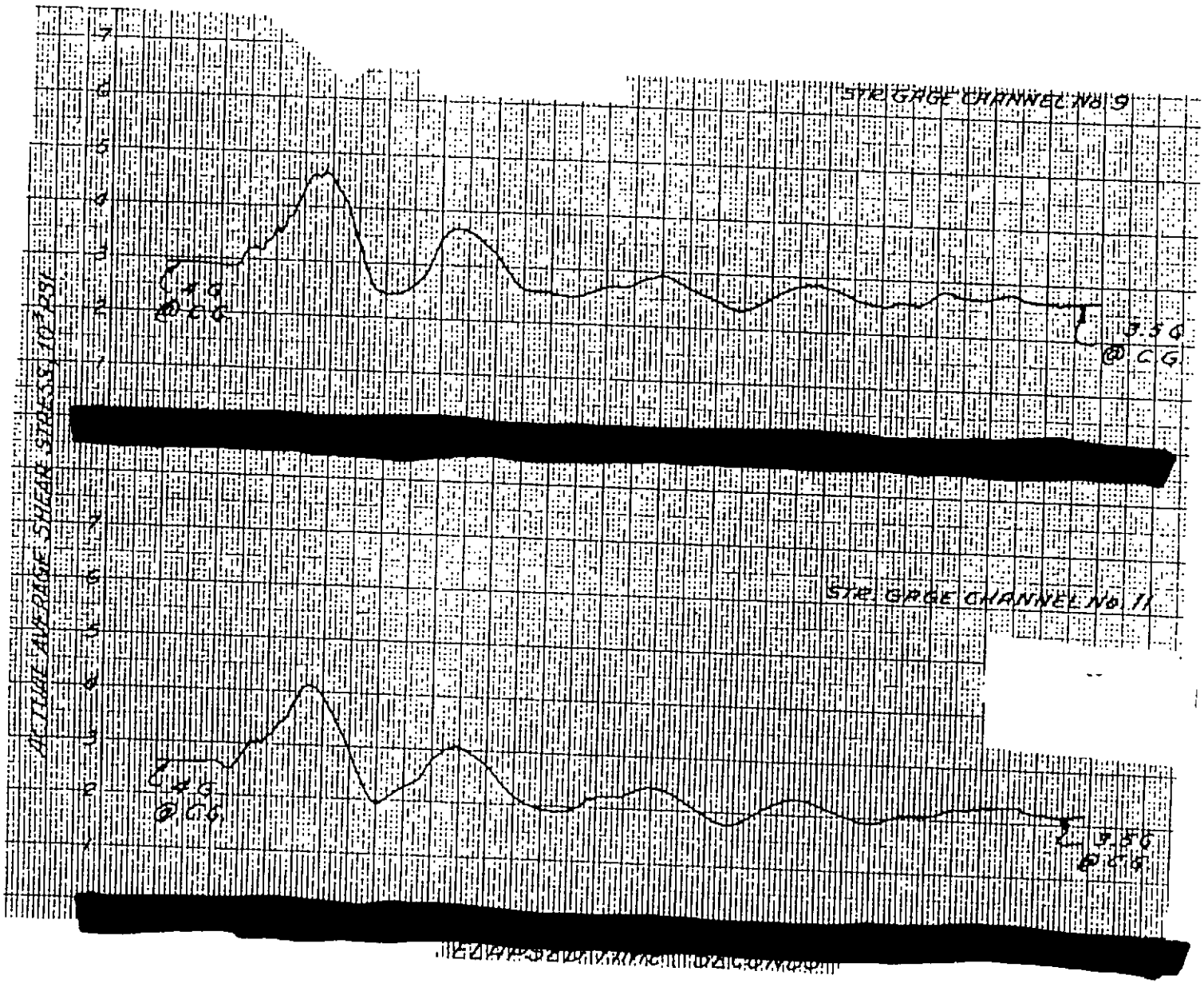

Figure 3.25 Side panel stress at shock arrival, strain gage Channels 9 and 11.

SECRET

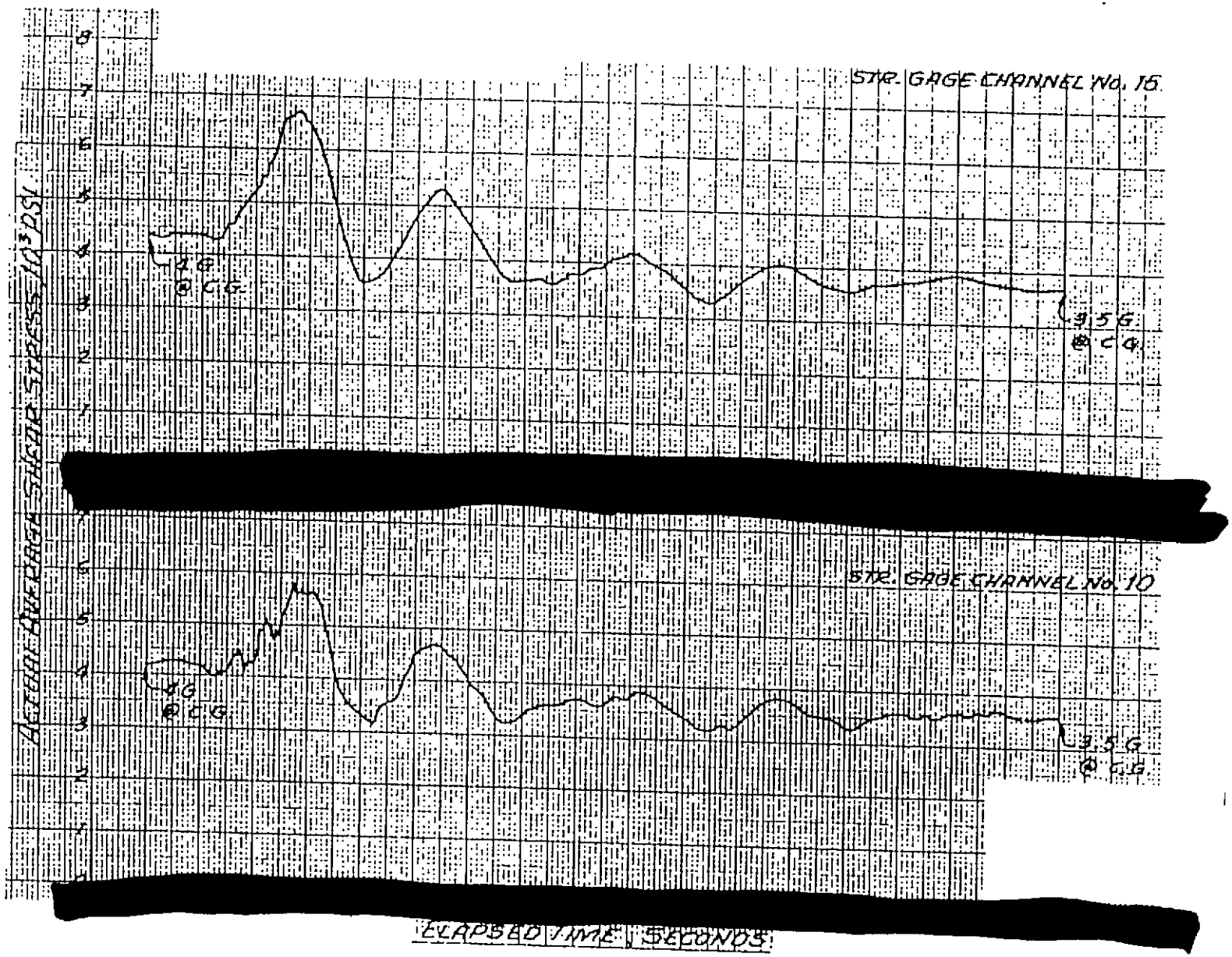

Figure 3.26 Side panel stress at shock arrival, strain gage Channels 15 and 10.

SECRET

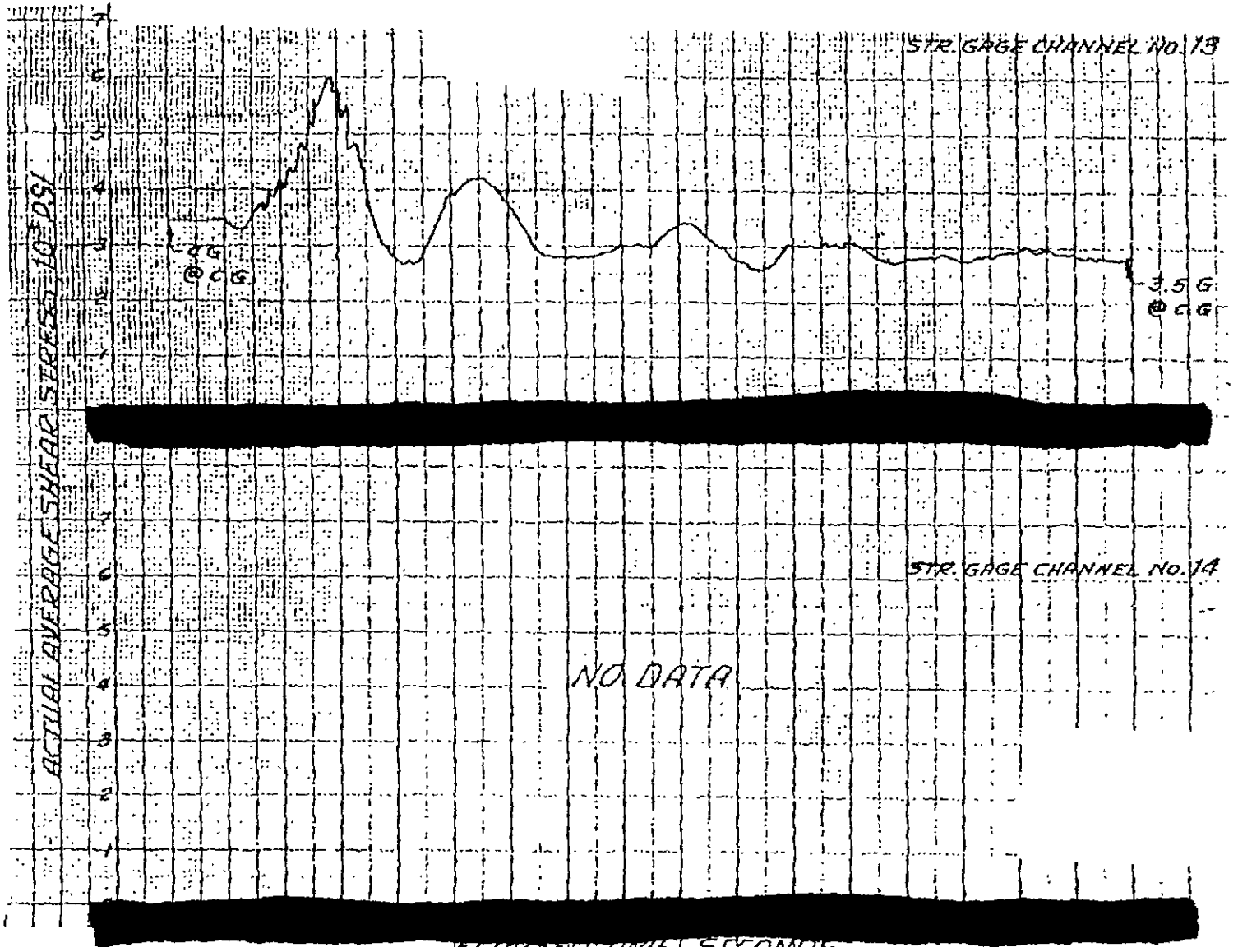

[redacted]

[redacted]

[redacted]

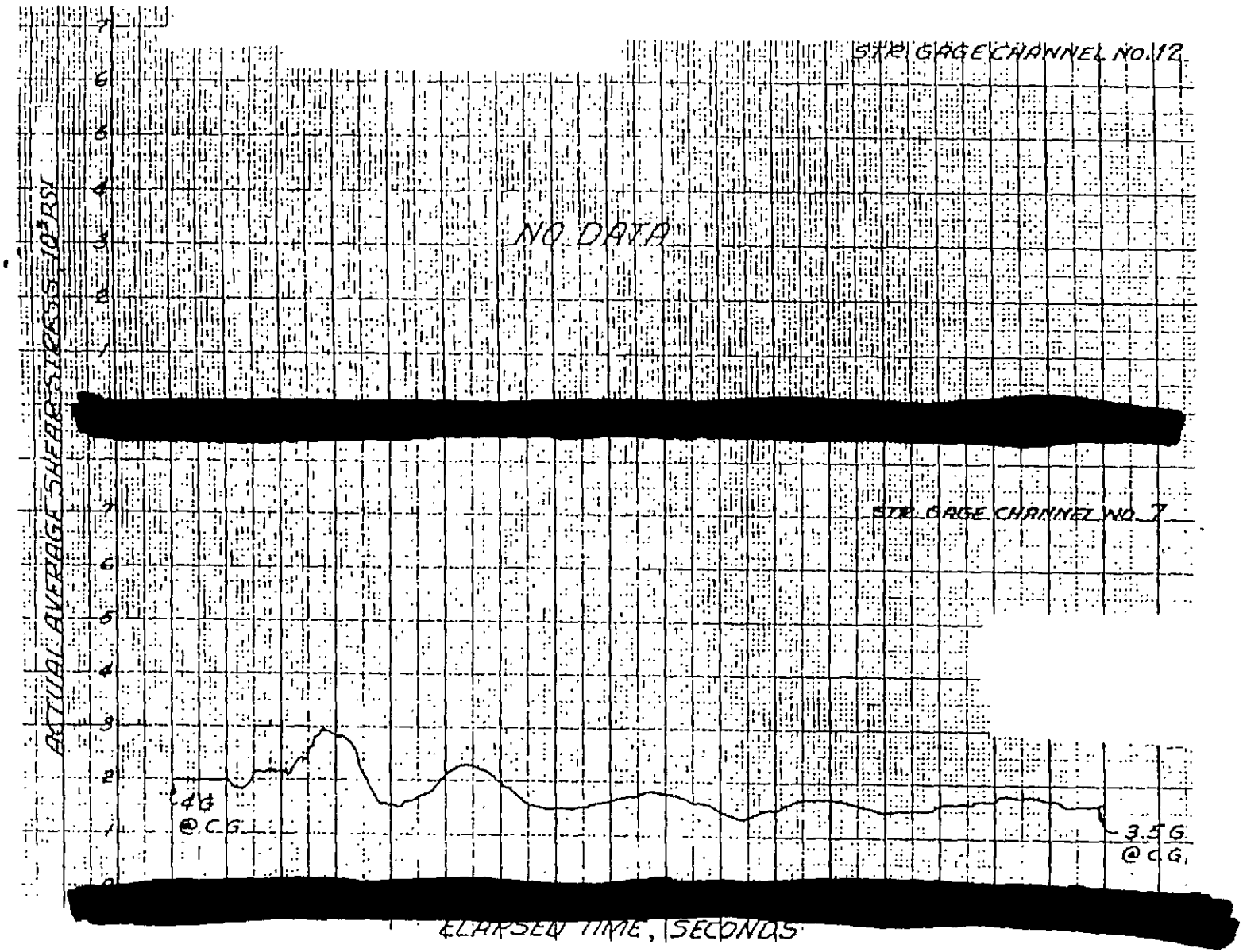

Figure 3.28 Side panel stress at shock arrival, strain gage Channels 12 and 7.

SECRET

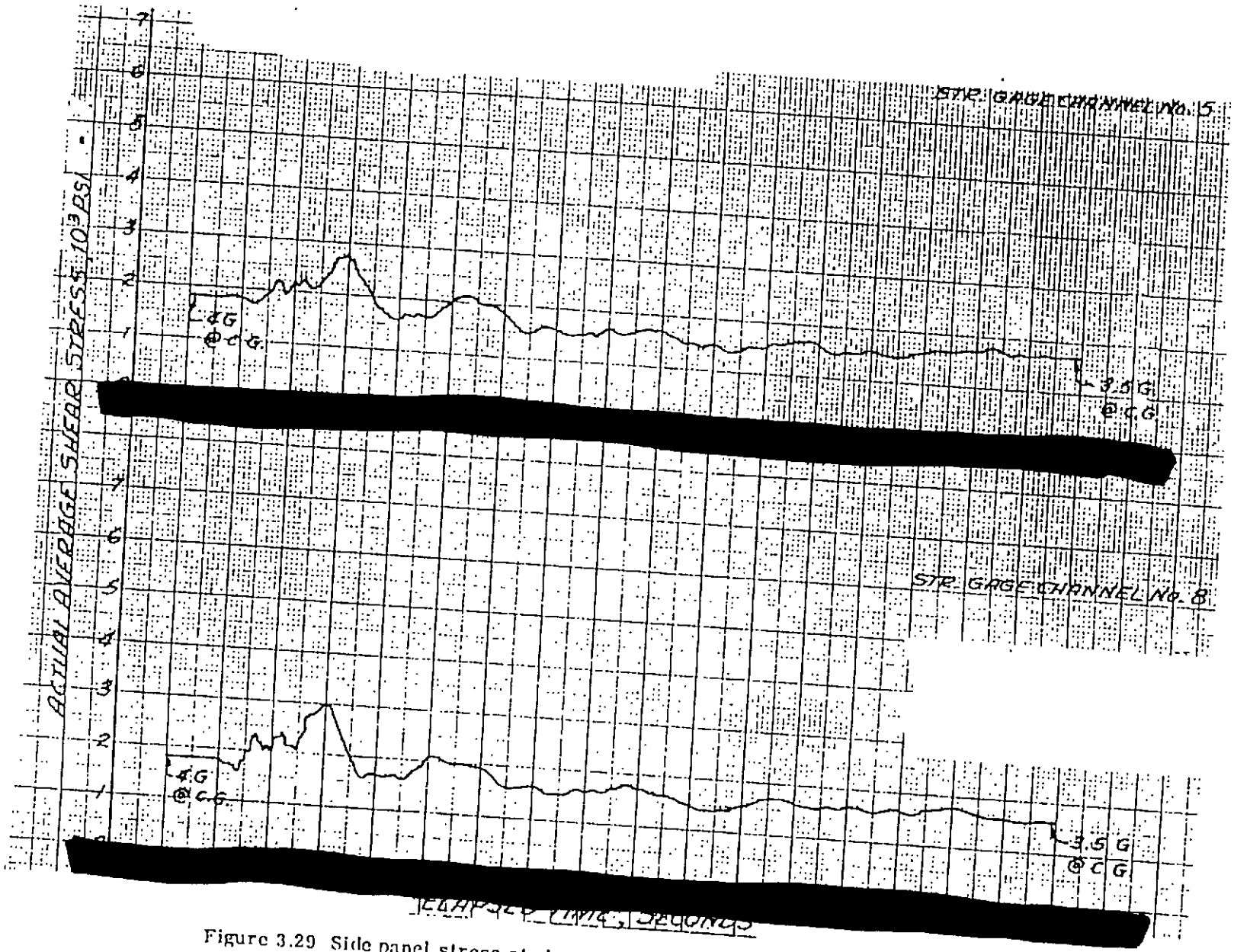

Figure 3.29 Side panel stress at shock arrival, strain gage Channels 5 and 8.

SECRET

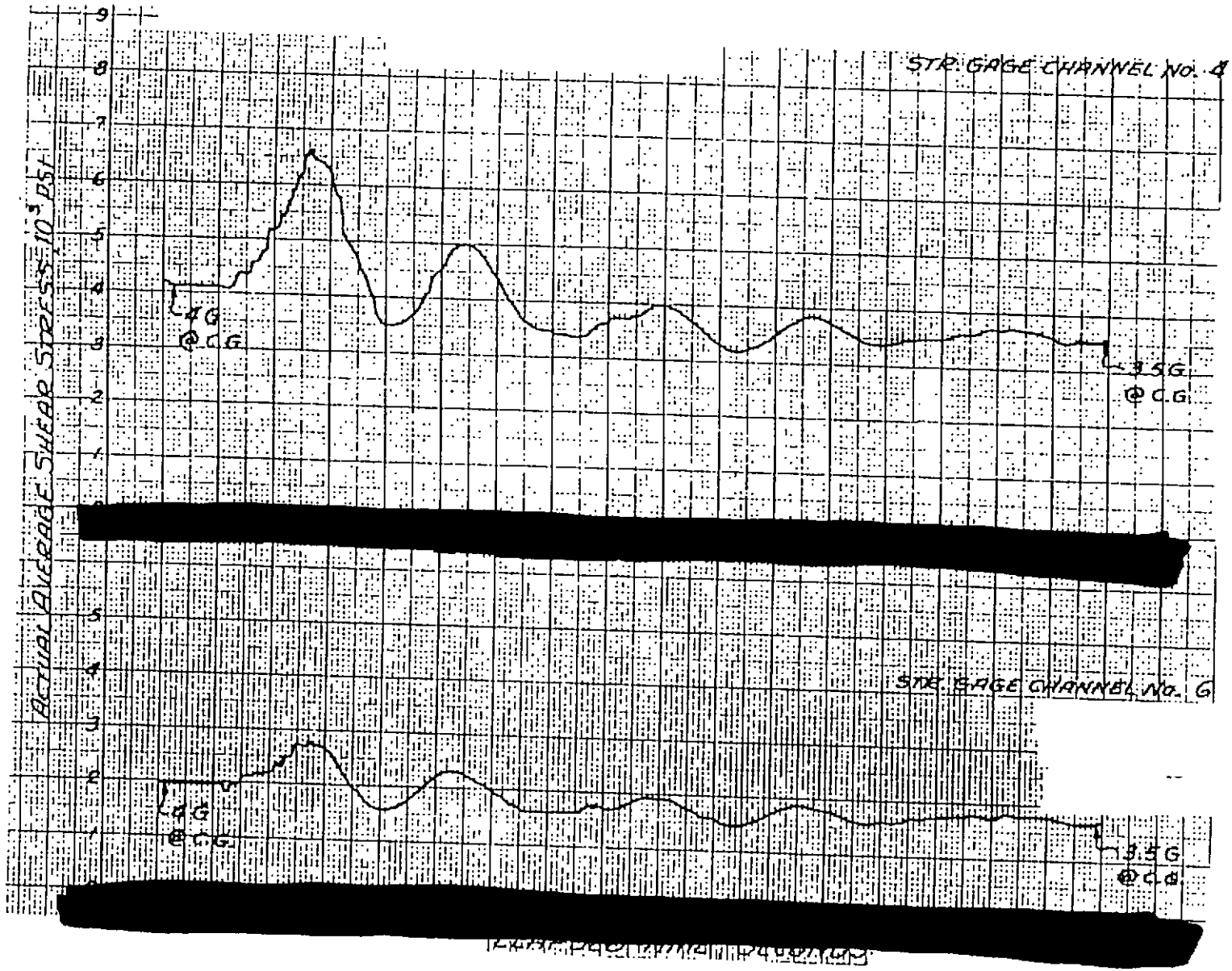

Figure 3.30 Side panel stress at shock arrival, strain gage Channels 4 and 6.

SECRET

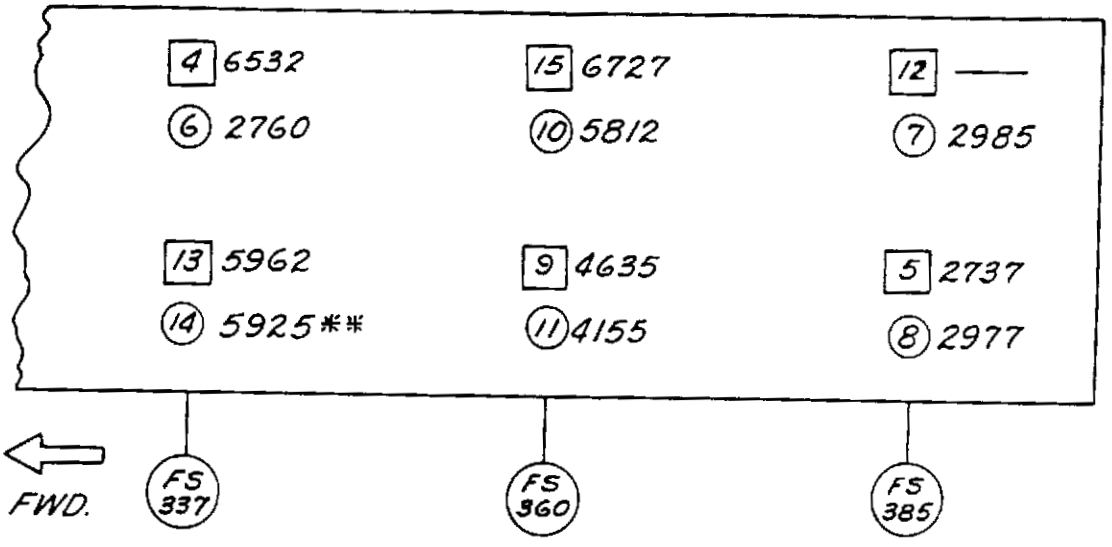

** STRESS ESTIMATED BY COMPARISON OF 13 & 14 FOR FLIGHT Nº 5

ALL SHEAR STRESSES SHOWN ARE PEAK STRESSES TAKEN FROM FIGS. 3.25 TO 3.30 INCL.

□ LEFT SIDE

○ RIGHT SIDE

Figure 3.31 Peak stresses inside panels.

SECRET

CHAPTER 4

DISCUSSION

4.1 FLIGHT PATH CONTROL CONCEPT

The positioning concept used in accurately locating the aircraft over a desired point at time of detonation has proved to be sound.

The actual technique used was a departure from methods used in previous tests. Consistent accuracies well within plus or minus 1 second [redacted] of desired position were attained within 10 practice runs, and after this, zero deviation was obtained approximately 50 percent of the time.

4.2 NUCLEAR RADIATION

The nuclear radiation doses at various locations in the cockpit, as determined by film badges, are listed in Table 3.3. The largest recorded exposure was 0.140 rem.

4.3 THERMAL RADIATION

Radiometer and calorimeter data are given in Figure 3.2. The radiometer is a flux-measuring device so there is no decay correction factor or integrating process to be applied to it. Therefore, one has merely to multiply the calibration factor to the sensor by the emf at any particular time to obtain the thermal flux at that time (cal/cm^2-sec). The radiometer curve in Figure 3.2 was obtained using this method. As shown, the maximum thermal radiation intensity measured by the radiometer in the cockpit was [redacted] cal/cm^2-sec and the duration of the pulse was [redacted] second.

Because the calorimeters are integrating devices, however, a more elaborate method of reading the oscillograph curves was used. This was necessary for two reasons:

SECRET

(1) Due to the continuous heat loss of the receiver button within the instrument from the moment of thermal energy impingement on the button, a correction for this decay must be applied to each successive point read in order to obtain an integrated curve.

(2) Due to the decay of the transducer output signal, one cannot be certain of the exact time after time-zero that the total energy was received unless a corrected curve is generated.

To correct for these factors, a method of corrective summation was developed at the US Naval Radiological Defense Laboratories (NRDL) and is here presented:

(1) Determine on the oscillograph trace the time point after which energy has ceased to be received by the calorimeters. It is not necessary that this be the point at which energy addition ceases — sometime after is satisfactory.

(2) Divide the time between the zero point and the selected cut-off point into equal convenient time increments (Δt).

(3) Read total trace deflection at each time interval.

(4) Obtain the true trace deflection at each time interval.

(5) Convert each value to millivolts (E), i.e., deflection (inches) times galvanometer calibration factor ($\frac{\text{millivolts}}{1 \text{ inch}}$)

$$\left(\frac{\text{IN}}{1}\right) \left(\frac{\text{millivolts}}{\text{inch}}\right) = \text{Millivolts}$$

The end-point millivolt reading is Ep.

(6) Add (E_1 E_2 E_3 . . . . Ep) = ΣE

(7) Subtract $\frac{Ep}{2}$ from ΣE to correct for averaging bias, thereby obtaining ΣE_c.

(8) Multiply ΣE_c by $\Delta t \Theta$. Θ is furnished with the instrument by NRDL.

(9) Add $\Delta t \Theta \Sigma E_c$ to the reading E_p.

(10) Multiply ($\Delta t \Theta \Sigma E_c + E_p$) by the inverse sensor calibration factor K to obtain calories/cm^2.

$$\left(\frac{\text{Millivolts}}{1}\right) \left(\frac{\text{Calories}}{\text{cm}^2 \text{ Millivolts}}\right) = \left(\frac{\text{Calories}}{\text{cm}^2}\right)$$

SECRET

The total thermal radiation as measured by the calorimeter in the cockpit was 0.23 cal/cm^2. It was found, however, that the indicated total thermal radiation increased with the elapsed time used in reducing the calorimeter data. Since for elapsed times greater than approximately 1 second, the aircraft was banked at a relatively large angle, it seems possible that some radiation could have been entering the calorimeter from the sun. In view of this and the fact that the radiometer indicated a pulse length of [redacted] second, it was decided to reduce the calorimeter data, using only the first 1 second of data. Theoretically the integral of the radiometer curve should be equal to the total thermal radiation. Integration of the radiometer curve yields a value of 0.15 cal/cm^2. This is considerably below the calorimeter value of 0.23 cal/cm^2. Considering the dependency of the calorimeter value on the elapsed time utilized, it seems likely that the value of 0.15 cal/cm^2 is more accurate than the 0.23 cal/cm^2 value.

4.4 RIGID-BODY DATA

Aircraft rigid-body data are presented in Figures 3.3, 3.4, and 3.5. Figure 3.3 indicates that at T_0 the aircraft velocity was approximately [redacted] At T [redacted] the velocity began to decrease and continued to do so throughout the maneuver. At the time of shock arrival the velocity was approximately [redacted] Figure 3.5 indicates that the roll maneuver was initiated at T = [redacted] and was largely completed by approximately T = [redacted] Figure 3.5 also indicates that the center of gravity acceleration, g, began to increase appreciably at about T [redacted] and by T = [redacted]

SECRET

the 4 g condition was obtained. Most of rigid-body data during the period of gust passage, is shown in Figure 3.5. Airspeed and altitude data for this period were not reduced since the overpressure effect would result in erroneous values. The rate gyros registered large fluctuations subsequent to the shock-wave arrival, but it is concluded that this is not indicative of the aircraft's motion. Rather, it is concluded that the shock-wave impingement resulted in vibration excitation of the structure to which the rate gyros were attached. As is evident, the frequency of the rate fluctuations was rather high——about 50 cps.

Using the roll attitude at $T = T_{sa}$ together with the aircraft position data from Figure 3.1, the direction of the shock-front propagation relative to the aircraft wing axis was determined. The angle so determined wa[redacted] degrees. That is, the direction of shock-front travel lacked onl[redacted] degrees being normal to the wing axis. Thus, a very near symmetrical gust input was obtained.

4.5 OVERPRESSURE DATA

Overpressure data are presented in Figure 3.3. These time histories represent the total pressure, in that static, dynamic, and weapon overpressure are included in the numerical values. Thus, the relatively rapid increase in pressure at approximately T = [redacted] is due to weapon effects. It can be seen that the maximum blast overpressures at the aircraft nose and vertical tail were approximately 0.4 psi. If the high-frequency fluctuations at the fuselage midsection are filtered out by eye, it is seen that the blast overpressure at

S[redacted]

this point was also about 0.4 psi. The duration of positive phase of the blast overpressure was approximately 0.6 second. Due to the variation in static and dynamic pressure with time, together with the relatively low magnitude of the blast overpressure, no apparent negative phase of the blast overpressure is evident in the data.

4.6 LATERIAL ACCELERATIONS

The lateral acceleration time histories during gust passage at various locations on the aircraft are shown in Figures 3.6 and 3.7. These data are considered relatively unimportant, since the gust input was almost normal to the aircraft coordinate system. These accelerometers were installed in the aircraft so that, in the event a large error in the actual positioning of the aircraft resulted in an appreciable side-gust component, dynamic response data could still be obtained.

4.7 NORMAL ACCELERATIONS

The normal acceleration time histories during gust passage at various locations on the aircraft are shown in Figures 3.8, 3.9, and 3.10. It should be emphasized again that high frequency filters were installed in the accelerometer circuits; thus the high-frequency components of the accelerations are attenuated.

Figure 3.8 indicates that the shock wave engaged the aircraft tail approximately 0.01 second previous to engaging the nose. Knowing the distance between these accelerometers and the speed of the shock wave (i.e., approximately Mach [redacted] at this point), the gust impingement angle was calculated to be about 110 degrees.

SECRET

This is in agreement with the impingement angle as determined from Figure 3.1, and the angle of attack.

Inspection of Figures 3.9 and 3.10 reveals one outstanding point: The wing responded strongly to the gust at a response frequency of about 6.5 cps. Ground-vibration survey results show this to be the frequency of the fundamental symmetrical mode of the aircraft. Although strong response occurred in the first flexible mode, inspection of Figures 3.8, 3.9, and 3.10 indicates practically no rigid-body response.

Results from the general theory of dynamic response of linear systems can be utilized to obtain interesting information from the normal acceleration curves. For example, if the high-frequency components in the wing traces are neglected, the response of the wing resembles closely the response of a lightly damped linear dynamic system which has been subjected to a step function input. If this is true, theory predicts that the maximum stress (i.e. the wing deformed concave upward its maximum amount) should occur at the time of maximum negative wing-tip acceleration, i.e. at the end of the first half-cycle of the response. For this system, this should occur at approximately T = [redacted] seconds. No strain gages were present on the wing, but strain gages located on the fuselage side panels all show peak values in the time interval T = [redacted] (Figures 3.25 through 3.30). Note, in fact, that the fuselage strain gages all exhibit time fluctuations which follow primarily the response in the fundamental mode. Note also

SECRET

that the high-frequency stress fluctuations are small in magnitude, in comparison to 6.5 cps fluctuations. It can also be seen that the maximum stress does not necessarily occur at the time of maximum acceleration. In the present system, for example, maximum (although attenuated) accelerations at the wingtips, fuselage, nose and tail all occur immediately after shock impingement, yet the stress peaks do not occur until sometime after shock impingement. Basically, this is due to the fact that virtually instantaneous acceleration can occur in aircraft structure but instantaneous relative displacements (or deformation) cannot.

A good approximation to the maximum wingtip deflection can be obtained from the normal-acceleration-time histories by considering the response to be that resulting from a step-function input. The system is approximated by an undamped single-degree-of-freedom system (i.e. the fundamental mode), and the analytical methods of Reference 5 are used. Taking the maximum wingtip negative acceleration as being minus 5g the maximum incremental upward wingtip deflection relative to the fuselage is calculated to be 4.2 inches. Note that this deflection is due to gust alone, i.e. in order to obtain the total deflection, the 4.2 inches would have to be added to the deflection due to the steady 4g load.

The fact that the gust load is applied to the wing in a sudden manner, rather than statically, causes an effective amplification

SECRET

of the load. That is, the stresses resulting from the suddenly applied load are greater than would result if the load were applied slowly (i.e. statically). For an undamped single degree of-freedom system the dynamic amplification resulting from a step input is equal to two, i.e. the maximum dynamic response is twice what the response would be statically, (Reference 5). Thus, it appears that, as a rule of thumb, the dynamic amplification at the wingtip can be taken as two. Note that this amplification refers to deflection and not to acceleration.

4.8 SHEAR STRESS IN FUSELAGE SIDE PANELS

Tensile and compressive strains were measured in the fuselage side panels at fuselage stations (FS) 337, 360, and 385. Sr-4 strain gages were bonded to the outer surface of the panels approximately 4 inches below the upper edge and approximately 4 inches above the lower edge of each side panel. Four gages were used at each location (as shown in Figure 3.11) to increase accuracy of reading and for temperature compensation. A sketch of the strain gage locations is shown in Figure 3.11.

The inner face of each panel was milled from a thickness of 0.125 inches to 0.098 inches in some areas and to 0.076 inches in other areas. Coincidently many of the strain gages were mounted directly opposite or nearly opposite to a change in panel thickness.

SECRET

Therefore, the strains measured should be considered as average values of strain for each respective location.

A condition of pure sheer existed throughout each instrumented panel, causing a state of biaxial stress on any element in either panel. Therefore, in the absence of buckling, $\tau max = \sigma_1 - \mu \sigma_2$. For the aluminum panels, $E = 10^7$psi; thus $\tau max = (\epsilon_1 - \mu\epsilon_2)\, 10^7$psi where μ is taken as 0.33.

Where: τmax = Maximum shear stress in psi

σ = Principal stress in psi

μ = Poisson's ratio

ϵ = Principal strain in inches/inch

E = Modulus of elasticity in psi.

Figure 3.11 shows strain gage locations and identifies them by oscillograph channel number, fuselage station and water plane. It is noted that no data were obtained from two of the twelve gages.

Figures 3.12 through 3.23 are plots for determining a delta stress between a zero reference and a true zero stress. Zero reference stress is the preflight calibration stress at one G condition with zero thrust and zero velocity. The delta stress value is obtained by extrapolating the zero G curve for stress versus velocity to zero velocity, then reading the delta stress between the extrapolated zero G point and the zero reference, one G point.

SECRET

No time-history plots of reference shear stresses for the period prior to shock arrival are shown. To convert the actual stresses to reference stresses, the respective delta stresses from Figures 3.12 through 3.23 should be subtracted. Figure 3.24 illustrates the sign convention for the shear measurements.

Figures 3.25 through 3.30 are time histories of actual stresses (reference stress plus delta stress) for a short period including shock arrival. The time span is from T = [redacted] to T = [redacted] As a result of the shock arrival, the greatest stresses were incurred during this period. Because of the dynamic conditions involved, no meaningful number of G's can be assigned to points on the curves. Therefore, G values are shown only for near-static conditions at T = [redacted] and T = [redacted]. A summary of peak stresses is shown in Figure 3.31. It is noted that the stress at strain gage channel number 6 has a relatively low value. This was probably due to slippage of two of the four strain gages at this location.

SECRET

CHAPTER 5

CONCLUSIONS

5.1 FLIGHT PATTERN CONCEPT

Rigorous and continuous coordination between aircraft pilot and radar controller produced a positioning concept capable of placing an aircraft, traveling a[redacted]ft/sec, within 100 ft of a desired point in space at a desired time.

5.2 POSITION ANALYSIS

Approximations and assumptions made in determining weapon effects during the mission resulted in conservative values, as anticipated.

5.3 RIGID-BODY RESPONSE

Rigid-body response, (translation and rotation of the aircraft) to the blast front was minor.

5.4 DYNAMIC RESPONSE

Appreciable structural dynamic response, particularly in the wing, was effected by the blast front. The response occurred primarily in the first symmetrical mode.

SECRET

Part 2

EYE PROTECTION IN F-100F/GAM 83B SIMULATION

CHAPTER 6

INTRODUCTION

6.1 OBJECTIVES

The objective of this project was to test the effectiveness of a 1-percent-transmission, gold-coated fixed filter in preventing retinal burn and debilitating flashblindness in the GAM-83B weapon system delivery.

6.2 BACKGROUND

The delivery of a visually guided air-to-ground missile with a nuclear warhead requires that the pilot be visually exposed to a nuclear detonation. An extreme hazard is created when the high thermal energy released is focused on the retina of the observer. In the typical delivery, the unprotected eye will suffer a retinal burn, resulting in a permanent blind area in the fovea, which is the area of most acute vision. With partial, but insufficient protection, a destructive lesion may be prevented, but flashblindness, which may persist long enough to prevent the pilot from retaining control of the aircraft, will occur.

The effects of thermal energy from nuclear detonations on the eyes have been a matter of deep concern to the military since the inception of nuclear testing. Beginning with Operation Buster in 1952, many experiments have been conducted to determine the effects on the eyes of exposure to nuclear fireballs. In Operation Upshot-Knothole, exposed

SECRET

rabbits received retinal burns up to a distance of 42.5 miles from a [redacted] low-altitude burst (Reference 6). In Operation Hardtack, a retinal burn was received by a rabbit at 305 nautical miles from a high-altitude burst of a [redacted] vice (Reference 7). [redacted]

Information on the extent and duration of flashblindness from exposure to nuclear bursts is more difficult to assess. Since there are no objective signs in flashblindness, tests must be subjective, requiring human subjects. Obviously, this limits the extent of participation in actual nuclear tests. Laboratory data is also very scanty, perhaps due to the fact that flashblindness very often has been considered only as a secondary and relatively minor effect, with retinal burn considered as the major problem. Most workers in the field now consider flashblindness to be a consideration of at least equal importance.

6.3 THEORY

Eye effects resulting from thermal radiation emitted by nuclear detonations are classified as retinal burns and flashblindness. Even though the difference in these effects is apparently one of degree, i.e., permanent as against temporary blindness, the mechanisms involved are quite different. Retinal burn results when there is a discrete retinal image of sufficient intensity to cause irreversible organic changes in the retinal and choroidal tissues. These changes are pathological.

The mechanisms underlying the phenomenon of flashblindness are not so well understood. Flashblindness occurs when a source, which is focused on the retina, is sufficiently bright to cause a persistence

SECRET

in the perception of the stimulus. This is referred to as an after-image.

Flashblindness can also occur when there is no discrete source but when the retina is flooded with an intense, dazzling light. The first effect results when a bright source is viewed directly, while the second is most likely to occur when the eye is exposed to diffusely reflected or scattered light of high intensity, such as might result from the scattering and reflection of light from a cloud cover.

SECRET

CHAPTER 7

PROCEDURE

7.1 EXPERIMENTAL DESIGN

Participation was in Shot Small Boy, with exposure of the observer's eyes [redacted] eapon burst. [redacted]

Prior to the mission, the observer underwent a complete visual and ophthalmoscopic examination, including fundascopic with dilated pupils, visual fields, and visual acuity tests at distance and near.

For the mission, the pilot and observer were both protected by a 1-percent-transmission, gold-coated, neutral-density visor; the pilot, however, did not view the detonation. Both wore the visor for at least one-half hour before the shot to become completely adapted to the ambient luminance through the visor. An eye patch was placed over the other eye of the observer.

Prior to takeoff, a measurement of the cockpit luminance was taken. A near visual-acuity chart was mounted on the instrument panel, and the lowest line that the observer could read through the visor was recorded.

The observer held two pocket stop watches, one in either hand. He observed the target and started both watches at the instant of detonation. He was instructed to blink and turn his head back in the cockpit as soon as he viewed the burst. He first attempted to read the air-speed indicator. When he was able to do so, he stopped the watch in his left hand and directed his attention to the visual-acuity chart.

SECRET

When he was able to read the same line that he could read on the pre-takeoff test, he stopped the second watch in his right hand.

After landing, the stop-watch readings were recorded and the comments of the observer regarding subjective reactions to the experiencewere noted. A complete visual and ophthalmoscopic examination was again performed on the observer.

7.2 INSTRUMENTATION

The 1-percent fixed filter was fabricated from a neutral density plastic which transmitted approximately 10 percent. The outer surface was then coated with gold to give 1-percent transmittance from 380 to 700 mμ and slightly less in the near infrared to 2,000 mμ. Specifications for this filter are contained in MIL-V-27446.

SECRET

CHAPTER 8

RESULTS

8.1 VISUAL

Complete ophthalmologic, visual, and perimetric examination revealed no damage or changes to the exposed eye in the form of retinal burn or otherwise. The observer stated that there was no period of flashblindness, or at least none long enough to record on his stop-watch.

8.2 CALCULATED

The retinal irradiance on the exposed eye through the 1 percent fixed filter was calculated to be approximatel[redacted]

SECRET

CHAPTER 9

DISCUSSION

This event provided an excellent opportunity to test the effectiveness of a 1-percent fixed filter under conditions encountered in a typical GAM-83B delivery, although the detonation was observed by the observer rather than the pilot.

The observer was blond and blue-eyed, with lightly pigmented retinas. Since the radiant energy is absorbed chiefly by the retinal and choroidal pigment, the damage threshold depends to a considerable extent on the degree of pigmentation. Thus, a dark-complexioned observer with a heavily pigmented retina would be more likely to suffer damage from the same energy dose.

The threshold irradiance necessary to cause a retinal burn has not yet been accurately determined. The results of laboratory studies with rabbits give threshold dose figures ranging from over 1 cal/cm^2 down to 0.2 cal/cm^2. Mild lesions, i.e. lesions visible ophthalmoscopically within 3 to 5 minutes after exposure, have been caused in rabbits by Dr. Ham and his associates with doses as low as 0.2 cal/cm^2 when delivered in 175 microseconds. (Reference 8.)

Clearly, the calculated irradiance [redacted] on the observer's retina in this event fallswell below the retinal-burn threshold level.

Figure 9.1 shows the irradiance levels at the retina from the first and second thermal pulses and the total, which is the summated

SECRET

total of the two pulses. The dotted line indicates the Small Boy yiel[redacted] Retinal irradiance levels from the entire range of possible yields from the GAM-83B warheads have been calculated for the same conditions as in Small Boy. The ordinate represents the retinal irradiance, unfiltered on the left, and through a 1-percent filter on the right.

Certain assumptions and approximations were necessary in order to calculate irradiation levels. Because of the paucity of data, and to prevent undue complication of the problem, the fireball was assumed to be uniformly radiating, with no consideration given to the spectral distribution of the emitted radiation, even though the absorption and scattering characteristics of both the atmosphere and the ocular media are known to be wavelength dependent. However, it is felt that these assumptions do not affect the irradiance levels significantly.

SECRET

page 83 is deleted in its entirety

CHAPTER 10

THERMAL ANALYSIS

10.1 DISCUSSION

The thermal energy from a nuclear detonation in the atmosphere is emitted in two pulses. The first pulse, which consists of only about 1/10 to 1/2 of 1 percent of the total thermal energy emitted is very rapid and short-lived. This is followed by the slower second pulse. Generally, the first pulse is not considered to be a hazard because of the small amount of energy emitted; however, when a focusing of energy occurs, as in the eyes, high-energy densities can occur. The first pulse occurs so fast that the fireball is still relatively small during this period, and the energy is focused onto a very small area of the retina. Therefore, the energy from the first pulse cannot be ignored when considering the thermal hazard to the eye.

In this report, the deposition of energy on the retina is determined separately for each pulse. Since the pulses are separated by a distinct trough, the light minimum, there is, no doubt, some dissipation of energy from the first pulse before the second occurs. However, since the 2 pulses of [redacted]eapon are separated only by about [redacted] seconds, the amount of heat loss during light minimum is not considered to be significant. The irradiances from the two pulses are therefore determined separately and then summated.

10.2 CALCULATION OF IRRADIANCE ON THE RETINA

<u>10.2.1 Energy From The Second Pulse.</u> The irradiance, or thermal-

SECRET

energy density at the cornea (at the front of the eye), if all attenuating factors are ignored, is determined by:

$$Q_C = \frac{E}{4\pi R^2} \tag{10.1}$$

Where: Q_C = irradiance at the cornea in calories/cm^2

E = total thermal emission in calories

R = slant range in centimeters

Taking the total thermal emission as $1/3 \times 10^{12} \times W$, where W is the yield in kilotons, we have: (Reference 4)

$$Q_C = \frac{1/3 \times 10^{12} \times W}{4\pi R^2}$$

or if all constants are combined

$$Q_C = 2.65 \times 10^6 \frac{W}{R^2} \tag{10.2}$$

Where: R = slant range in meters

To determine the irradiance at the retina:

$$Q_{R_2} = Q_C \frac{D_p^2}{D_i^2} \tag{10.3}$$

Where: Q_{R_2} = retinal irradiance from the second pulse in calories/cm^2

D_p = diameter of pupil in millimeters

D_i = diameter of retinal image in millimeters

The image diameter D_i can be evaluated in terms of the fireball diameter, the nodal length of the eye, and the slant range. The nodal length is defined as the distance from the posterior nodal point of the eye to the posterior focal point, and is equal to the posterior focal length divided by the index of refraction of the image medium. The focal length of the eye cannot be used to determine

SECRET

retinal image sizes because the indices of refraction of the object and image media are not the same. The nodal length of the eye is approximated at 17 millimeters.

$$D_i = \frac{D_f N}{R} \tag{10.4}$$

Where: D_f = fireball diameter in meters

R = slant range in meters

N = nodal length of the eye

Then, substituting values for Q_C from Equation (10.2) and values for D_i from Equation (10.4) in Equation (10.3), we have:

$$Q_{R_2} = \left[2.65 \times 10^6 \frac{W}{R^2}\right]\left[\frac{D_p^2}{D_f^2} \frac{R^2}{(17)^2}\right] \tag{10.5}$$

It is now clearly seen that the range cancels out of the equation. This demonstrates analytically that the irradiance of a focused system is independent of the distance of the source. As the distance of the receiver from the source increases, the total energy falling on the receiver decreases; however, the image area also decreases to the same degree. The energy density, therefore, remains the same. Thus, the only protection to the eye offered by an increase in distance from the detonation is the increased atmospheric attenuation.

Equation (10.5) becomes:

$$Q_{R_2} = 9.17 \times 10^3 \frac{W \; D_p^2}{D_f^2} \tag{10.6}$$

The fireball diameter is now evaluated in terms of W at 150 milliseconds, at which time the exposed eye is considered to have blinked.

SECRET

The Edgerton, Germeshausen and Grier (EG&G) semiempirical formula for fireball growth from minimum time out to several hundred milliseconds is used. This formula represents the best fit of the EG&G fireball diameter data of weapons [redacted] (Reference 9).

[redacted]

(10.7)

Where: D_f = fireball diameter in meters

t = time in milliseconds

Substituting the value for D_f from Equation (10.7) into Equation (10.6) gives:

[redacted]

(10.8)

Q_{R_2} in Equation (10.8) represents the retinal irradiance from the unattenuated radiation of the second pulse. Taking into consideration all the attenuation factors, the final equation now takes the form:

[redacted] (10.9)

Where: $A = T_a T_c T_o$

T_a = atmospheric transmission

T_c = aircraft canopy transmission

T_o = ocular transmission

E_f = fractional transmission in 150 milliseconds (blink time)

Atmospheric transmission was estimated at 0.83 for a visibility of

SECRET

50 miles at a slant range of [redacted]

The transmission of the canopy was estimated at 0.88. A reading of the sky luminance was taken from the cockpit first with the canopy open and then through the closed canopy. The luminance was measured at 1,700 foot lamberts on direct measurement and 1500 foot lamberts through the closed canopy. The ratio of 1,500/1,700 or 0.88 was taken as the canopy transmission factor.

The ocular transmission was estimated at 0.80.

Thus, A = (0.83) (0.88) (0.80) = 0.58

The fractional energy E_f emitted in 150 milliseconds was determined by first evaluating the ratio t/t_{max}, where t_{max} is the time in milliseconds to the second pulse maximum, and t is the cutoff time of 150 milliseconds.

$t_{max} = 24\ W^{0.5}$ (Reference 9)

t_{max} = [redacted]

The scaled time becomes 150 [redacted] and the fractional thermal energy is determined to be abou[redacted] the graph relating fraction of thermal energy to scalled time in second thermal pulse (Reference 4).

The pupillary diameter was estimated at 4 millimeters. Since it proved to be impossible to measure the pupil behind the visor, an indirect method was used. The pupil was measured at 4 millimeters indoors with an ambient luminance of 15 foot lamberts. Since the outdoor luminance of 1,500 foot lamberts would approximate the indoor luminance of 15 foot lamberts through a 1-percent filter, 4 millimeters was taken as the actual

SECRET

measurement of the pupillary diameter.

The retinal irradiation from the second thermal pulse is now calculated from Equation (10.9):

[redacted] (10.10)

[redacted] (10.11)

10.2.2 Energy From The First Pulse. Since the fireball diameter and consequently the retinal image size is increasing rapidly during the first pulse, it is evident that the energy falling on the retina is not evenly distributed. An accurate profile of the distribution of energy over the retinal image as a function of time requires exact values for the energy rise and fireball diameters from time zero. This information, unfortunately, is not available for times prior to the first peak. Therefore, in this report, the total energy from the first pulse is considered to occur at the first peak. The error at the center of the retinal image, caused by this approximation, is not deemed to be significant. The center of the image is, of course, the hottest point, because of the accumulation of energy there due to the increasing fireball size. It is therefore the point of greatest concern.

Since only about 1/2 of 1 percent of the total emission occurs in the first pulse, the irradiance at the cornea from the first pulse becomes:

SECRET

$$Q_{C_1} = 2.65 \times 10^6 \frac{W}{R^2} (0.005) \text{ (from Equation 10.2)} \quad (10.12)$$

Or $$Q_{C_1} = 1.33 \times 10^4 \frac{W}{R^2} \quad (10.13)$$

To determine the irradiance at the retina:

$$Q_{C_1} = \left[1.33 \times 10^4 \frac{W}{R^2}\right]\left[\frac{D_p^2 \; R^2}{D_f^2 \; (17)^2}\right] \text{ (from Equation 10.5)}$$

Or $$Q_{C_1} = 46.02 \frac{W \; D_p^2}{D_f^2} \quad (10.14)$$

The fireball diameter is now evaluated in terms of W at the time of the first peak. This is determined by the EG & G ϕ^5 law for fireball growth prior to time of minimum. (Reference 9.)

$$W = 1.27 \times 10^{-8} \frac{D_f^5}{t^2}$$

Or $$D_f = 37.96 \; W^{0.2} \; t^{0.4} \quad (10.15)$$

Where: D_f = fireball diameter in meters

t = time in milliseconds

The time to first peak is approximated by:

$t = 10^{-1} \; W^{0.42}$ (Reference 10)

Where: t = time in milliseconds

Substituting this value for D_f in Equation 10.15 gives:

$$D_f = (37.96)(W^{0.2})\left[(10^{-1})(W^{0.42})\right]^{0.4}$$

Or $$D_f = 15.1 \; W^{0.368} \quad (10.16)$$

Now, substituting this value for D_f in Equation (10.14) gives:

SECRET

[redacted]

$$Q_{R_1} = 46.02 \frac{W \; D_p^{\,2}}{(15.1)^2 \; (W^{0.368})^2}$$

or $$Q_{R_1} = 0.202 \; W^{0.264} \; D_p^{\,2} \; A \qquad (10.17)$$

"A" is the combined transmission factor and is again taken as 0.58. The pupillary diameter is again taken as 4 millimeters.

The retinal irradiance from the first thermal pulse in this event is now calculated from Equation (10.17):

[redacted]

[redacted]

SECRET

CHAPTER 11

CONCLUSIONS AND RECOMMENDATIONS

It can be concluded that retinal burn and flashblindness present no hazard when [redacted] etonation is observed through a 1-percent transmission, gold-coated neutral-density filter, under the conditions of this test. The level of retinal irradiance is clearly below the retinal burn threshold for bursts fro[redacted]nder similar conditions. [redacted]

From the results of this experiment, it is predicted that retinal burn and flashblindness would not occur when any burst in the GAM-83B range is observed through a similar filter under any conditions.

It is recommended that similar experiments be conducted in any future nuclear testing. It is necessary that the filter be tested under conditions of maximum burst and minimum distance for the system and with many more exposures.

High resolution emission data, both photographic and electronic, are necessary to determine the minimum density required in the filter. It is felt that further testing may indicate that the safe transmission of the filter can be doubled or even tripled.

SECRET

APPENDIX

INSTRUMENTATION LOCATIONS AND CONFIGURATIONS

SECRET

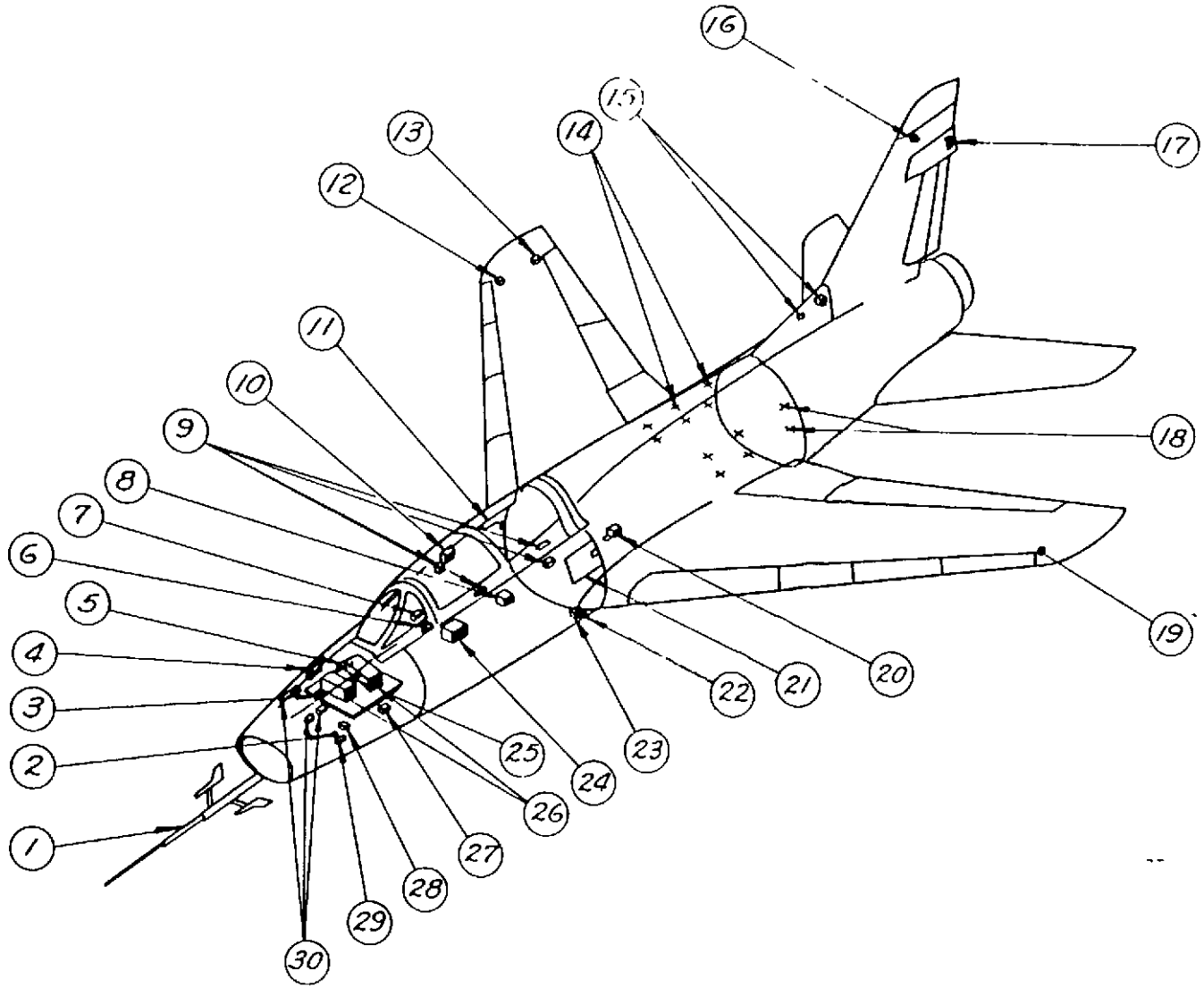

Figure A.1 General aircraft instrumentation.

SECRET

1 BOOM ASSY.
2 ACCELEROMETER INSTL.
3 ACCELEROMETER INSTL.
4 RELOCATION
5 RELOCATION
6 INSTRUMENT INSTL.
7 INSTRUMENT INSTL.
8 GYRO INSTL.
9 INSTL.-OSCILLOGRAPH, PWR CONTROL & CORRELATOR
10 INSTL.-SPECIAL EFFECTS
11 DOOR ASSY.
12 ACCELEROMETER INSTL.
13 ACCELEROMETER INSTL.
14 INSTL.-STRAIN GAGE
15 ACCELEROMETER INSTL.
16 ACCELEROMETER INSTL.
17 PRESSURE TRANSDUCER INSTL.
18 INSTL.-STRAIN GAGE
19 ACCELEROMETER INSTL.
20 ACCELEROMETER INSTL.
21 DOOR ASSY.
22 PRESSURE TRANSDUCER INSTL.
23 GYRO INSTL.
24 INSTL.-POWER SUPPLY
25 INSTL.-OSCILLOGRAPH & EQUIP.
26 RELOCATION
27 PRESSURE TRANSDUCER INSTL.
28 PRESSURE TRANSDUCER INSTL.
29 PRESSURE TRANSDUCER INSTL.
30 RELOCATION

Figure A.2 Legend.

SECRET

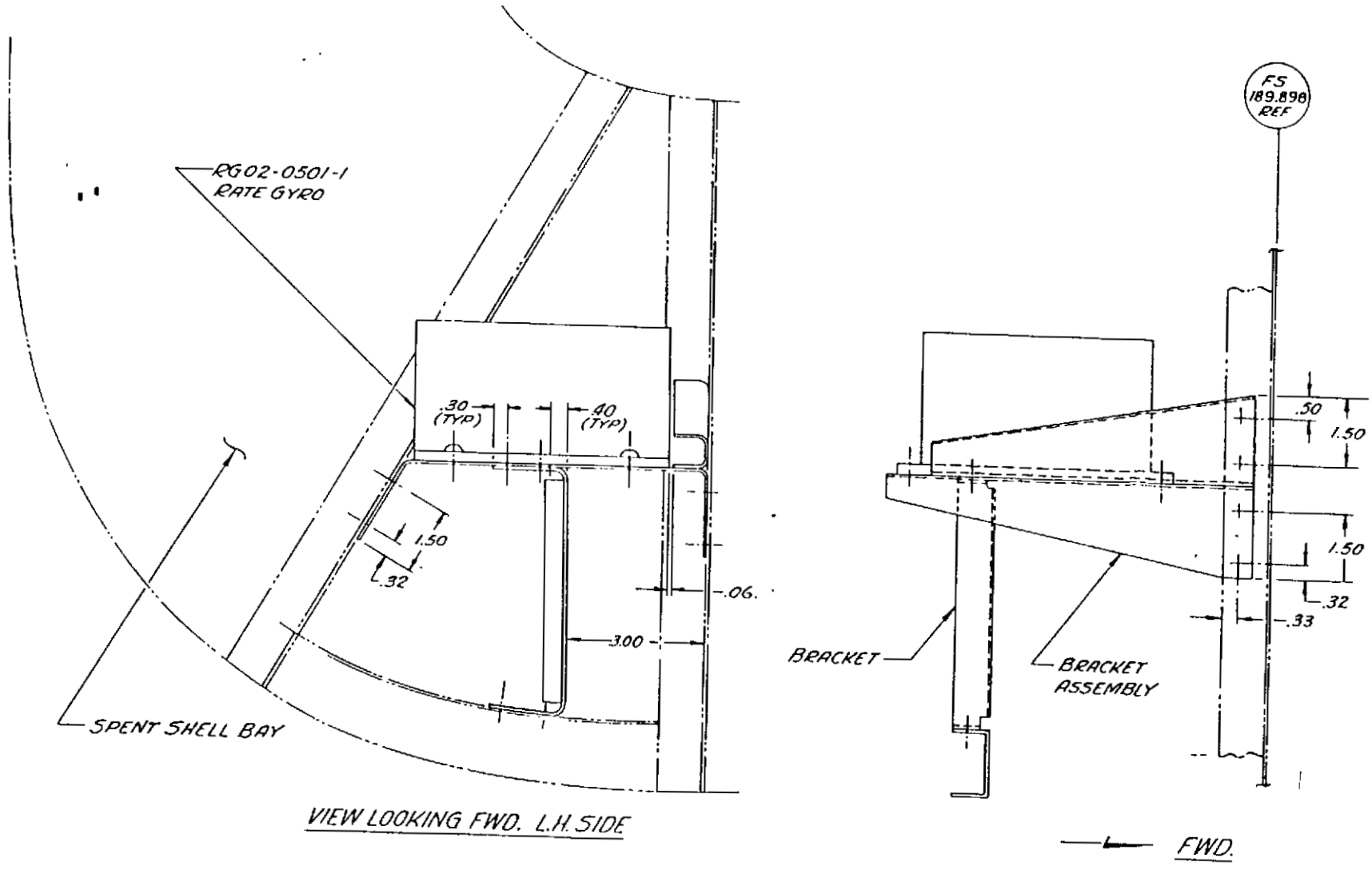

Figure A.3 Attitude gyro installation, FS 189.898.

SECRET

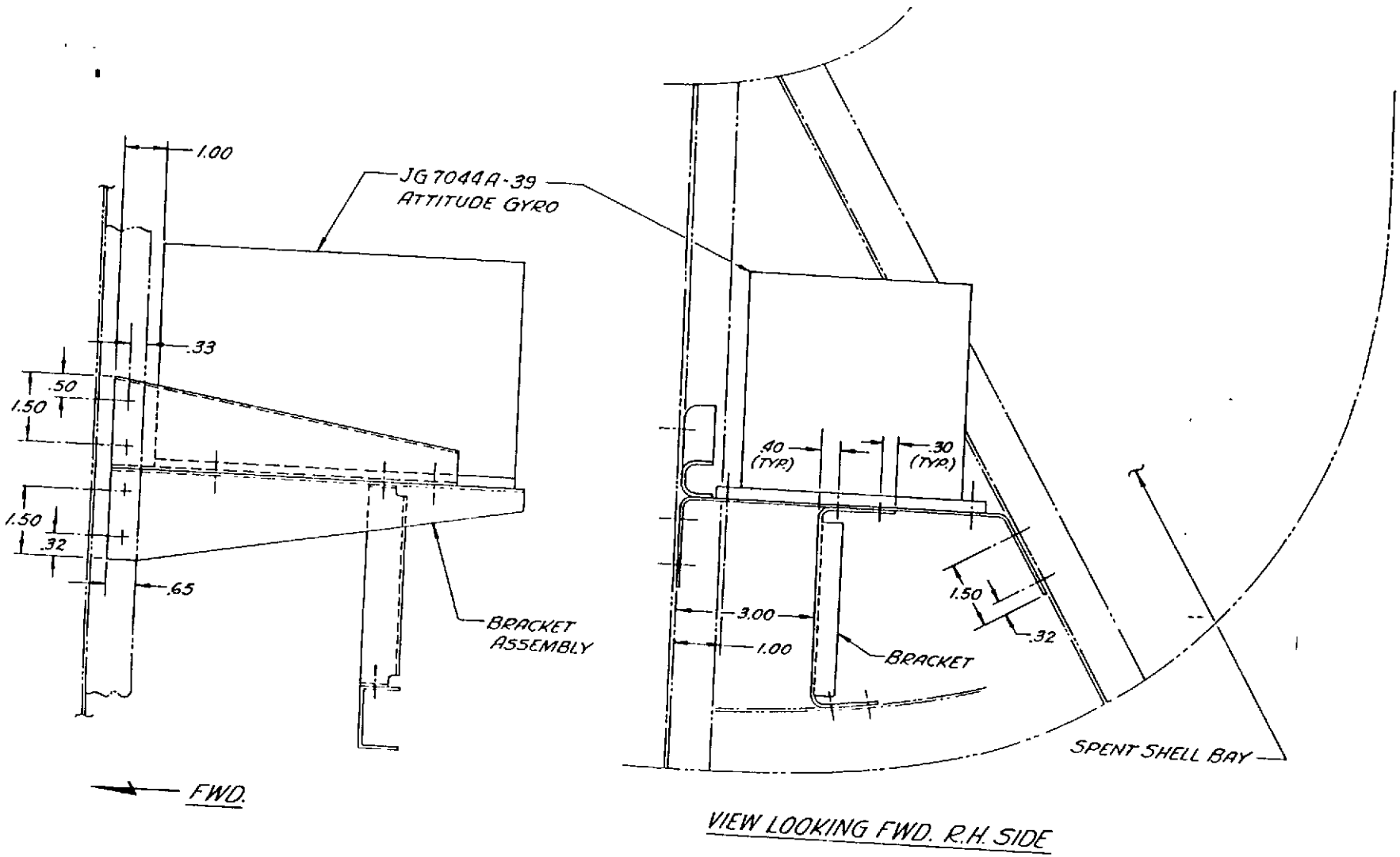

Figure A.4 Rate gyro installation, FS 189.898.

SECRET

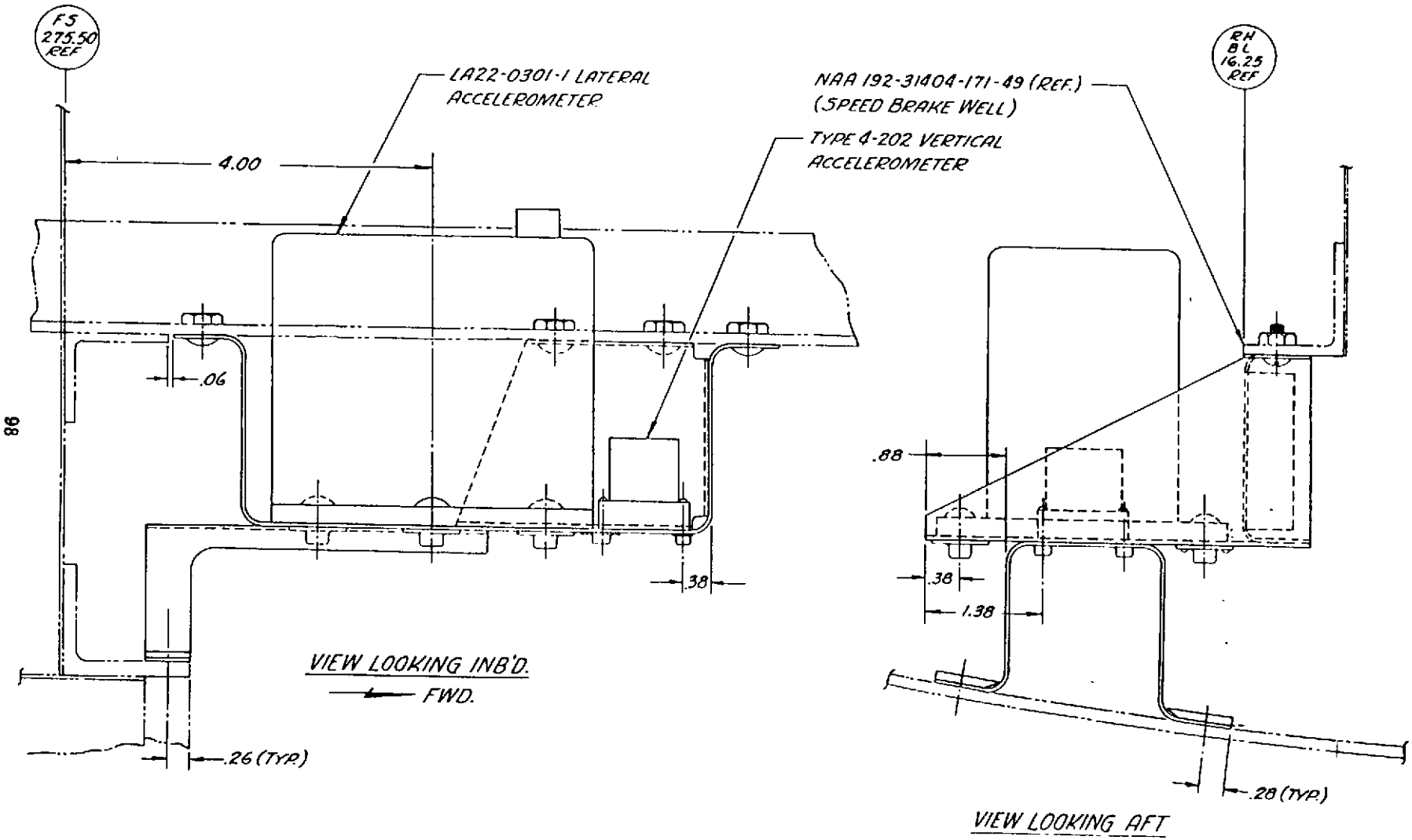

Figure A.5 Lateral and vertical accelerometer installation, FS 275.50.

SECRET

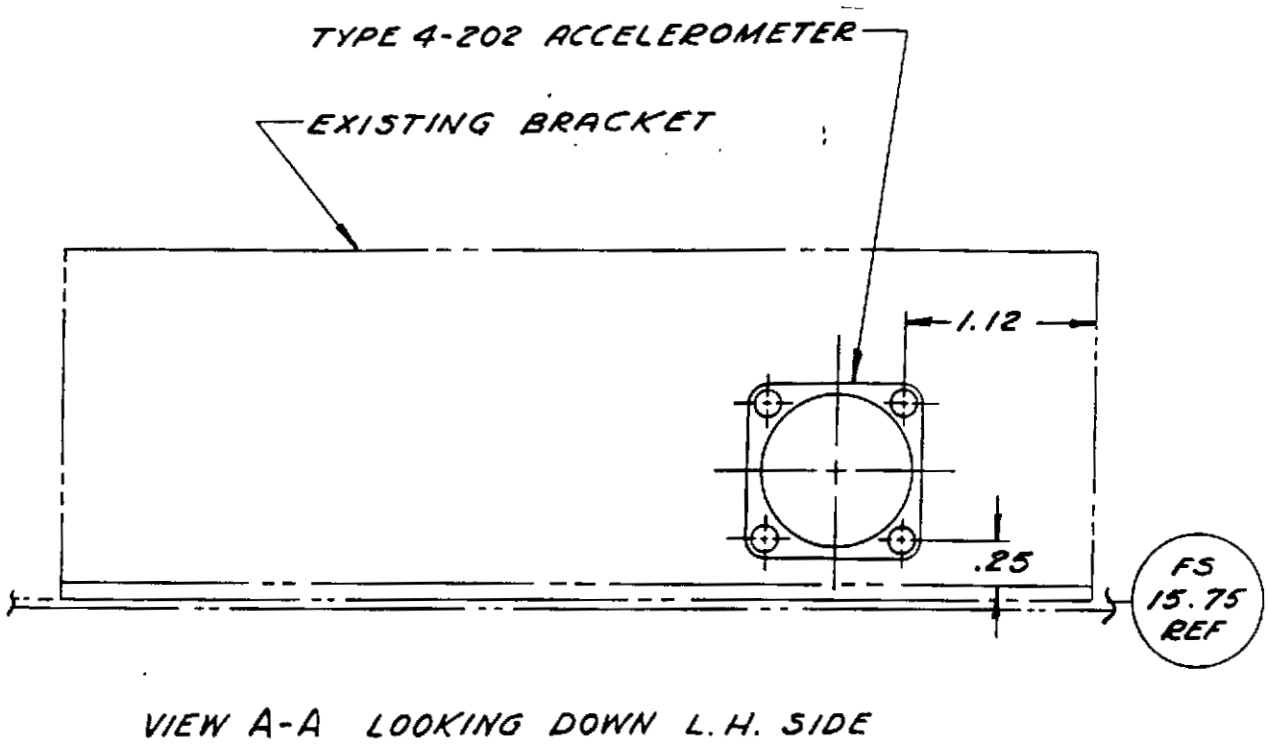

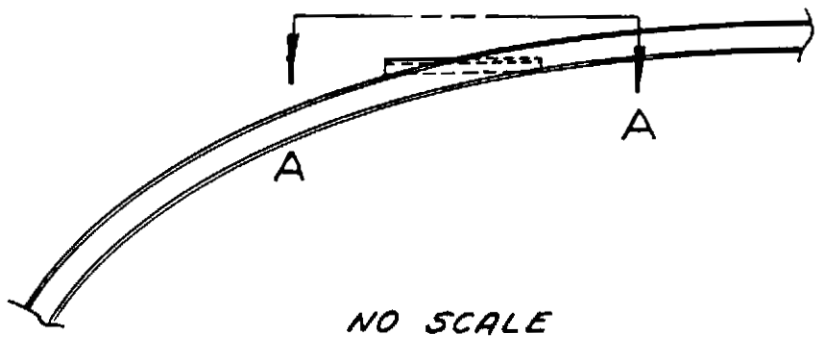

Figure A.6 Accelerometer installation, FS 15.75.

SECRET

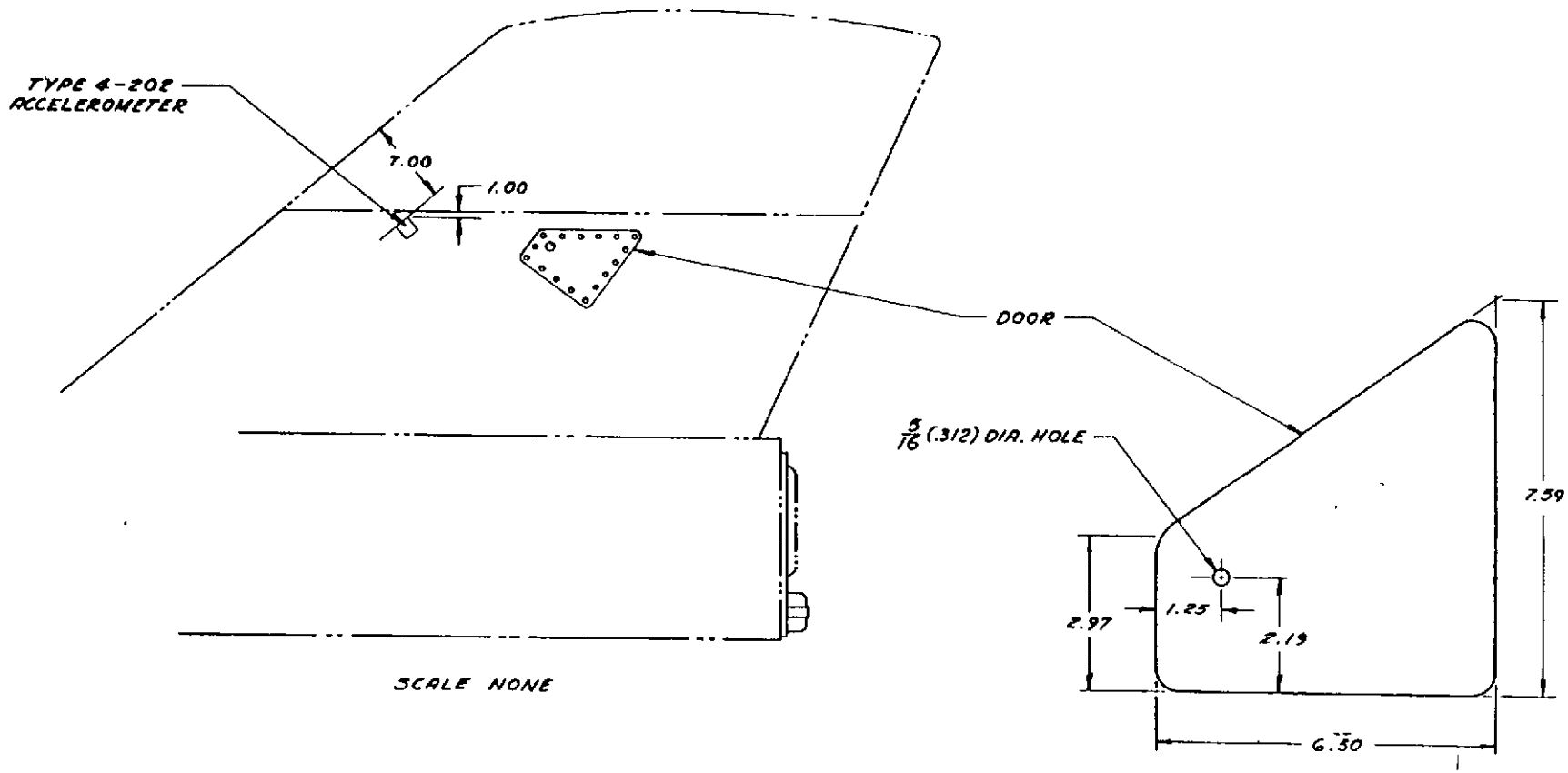

Figure A.7 Vertical stabilizer accelerometer installation.

SECRET

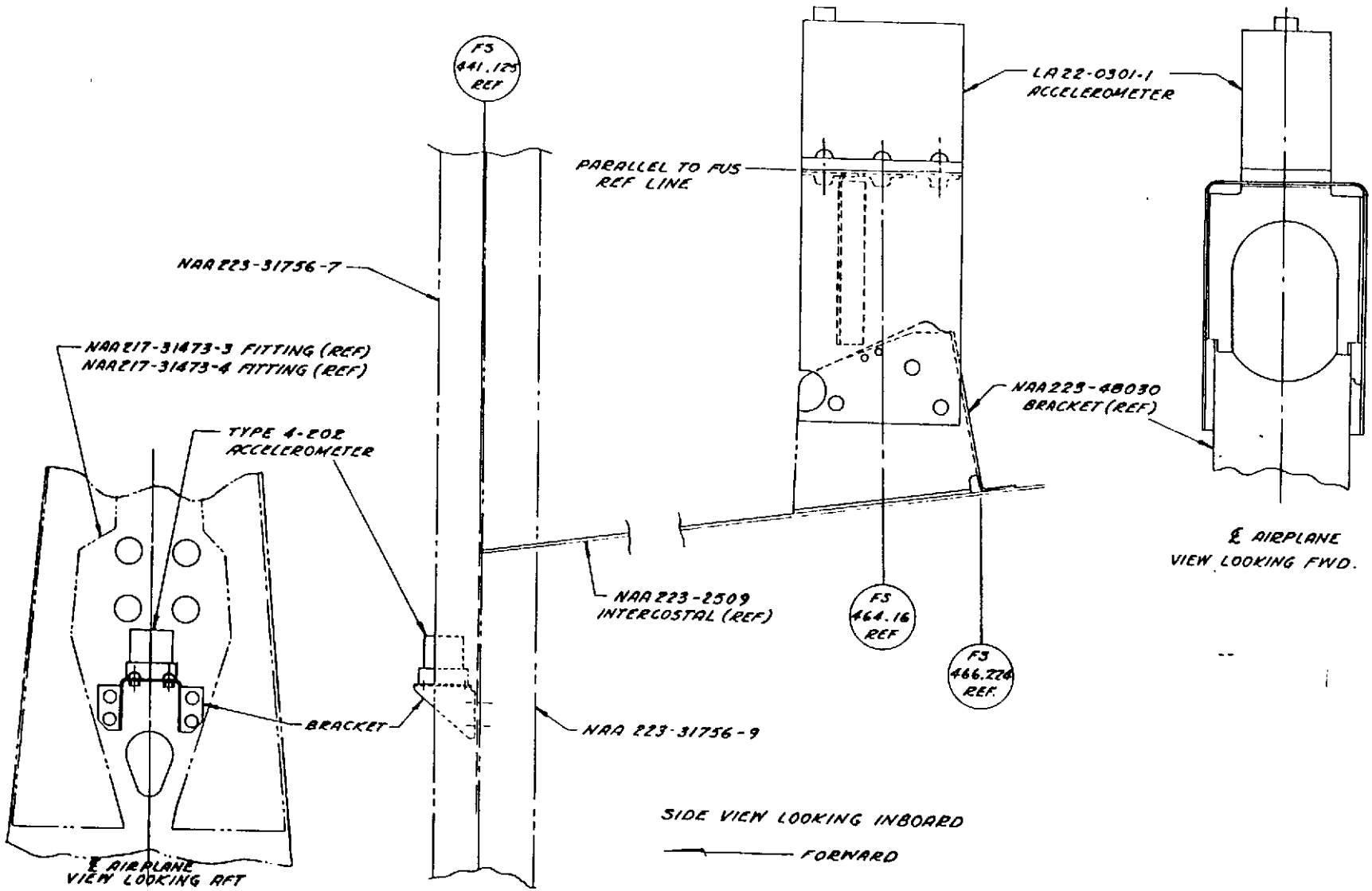

Figure A.8 Accelerometer Installation, FS 464.16.

SECRET

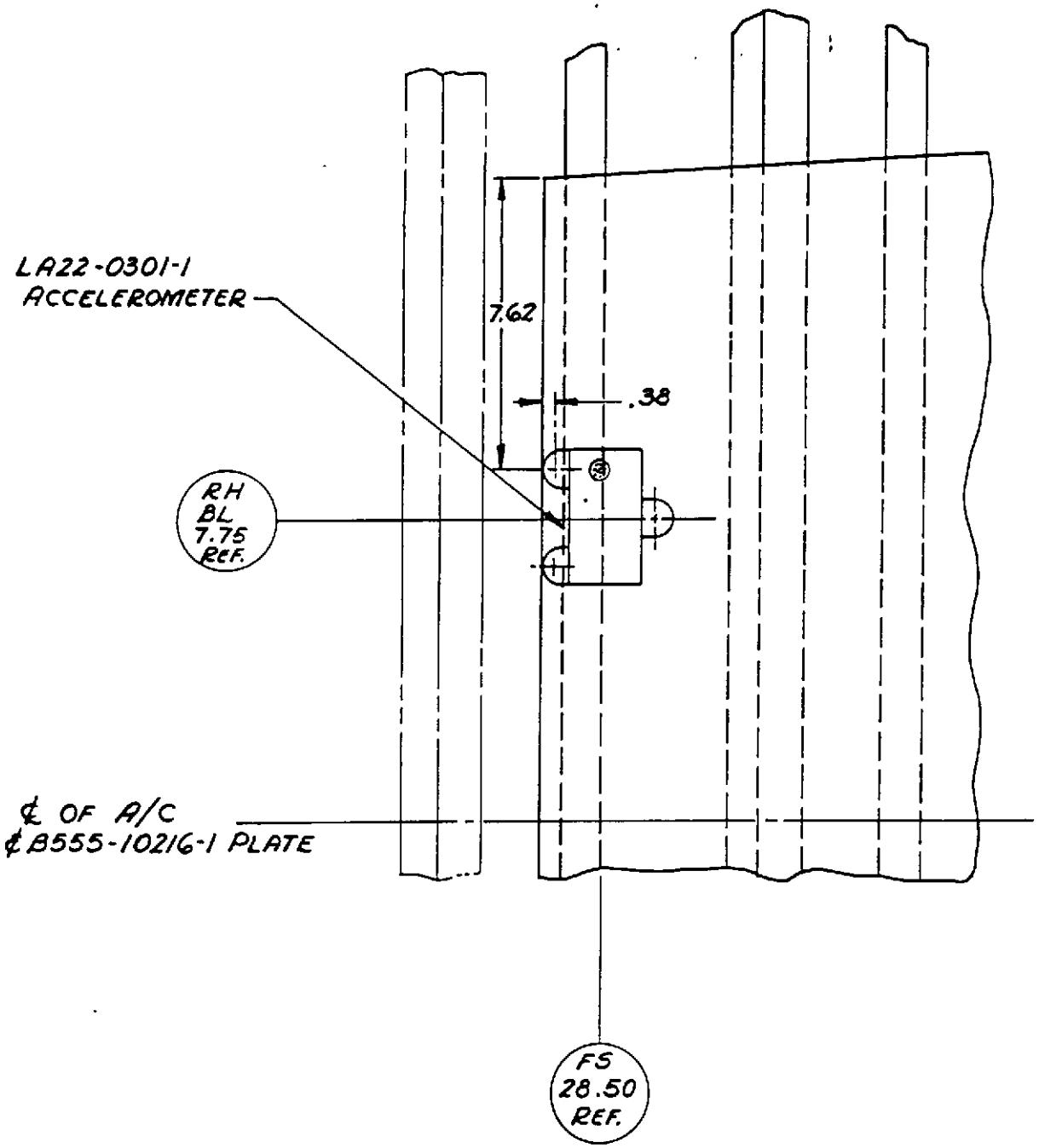

Figure A.9 Accelerometer installation, FS 28.50.

SECRET

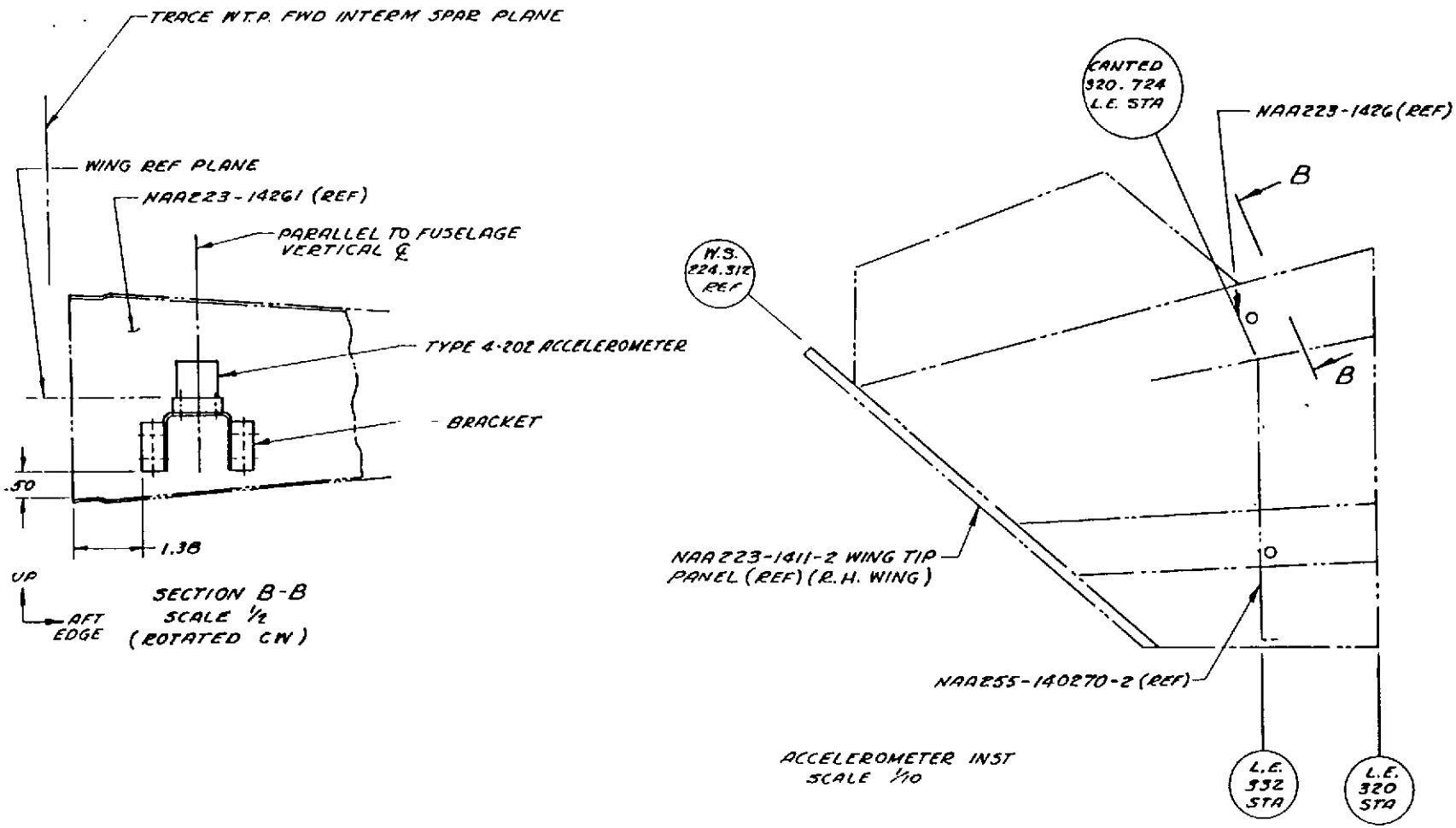

Figure A.10 Wingtip accelerometer installation, right wing.

SECRET

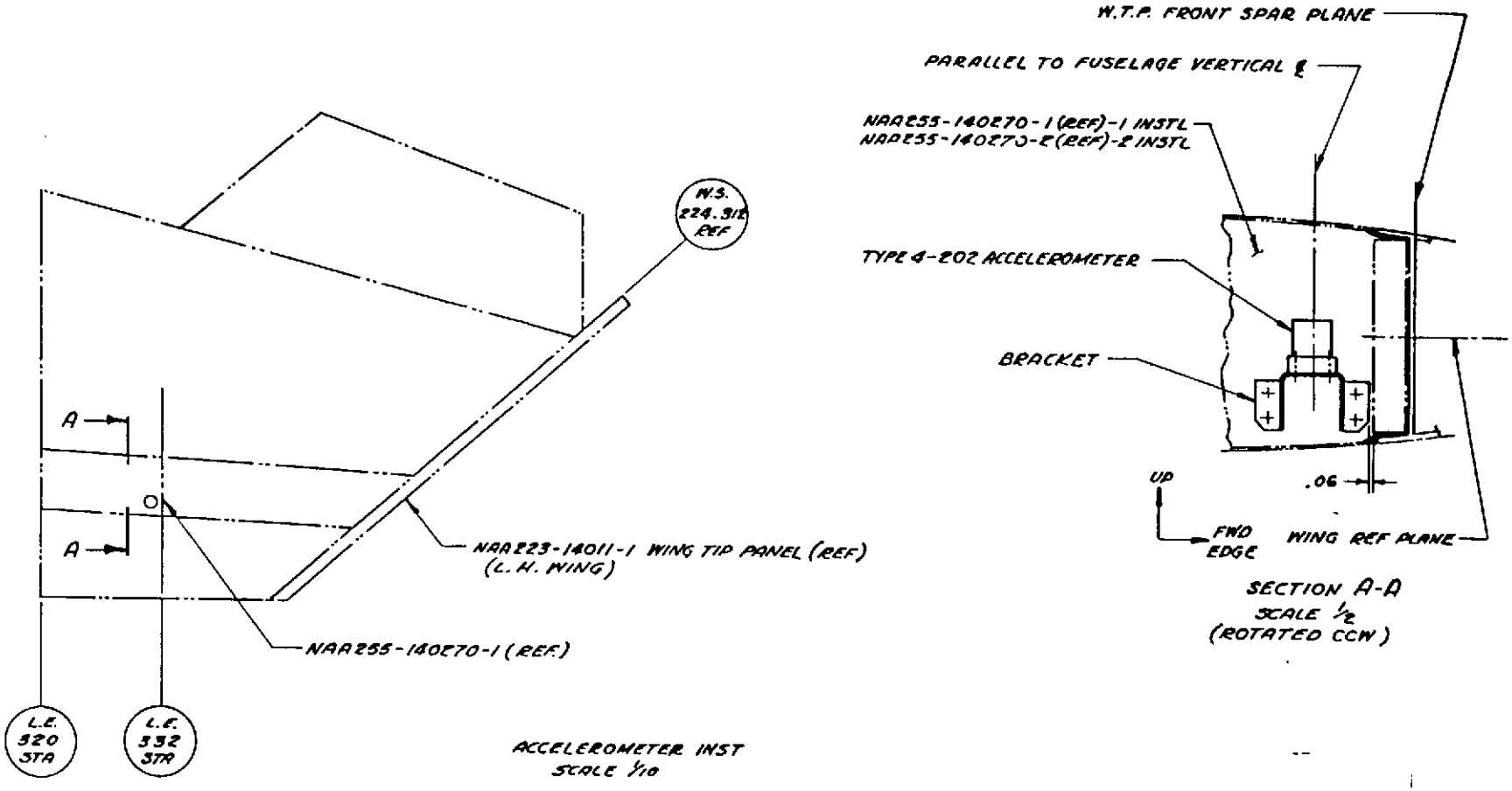

Figure A.11 Wingtip accelerometer installation, left wing.

SECRET

REFERENCES

1. "F-100D/F Gust Limits"; Report Nr. TFD-61-783; 10 October 1961; North American Aviation, Inc., Downey, California; Confidential.

2. "GAM-83B, Pilot Safety Study"; Report Nr. OR2128; December 1961; The Martin Company, Orlando, Florida; Secret.

3. "Nuclear Weapon Delivery Capability Study for the F-100D Airplane"; Report Nr. NA 56-1076, January 1947; North American Aviation, Inc., Downey, California; Secret.

4. S. Glasstone; "The Effects of Nuclear Weapons"; US Department of Defense, June 1957. (1962 edition is available from the US Government Printing Office, Washington 25, D.C.)

5. R.L. Bisplinghoff, H. Ashley, R.L. Halfman; "Aeroelasticity"; Addison-Wesley Publishing Co., Inc.; 1955.

6. Victor A. Byrnes and others; "Ocular Effects of Thermal Radiation from Atomic Detonation—Flashblindness and Chorioretinal Burns"; Project 4.5, Operation Upshot-Knothole, WT-745, November 1955; School of Aviation Medicine, USAF, Randolph Air Force Base, Texax; Unclassified.

7. J.E. Pickering and others; "Effects on Eyes from Exposure to Very-High-Altitude Bursts (U)"; Project 4.1, Operation Hardtack, WT-1633, October 1960; School of Aviation Medicine, USAF, Randolph Air Force Base, Texas; Secret Formerly Restricted Data.

8. Personal Communication; Dr. W.T. Ham, Jr., Medical College of Virginia, Richmond, Virginia.

9. Personal Communication; D.F. Seacord, Jr., Edgerton, Germeshausen and Grier, Boston, Massachusetts.

10. R.W. Hillendahl; "Characteristics of the Thermal Radiation from Nuclear Detonations"; Vol. III, R and D Technical Report USNRDL-TR-383; US Naval Radiological Defense Laboratory, San Francisco 24, California; Unclassified.

~~SECRET~~

Page 107 is deleted in its entirety